1-1-1997

Fractal relationships and spatial distribution of ore body modelling

D. J. Kentwell
Edith Cowan University

Edith Cowan University

Copyright Warning

Fractal Relationships and Spatial Distributions in Ore Body Modelling

Thesis

Master of Science (Mathematics and Planning)

D. J. Kentwell

Faculty of Science, Technology and Engineering
School of Computer, Information and Mathematical Sciences
Edith Cowan University

August 1997

USE OF THESIS

The Use of Thesis statement is not included in this version of the thesis.

Table of Contents

Abstract

The nature of spatial distributions of geological variables such as ore grades is of primary concern when modelling ore bodies and mineral resources. The aim of any mineral resource evaluation process is to determine the location, extent, volume and average grade of that resource by a trade off between maximum confidence in the results and minimum sampling effort. The principal aim of almost every geostatistical modelling process is to predict the spatial variation of one or more geological variables in order to estimate values of those variables at locations that have not been sampled. From the spatial analysis of these variables, in conjunction with the physical geology of the region of interest, the location, extent and volume, or series of discrete volumes, whose average ore grade exceeds a specific ore grade cut off value determined by economic parameters can be determined. Of interest are not only the volume and average grade of the material but also the degree of uncertainty associated with each of these. Geostatistics currently provides many methods of assessing spatial variability. Fractal dimensions also give us a measure of spatial variability and have been found to model many natural phenomenon successfully (Mandelbrot 1983, Burrough 1981), but until now fractal modelling techniques have not been able to match the versatility and accuracy of geostatistical methods. Fractal ideas and use of the fractal dimension may in certain cases provide a better understanding of the way in which spatial variability manifests itself in geostatistical situations. This research will propose and investigate a new application of fractal simulation methods to spatial variability and spatial interpolation techniques as they relate to ore body modelling. The results show some advantages over existing techniques of geostatistical simulation.

Declaration

I certify that this thesis does not incorporate without acknowledgement any material previously submitted for a degree or diploma in any institution of higher education; and that to the best of my knowledge and belief it does not contain any material previously published or written by another person except where due reference is made in the text.

Signature .

Date 16-12-97

Acknowledgements

I would like to thank Western Mining Corporation and Mr. Ian Glacken for providing the gold data from the Goodall Mine as well as Gemcom Australia and Mr. Chris Cusack for providing the GS32 and PCXPLOR software and for providing industry contacts. I would also like to thank my supervisors Mr. Geoff Comber and Dr. Lyn Bloom for their tireless editing and moral support.

1 Introduction

In this chapter we will outline the need for techniques that predict spatial variability of geological variables, present a preview summary of the thesis and give a brief description of the software used.

1.1 The Problem in Relation to Ore Body Modelling

The aim when evaluating any prospect or potentially mineable orebody is to determine the physical extent and economic value of the mineralisation whilst at the same time using the minimum amount of sampling necessary to give a reliable estimate. Minimising sampling is a major component in minimising exploration and development costs. Geostatistical techniques, along with various rules of thumb, are currently used to achieve this. The basis of an ore body model comes firstly from the geological structures present and secondly from a set of sample values of some geological variable or variables taken from known locations throughout the region of interest. In other words, an ore body model is, in part, a spatial distribution of sample values in three dimensions. The more samples (appropriately distributed) that are taken the better the results of the modelling process should be. But more samples mean more costs and more time spent, not only with the sampling procedure itself but also with access to the sites that need to be sampled. For example it is physically more difficult to sample locations that are on steep hillsides or underwater. Therefore the number of samples taken and the choice of sample locations is always a trade off between maximum confidence in the overall results and minimum sampling effort.

The principal aim of almost every geostatistical modelling process is to predict the spatial variation of one or more geological variables in order to estimate values of those variables at locations that have not been sampled. Such a variable may be any geological property that varies over distance and that can be measured in numeric or categorical values. The main variable of interest is usually the mineral grade, in grams per tonne, but other variables such as vein widths or veining densities are often used as an indicator of the degree of mineralisation. From the spatial analysis of these variables, in conjunction with the physical geology of the region of interest, the object is to define the location, extent and volume, or series of discrete volumes, whose average ore grade exceeds a specific ore grade cut off value determined by economic parameters. Of interest are not only the volume and average grade of the material but also the degree of uncertainty associated with each of these.

Geostatistics currently provides many methods of assessing spatial variability. Fractal dimensions also give us a measure of spatial variability and have been found to model many natural phenomenon successfully (Mandelbrot 1983, Burrough 1981), but until now fractal modelling techniques have not been able to match the versatility and accuracy of geostatistical methods.

1.2 Aim of the Thesis

The aim of this thesis is to investigate fractal modelling methods and determine whether and how they can be applied in a geostatistical framework to ore body modelling, and in particular to gold deposits, and to determine whether they offer any advantages over existing geostatistical techniques.

1.3 Significance of the research

With the price of gold currently at a twelve year low and with Australia now being the world's most expensive gold producer (Dunn 1997, p22) gold exploration and production companies are more and more concerned with obtaining an accurate assessment of their potential reserves. Any techniques that improve the accuracy of that assessment without substantially increasing the costs involved will therefore be of great benefit to the industry.

1.4 Outline of the thesis

In chapter two we will examine the mathematical details of the theory of regionalised variables underlying geostatistics and explain, with examples, the basic estimation process of *kriging*. In chapter three we will look at some of the different methods of geostatistical simulation and give theoretical details plus examples of two methods in particular, namely *sequential Gaussian simulation* and *LU decomposition*. In chapter four we will detail fractal theory focusing on stochastic fractals and the model of *fractional Brownian motion* before going on to propose a new scheme, SGFRACT, that incorporates the fractal dimension into geostatistics. The data used in the examples in chapters two and three are used to test the new simulation scheme. Chapter five shows the application of SGFRACT to an actual industrial situation using data from a completed gold mining operation in the Northern Territory. Chapter six contains a review, conclusions and recommendations for further research.

1.5 Software Summary

The software used for calculation, manipulation and visualisation of data is briefly described here and is then referred to throughout the thesis by its program name in capitals.

The GEMCOM (Gemcom 1996) suite of mining software includes:

GS32 - A three dimensional visualisation and solids creation mining software package.

PCXPLOR - An exploration database management, statistics and geostatistics processing package.

The GSLIB (Deutsch & Journel 1992) suite of geostatistical routines includes:

OKB2D - A basic two dimensional kriging estimation routine.

SGSIM - A sequential Gaussian simulation routine.

NSCORE & BACKTR - transformation routines.

Other statistics and presentation software used include:

UPFILE (Kanevski 1997)

VARIOWIN 2.1 (Pannatier 1994).

2 Estimation

Consider a continuous variable distributed in one, two or three dimensional space. In order to understand the nature of this variable we need to have a model of how it changes with distance and direction. The phenomenon can be sampled at different discrete locations but this only gives us information about those specific points and does not by itself tell us anything about the unsampled areas. We know from experience that, in general, things found close together tend to be similar and that things that are further away from each other tend to be different. This being the case, we would expect that some sort of spatial continuity exists that could be accurately modelled if we knew the exact relationship between all possible point values. However most situations that occur in nature, including the distribution of mineral grades throughout a deposit, do not show such regularity or conformity. In fact, upon initial examination many natural phenomena show what appears to be totally random behaviour. The task of looking for some sort of spatial continuity within these at least partially random phenomena therefore requires some sort of *probabilistic model* that takes account of both the random and the structured aspects. Geostatistics is a branch of mathematics that deals with modelling and estimation in such situations.

In this chapter we will examine regionalised variable theory which is the basis of geostatistics and go on to outline the framework and mathematical tools that allow the estimation of spatial variables within a probabilistic model. The notation and methodology we will use mostly follows Deutsch & Journel (1992). Where conflicting notation could lead to confusion some amendments have been made.

2.1 Regionalised Variable Theory

Regionalised variable theory states that where a property is sampled in a region of space each individual sample value can be considered as the outcome from a single but unknown *random process,* and that a set of sample values from different locations in a region of space can be considered as one outcome of a set of random processes that are not necessarily the same. A random process in this context is a general term covering any natural or artificial mechanism which produces results that appear to be without any pattern or order. Consider a particular location $\mathbf{u}_\alpha$ which is a vector of up to three components $(u_\alpha^x, u_\alpha^y, u_\alpha^z)$ within a region R and where α is an index representing the particular location. When the variable under consideration is continuous and the locations are points there is an infinite number of possible sample locations within R. The random process at location $\mathbf{u}_\alpha$ is called a *random variable* $Z(\mathbf{u}_\alpha)$. The set of all random variables within R is called a *random function* $\{Z(\mathbf{u}) : \mathbf{u} \in R\}$. A *regionalised value* $z(\mathbf{u}_\alpha)$ is an individual sample value and represents one realisation of the random variable $Z(\mathbf{u}_\alpha)$. A *regionalised variable* $\{z(\mathbf{u}) : \mathbf{u} \in R\}$ is the set of all possible sample values in R and represents one realisation of all the random variables in R. From this point on we will use $Z(\mathbf{u})$ to denote a random function and $z(\mathbf{u})$ to denote a regionalised variable. To accommodate the deterministic aspects as well as the random aspects of regionalised variables the random function model of $Z(\mathbf{u})$ can be considered as being made up of three major components for all locations $\mathbf{u}$ within the region,

$$Z(\mathbf{u}) = m(\mathbf{u}) + Y(\mathbf{u}) + e \qquad \forall \mathbf{u} \in R \tag{2.1}$$

where $m(\mathbf{u})$ is a deterministic, linear or non-linear, function describing the trend or *drift* component, $Y(\mathbf{u})$ represents the random spatially dependent residuals from $m(\mathbf{u})$ and e is a residual spatially independent noise term. We will investigate each of these terms in more detail in the following sections. This model deals with random functions whose joint probability distributions are unknown and we must now establish a probabilistic framework in which we can study and make inferences about the forms of these distributions.

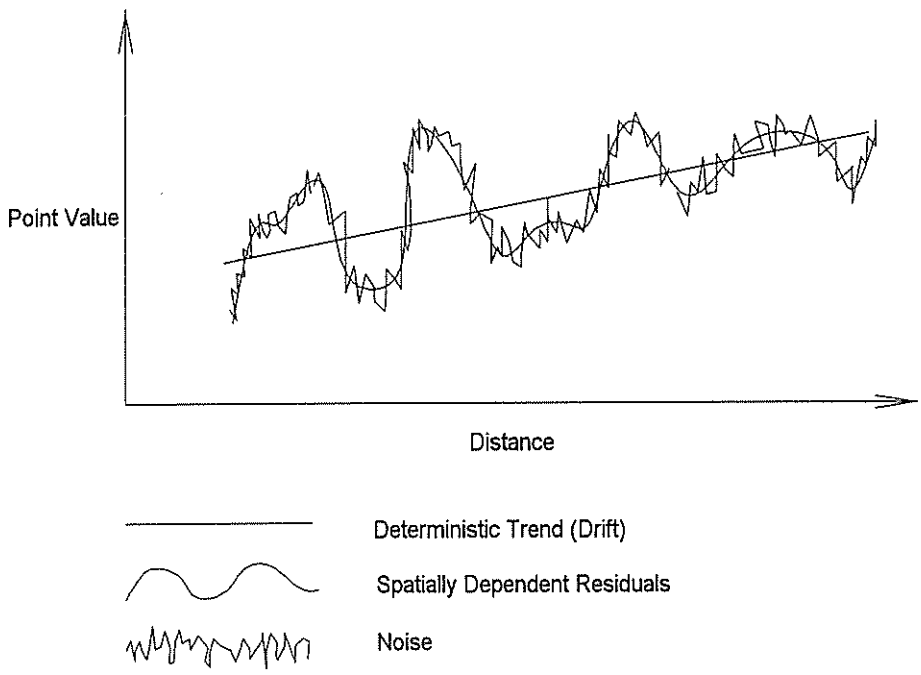

Figure. 2.1. One dimensional data profile with linear drift showing random function model components.

Each random variable $Z(\mathbf{u}_\alpha)$ within the random function $Z(\mathbf{u})$ has an unknown cumulative distribution function F given by

$$F(\mathbf{u}_\alpha; z) = P(Z(\mathbf{u}_\alpha) < z). \tag{2.2}$$

Similarly the unknown joint probability distribution of the random function $Z(\mathbf{u})$ with n random variables is defined by

$$F(\mathbf{u}_1, \ldots, \mathbf{u}_n; z_1, \ldots, z_n) = P(Z(\mathbf{u}_1) < z_1, \ldots, Z(\mathbf{u}_n) < z_n) \; . \qquad (2.3)$$

In order to obtain a probabilistic interpretation of any random variable it is necessary to be able to infer its probability distribution. To approximate a statistical distribution it is often sufficient to define its first two moments, if they exist. This does not completely define the distribution as it can be shown that two different distributions can have the same first two moments, but it does define certain characteristics of a distribution which turn out to be sufficient to provide approximate solutions for most geostatistical purposes (Journel & Huijbregts 1978). The first order moment of a distribution is its mean or its expectation. The expectation of a random variable $Z(\mathbf{u}_\alpha)$, assuming it exists, is usually a function of $\mathbf{u}$ and is written as

$$E[Z(\mathbf{u})] = m(\mathbf{u}). \qquad (2.4)$$

There are three second order moments we shall consider. The first is the *variance* of a random variable which is a measure of the dispersion of a distribution away from its mean. The next second order moment is the *covariance* which is a measure of the nature of association between two random variables. The third is the *variogram* which is the variance of the increments of two random variables and is therefore a measure of the dispersion of the distribution of the increments.

Definition 2.1 The *variance* of a random variable $Z(\mathbf{u}_\alpha)$, if it exists, is defined as,

$$\sigma^2 = Var(Z(\mathbf{u}_\alpha)) = E[(Z(\mathbf{u}_\alpha) - m(\mathbf{u}_\alpha))^2]. \qquad (2.5)$$

Definition 2.2 The *covariance* of the random variables, $Z(\mathbf{u}_\alpha)$ and $Z(\mathbf{u}_\beta)$, assuming both exist, is defined as

$$C(\mathbf{u}_\alpha, \mathbf{u}_\beta) = E[(Z(\mathbf{u}_\alpha) - m(\mathbf{u}_\alpha))(Z(\mathbf{u}_\alpha) - m(\mathbf{u}_\beta))]\,. \tag{2.6}$$

Definition 2.3 The *variogram* is the variance of the increment $Z(\mathbf{u}_\alpha) - Z(\mathbf{u}_\beta)$ and is defined as

$$2\gamma(\mathbf{u}_\alpha, \mathbf{u}_\beta) = Var(Z(\mathbf{u}_\alpha) - Z(\mathbf{u}_\beta)). \tag{2.7}$$

To carry out statistical inference we require a number of samples from a distribution, the more samples there are the closer the estimation of the parameters will be to the true distribution parameters. However in geostatistical situations we only have one sample set from the random function which is in turn made up of single sample values from individual random variables. This is insufficient for statistical inference. To overcome this problem certain assumptions of homogeneity are necessary. These are broadly covered by the term *stationarity*. If we consider the region of interest to be *homogeneous*, that is that the phenomena under investigation have been formed by a uniform process for that region, and hence assume that the regionalised variable repeats itself in space, this then provides the equivalent of many realisations of the random function which permits a certain amount of statistical inference. For example, imagine a two dimensional grid of sample locations and a small window which is allowed to move around that grid. Each possible position of that smaller window is considered to be a different realisation of the same random function (see figure 2.2). We assume that the characteristics of the random function do not change when shifting a given set of points from one area to another. This is known as *translation invariance*.

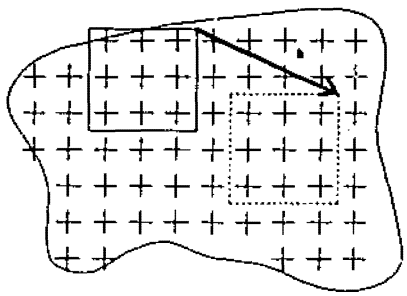

Figure. 2.2. Different realisations of the same random function with translation vector **h**.

Definition 2.4 A random function $Z(\mathbf{u})$ is said to be *strictly stationary* if for any set of n points $\mathbf{u}_1, \ldots, \mathbf{u}_n$ and any translation vector $\mathbf{h}$

$$F_{\mathbf{u}_1,\ldots,\mathbf{u}_n}(z_1, \ldots, z_n) = F_{\mathbf{u}_1+\mathbf{h},\ldots,\mathbf{u}_n+\mathbf{h}}(z_1, \ldots, z_n). \tag{2.8}$$

From this it follows that any two random variables $Z(\mathbf{u}_\alpha)$ and $Z(\mathbf{u}_\alpha+\mathbf{h})$ from a stationary random function have the same probability distribution and that all random variables, within a particular stationary random function, have a constant mean m which therefore does not depend on the location $\mathbf{u}$. From equation 2.4 we now get

$$E[Z(\mathbf{u}_\alpha)] = m \qquad \forall \mathbf{u}_\alpha \in R. \tag{2.9}$$

Another implication of the assumption of strict stationarity is that the functions in equations 2.6 and 2.7 depend only on the translation vector $\mathbf{h}$ and not on the location $\mathbf{u}$. Therefore any given pair of random variables $[Z(\mathbf{u}_\alpha), Z(\mathbf{u}_\alpha+\mathbf{h})]$ can be considered as having the same bivariate probability as any other pair from the stationary random function. Thus, assuming the covariance for each pair of random variables exists, from equations 2.6 and 2.9 we now get

$$\begin{aligned} C(\mathbf{u}_\alpha, \mathbf{u}_\beta) &= C(\mathbf{u}_\alpha, \mathbf{u}_\alpha+\mathbf{h}) \\ &= E[(Z(\mathbf{u}_\alpha) - m)(Z(\mathbf{u}_\alpha+\mathbf{h}) - m)] \\ &= E[Z(\mathbf{u}_\alpha) Z(\mathbf{u}_\alpha+\mathbf{h})] - E[Z(\mathbf{u}_\alpha)]m - E[Z(\mathbf{u}_\alpha+\mathbf{h})]m + m^2 \end{aligned} \tag{2.10}$$

hence,

$$E[Z(\mathbf{u}_\alpha)Z(\mathbf{u}_\alpha+\mathbf{h})] - m^2 = C(\mathbf{h}) \qquad \forall \mathbf{u}_\alpha \in R. \tag{2.11}$$

Definition 2.5 A random function is *second order stationary* if, for all vectors **h,**

$$E[Z(\mathbf{u}_\alpha)] = m \qquad \forall \mathbf{u}_\alpha \in R$$

and

$$E[Z(\mathbf{u}_\alpha)Z(\mathbf{u}_\alpha+\mathbf{h})] - m^2 = C(\mathbf{h}) \qquad \forall \mathbf{u}_\alpha \in R.$$

Second order stationarity is weaker than strict stationarity in that it does not require the full probability distribution to be known, only the expectation and covariance function of the random variables must exist and the variance of the random function must be finite. The existence of the covariance function implies the existence of a finite variance because at a separation of $\mathbf{h}= 0$ the covariance is equal to the variance.

$$C(0) = E[(Z(\mathbf{u}_\alpha) - m)^2] = Var(Z(\mathbf{u}_\alpha)) \qquad \forall \mathbf{u} \in R \tag{2.12}$$

If we now consider the stationary variogram function, equation 2.7 becomes

$$2\gamma(\mathbf{u}_\alpha, \mathbf{u}_\beta) = Var(Z(\mathbf{u}_\alpha) - Z(\mathbf{u}_\alpha+\mathbf{h})) \tag{2.13}$$

and the existence of the right hand side does not require $Var(Z(\mathbf{u}_\alpha))$ to be finite nor does it require the existence of the covariance function.

Definition 2.6 A random function is *intrinsic second order stationary* when, for all vectors **h,**

$$E[Z(\mathbf{u}_\alpha+\mathbf{h}) - Z(\mathbf{u}_\alpha)] = 0 \qquad \forall \mathbf{u} \in R \tag{2.14}$$

and

$$Var(Z(\mathbf{u}_\alpha+\mathbf{h}) - Z(\mathbf{u}_\alpha)) = 2\gamma(\mathbf{h}). \tag{2.15}$$

If we relate the concept of stationarity under the covariance or variogram function (equations 2.9, 2.11, 2.14 and 2.15) back to our model in equation 2.1 we now have what is known as a *stationary random function model*

$$Z(\mathbf{u}) = m + Y(\mathbf{u}) + e \tag{2.16}$$

where m is a constant mean, $Y(\mathbf{u})$ represents the spatially correlated random variation that remains once the mean has been subtracted and e is a residual error term. The variation with distance and direction $\mathbf{h}$ of the term $Y(\mathbf{u})$ can be modelled by the covariance function in some circumstances and by the variogram function in all circumstances.

2.2 Variogram and Covariance Functions

Having established our stationary random function model we will now concentrate on the component $Y(\mathbf{u})$ which contains any spatially correlated structure that exists in a particular regionalised variable. The principal tool used to study this structure is the *semi-variogram* for an intrinsic second order stationary process which is a plot of the semi-variogram function

$$\gamma(\mathbf{h}) = \tfrac{1}{2}E[(Z(\mathbf{u}_\alpha + \mathbf{h}) - Z(\mathbf{u}_\alpha))^2] \tag{2.17}$$

against the separation distance $|\mathbf{h}|$. For the moment we will only consider models that come from data sets that are *isotropic*, that is data that show the same structure in all directions. The semi-variogram is usually used in modelling in preference to the covariance function because it can handle random functions that are both second order stationary and intrinsic second order stationary. The covariance function and the semi-variogram function are related by the equation

$$\gamma(\mathbf{h}) = C(0) - C(\mathbf{h}) \tag{2.18}$$

which can be derived from equations 2.12 and 2.13. It should be noted that the semi-variogram can always be derived from the covariance but the converse is not

always possible because the semi-variogram may only be derived from a process which is intrinsic second order stationary. One example of a process for which the semi-variogram function exists but the covariance function does not is that of *Brownian motion* (Cressie 1991).

When using covariance or semi-variogram functions to compute variances of a sample set from a stationary random function we are in fact using a linear combination,

$$Y = \sum_{\alpha=1}^{n} \lambda_\alpha Z(\mathbf{u}_\alpha) \tag{2.19}$$

where λ_α is any real number, of the individual random variables which itself is also a random variable. This linear combination must adhere to the condition that its covariance or semi-variogram function is in some sense *positive definite*, ensuring that the variance of the random variable is never negative. The following properties used in definitions 2.7 and 2.8 are classical results of the theory of stochastic processes taken from Journel and Huijbregts (1978).

Definition 2.7 The covariance function $C(\mathbf{h}) = C(\mathbf{u}_\alpha, \mathbf{u}_\beta)$ is *positive definite* if,

$$Var(Y) = \sum_{\alpha=1}^{n} \sum_{\beta=1}^{n} \lambda_\alpha \lambda_\beta C(\mathbf{u}_\alpha, \mathbf{u}_\beta) \geq 0 \tag{2.20}$$

where λ_α and λ_β are any real numbers.

It follows from definition 2.7 that not just any function can be considered as the covariance function of a stationary random function.

Definition 2.8 When $C(0)$ does not exist, the semi-variogram function $\gamma(\mathbf{h}) = \gamma(\mathbf{u}_\alpha, \mathbf{u}_\beta)$ is *conditional positive definite* if,

$$\sum_{\alpha=1}^{n} \lambda_\alpha = 0$$

and

$$Var(Y) = -\sum_{\alpha=1}^{n}\sum_{\beta=1}^{n}\lambda_\alpha\lambda_\beta\gamma(\mathbf{u}_\alpha, \mathbf{u}_\beta) \geq 0 \qquad (2.21)$$

where λ_α and λ_β are any real numbers.

In some texts this condition on the semi-variogram is called *conditional negative definite* (Wackernagel 1995). In the rest of this chapter we will mainly refer to semi-variogram models and not covariance models because, as stated above, the semi-variogram model can always be derived from the covariance model but the converse is not always possible. The general form of the theoretical semi-variogram is $\gamma(0) = 0$ and $\gamma(\mathbf{h})$ increases as $|\mathbf{h}|$ increases. The semi-variogram is also an even function, that is

$$\gamma(\mathbf{h}) = \gamma(-\mathbf{h}). \qquad (2.22)$$

In the case where the covariance function exists, as $|\mathbf{h}|$ gets very large, $\gamma(\mathbf{h})$ reaches, or approaches asymptotically, a particular value and remains at this value for any larger values of $|\mathbf{h}|$. This value is known as the *sill* $(c_0 + c_1)$ where c_0 is the *nugget variance*, also known as the *nugget effect*, and c_1 is the *partial sill* (see figure 2.3). The existence of the sill indicates an absence of correlation between the two random variables $Z(\mathbf{u}_\alpha)$ and $Z(\mathbf{u}_\alpha+\mathbf{h})$ at large values of $|\mathbf{h}|$. Models with a sill are often called *bounded* models. The sill corresponds to the variance of the random function and is defined as

$$c_0 + c_1 = \gamma(\infty) = Var(Z(\mathbf{u})) = C(0) \qquad (2.23)$$

The other parameter in a semi-variogram model, where the covariance function exists, is the *range a* which is the value of $|\mathbf{h}|$ at which $\gamma(\mathbf{h})$ effectively reaches the sill. We say 'effectively reaches the sill' because with models where $\gamma(\mathbf{h})$ approaches the sill asymptotically the range is usually defined at the value of $|\mathbf{h}|$ at which $\gamma(\mathbf{h})$ is 95% of the sill and is referred to as the *practical range*. The range represents the distance beyond

which there is no spatial correlation. In cases where a sill exists the theoretical semi-variogram models are known as transition or bounded models and relate to random functions that are second order stationary and hence also intrinsic second order stationary. In the case where $\gamma(\mathbf{h})$ continues to increase as $|\mathbf{h}|$ increases with no apparent limit, the theoretical semi-variogram model is said to be unbounded and corresponds to a random function that can only be characterised as intrinsic second order stationary and not second order stationary.

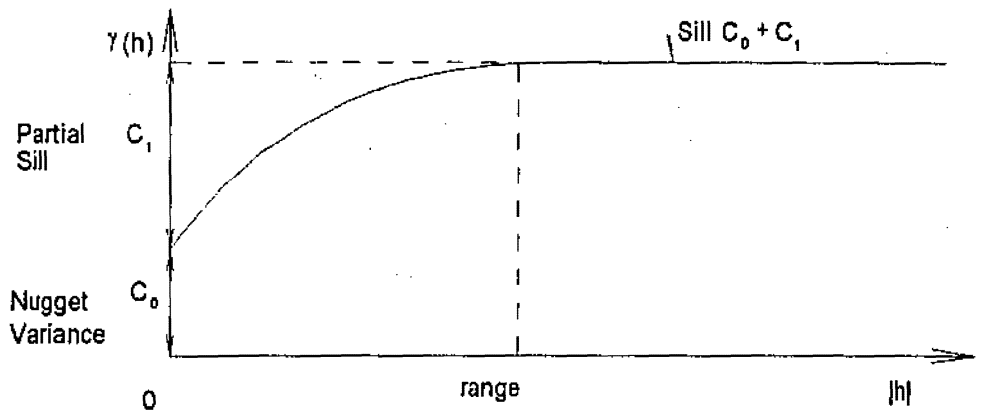

Figure. 2.3. Semi-variogram components.

Definition 2.9 The *experimental semi-variogram* (see figure 2.4) is defined from the sample data by

$$\gamma(\mathbf{h}) = \frac{1}{2N}\sum_{\alpha=1}^{N}(z(\mathbf{u}_\alpha) - z(\mathbf{u}_\alpha + \mathbf{h}))^2 \qquad (2.24)$$

where N is the number of sample pairs.

Equation 2.24 is known as the classical estimator of the semi-variogram. The sample pairs are defined by searching for all possible pairs within a stationary region that, when taken as a vector, match a particular distance and direction $\mathbf{h}$ within a given set of tolerances (see figure 2.5). There are a number of bounded models commonly used in practice, the choice of which depends on both the fitting of the data that form the experimental semi-variogram and a knowledge of the expected behaviour of the

phenomenon under investigation. The models most often used in ore body modelling are described below.

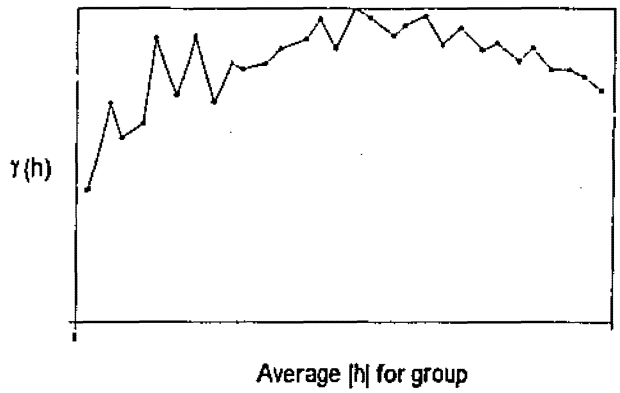

Figure. 2.4. One example of an experimental semi-variogram.

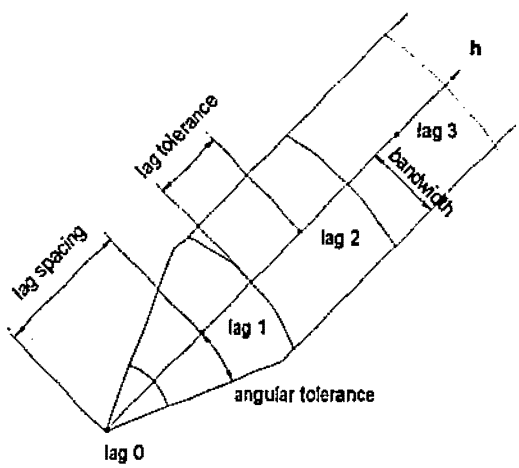

Figure 2.5. Pair selection tolerances (lag, angle and bandwidth) where each successive lag defines the pair separation distance |h|.

The *pure nugget effect model*, figure 2.6, is a special case which is a model with no spatial structure. It represents a complete absence of spatial correlation and therefore absence of structure and complete randomness of the random function. It can be considered to be made up of two separate but indistinguishable parts. The first, from which it gets its name, relates to gold mining where there is a tendency to find very high concentrations, or nuggets, amongst the more even general distribution of the gold within the geological formation. Therefore two sample values taken very close together, which would normally be expected to show almost identical values, may sometimes

show very different values. The second part of the pure nugget effect model relates to random errors in the sampling and measuring process itself. Although two samples taken very close together may actually have the same value, errors in the sampling and measuring process indicate that they do not. Another interpretation of the nugget efffect is that it represents variation at a scale smaller than that of the accuracy of the measurements. If we relate the pure nugget effect back to equation 2.16 we see that it corresponds to the parameter e which we defined as a residual error term with mean zero. The pure nugget effect shows up on the experimental semi-variogram as a discontinuity at the origin and is usually modelled as a constant term together with other semi-variogram models. The pure nugget model also corresponds to the variance of the random function.

Definition 2.10 The *pure nugget model* is defined by,

$$\gamma(\mathbf{h}) = \begin{cases} 0 & , \quad |\mathbf{h}|=0 \\ c_0 & , \quad \forall |\mathbf{h}|>0 \end{cases}. \tag{2.25}$$

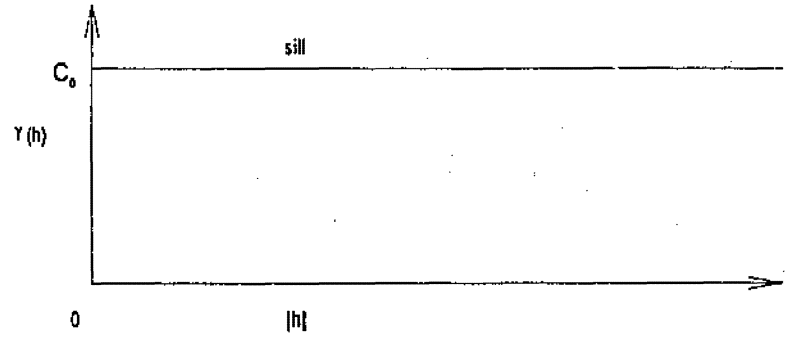

Figure 2.6. Pure nugget effect.

The following models do not contain terms for pure nugget effect. The term c_1 will denote the partial sill.

Definition 2.11 The *spherical model* is defined by,

$$\gamma(\mathbf{h}) = \left\{ \begin{array}{cc} c_1\left(\frac{3|\mathbf{h}|}{2a} - \frac{1}{2}\frac{|\mathbf{h}|^3}{a^3}\right), & 0 \le |\mathbf{h}| \le a \\ c_1, & |\mathbf{h}| > a \end{array} \right\}. \qquad (2.26)$$

In the case of the spherical model the parameter a is equal to the range. The spherical model, in association with nugget effect, is of the form that is most commonly encountered in geological situations. It is characterised by a steep linear behaviour near the origin then a gradual flattening to reach its sill at a finite distance which is the range a (see figure 2.7). It corresponds to random function with very irregular variation at small values of $|\mathbf{h}|$.

Definition 2.12 The *exponential model* is defined by,

$$\gamma(\mathbf{h}) = c_1\left(1 - \exp(-\frac{3|\mathbf{h}|}{a})\right). \qquad (2.27)$$

The exponential model also displays linear behaviour at the origin, is steeper than the spherical model and only approaches its sill asymptotically. The (practical) range a is reached at 95% of the partial sill. This form (Isaaks & Srivastava 1989, Deutsch & Journel 1992), although not the classical form, makes more sense when practically fitting an experimental semi-variogram. For the exponential model used in some texts (Journel & Huijbregts 1978, Wackernagel 1995) a is still called the range but is equal to a third of the practical range.

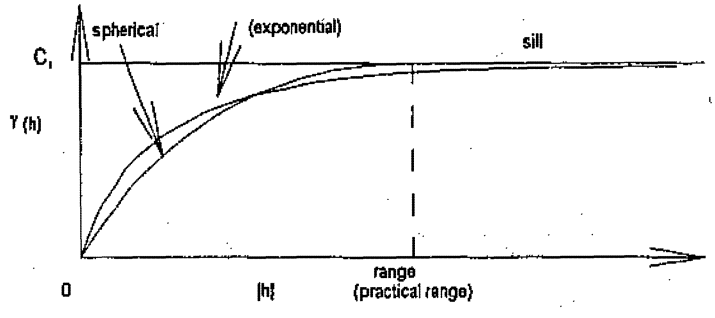

Figure. 2.7. Bounded semi-variogram models.

The *power model* is an *unbounded* model which, by definition, does not have a sill (see figure 2.8).

Definition 2.13 The *power model* is defined by,

$$\gamma(\mathbf{h}) = b|\mathbf{h}|^{\theta} \quad \text{where } 0 < \theta < 2 \tag{2.28}$$

and b is the slope of the line between the origin and $|h| = 1$.

The *linear model* is a special case of the power model where θ equals 1 and hence produces a straight line. It is defined by

$$\gamma(\mathbf{h}) = b|\mathbf{h}|. \tag{2.29}$$

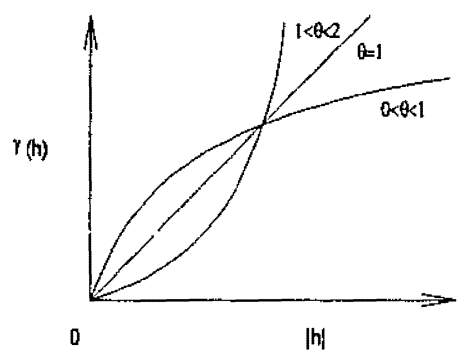

Figure. 2.8. Typical power semi-variogram models.

Nested models are models made up of linear combinations of variogram models, bounded or unbounded, and can be justified in practice by imagining different sets of physical causes operating at different scale ranges that combine to make up the entire phenomenon under investigation. For example different geological processes act at different scales; sedimentary processes act on fine particles in the order of millimetres and centimetres and volcanic processes act in the order of tens to hundreds of metres.

Formally, a nested semi-variogram is made up of $n+1$ elemental semi-variograms numbered with an index $u = 0, \ldots, n$ and is defined by

$$\gamma(\mathbf{h}) = \sum_{u=0}^{n} \gamma_u(\mathbf{h}). \tag{2.30}$$

Note that when a nested model is made up of bounded models and includes a pure nugget effect model the *sill* is made up of a summation of the nugget variance and the partial sills of the other models in the nest

$$sill = c_0 + \sum_{w=1}^{n} (c_1)_w. \tag{2.31}$$

where $(c_1)_w$ denotes the partial sill of the wth bounded model. Note also that if unbounded models are included in a nest a sill will not exist.

2.3 Anisotropy

So far we have been looking at situations where the spatial structure is the same in all directions in two or three dimensional space. This often does not occur in real data sets and we have to model separate semi-variograms for different directions of our translation vector **h**. We may find that the region under examination contains some sort of anisotropy. *Range anisotropy* exists when all the directional semi-variogram models for a particular set of data have the same type of model with the same sill but different ranges. *Geometric anisotropy* is a form of range anisotropy that is described by finding the directions of the axes of an ellipse, in two dimensions, or an ellipsoid in three dimensions. These directions are found with the use of an *iso-semi-variogram diagram*, (see figure 2.9). An iso-semi-variogram in two dimensions is a plot of the values of each directional semi-variogram function at selected values of **h** along each of their

respective directional vectors from the origin. The last value, if it exists, along the vector is the range in that direction.

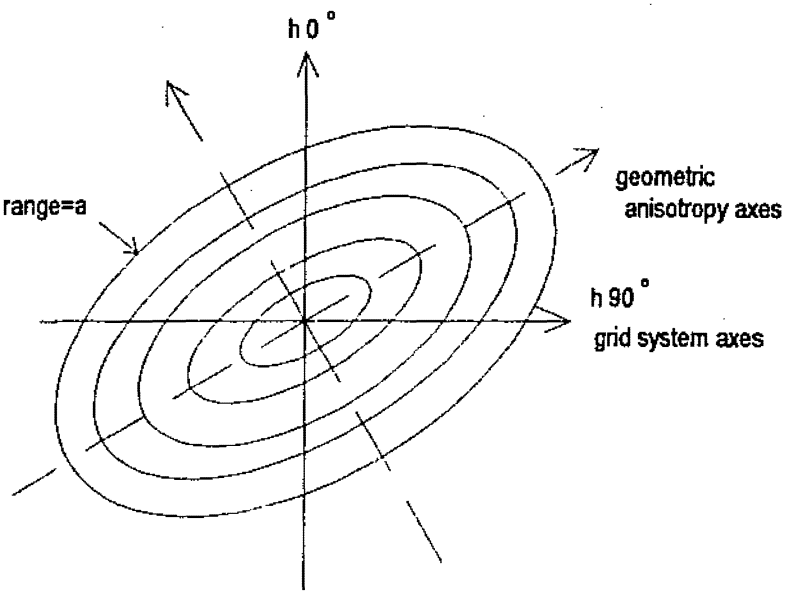

Figure. 2.9. Iso-semi-variogram diagram.

To handle two dimensional geometric anisotropy a rotation and dilation can be performed on the initial rectangular co-ordinates of the data locations. The rotation brings the co-ordinate system into line with the major axis of the ellipse of geometric anisotropy and the dilation then turns the ellipse into a circle with radius equal to the major semi-axis. The initial orientation of the co-ordinates is then restored by reversing the rotation. The transformation for each co-ordinate pair is as follows,

$$\begin{bmatrix} u'^{x}_{\alpha} \\ u'^{y}_{\alpha} \end{bmatrix} = \begin{bmatrix} \cos(-\varphi) & \sin(-\varphi) \\ -\sin(-\varphi) & \cos(-\varphi) \end{bmatrix} \begin{bmatrix} 1 & 0 \\ 0 & \tau \end{bmatrix} \begin{bmatrix} \cos\varphi & \sin\varphi \\ -\sin\varphi & \cos\varphi \end{bmatrix} \begin{bmatrix} u^{x}_{\alpha} \\ u^{y}_{\alpha} \end{bmatrix} \qquad (2.32)$$

where φ is the rotation angle from the grid axis to the major geometric anisotropy axis and $\tau = \frac{a_1}{a_2} < 1$ is the ratio of anisotropy derived from the ranges of the directional semi-variogram models aligned with the major and minor axes of anisotropy. In matrix form this is written as,

$$\mathbf{u}' = \mathbf{R}_{-\varphi} \Upsilon \mathbf{R}_{\varphi} \mathbf{u} = \mathbf{A}\,\mathbf{u}\,. \qquad (2.33)$$

where the prime denotes a transform. To obtain an isotropic semi-variogram model we can now take the matrix **A** and multiply it by any two dimensional separation vector **h** such that, $\mathbf{h}' = \mathbf{Ah}$ and therefore,

$$\gamma_{anisotropic}(\mathbf{h}) = \gamma'_{isotropic}(\mathbf{h}'). \qquad (2.34)$$

This is then used with the original untransformed data. Three dimensional anisotropy in practice is almost never geometric, however the theoretical procedure for dealing with it is similar to the two dimensional case. It is more usual to deal with three dimensional anisotropy as a mixture of geometric anisotropy and *zonal anisotropy*. We define zonal anisotropy as the case where the sill changes with direction and the range remains the same for all directional component semi-variograms. Zonal anisotropy is modelled as if the phenomenon under investigation was made up of a number of separate structures. A single semi-variogram model for zonal anisotropy can be considered as being a nested semi-variogram model with a sill value equal to the sum of the individual component models' partial sill values. Each directional component is modelled as for geometric anisotropy but with infinite ranges in the directions perpendicular to the component. This sets the anisotropy ratio to 0 in the perpendicular directions and eliminates their influence. For the two dimensional example

$$\tau = \lim_{a_1 \to \infty} \frac{a_2}{a_1} = 0.$$

The appropriate transformation

$$\mathbf{h}' = \mathbf{Ah} \text{ where } \mathbf{A} = \mathbf{R}_{-\varphi} \begin{bmatrix} 1 & 0 \\ 0 & 0 \end{bmatrix} \mathbf{R}_{\varphi} \qquad (2.35)$$

is applied to each component which can then be treated as a set of nested models and summed to give a final isotropic model.

$$\gamma(\mathbf{h}) = \sum_{n=0}^{w} \gamma_n(\mathbf{h}'_n) \qquad (2.36)$$

Here w is the number of reduced component directional models and n is the associated index. A general structural isotropic model that is a combination of geometric and zonal anisotropy is obtained in a similar way by nesting reduced geometric and zonal component models.

2.4 Change of Support

So far we have been looking at theoretical models that treat the individual regionalised values $z(\mathbf{u}_\alpha)$ as point data with no dimension and no size. This is not the case in practice. In most cases and particularly in mining applications we are in fact dealing with an amount of material of some volume v from which the regionalised value $z_v(\mathbf{u}_\alpha)$ is derived. This volume is known as the point support $v(\mathbf{u}_\alpha)$. In general, random variable populations derived from small supports have a higher variance than random variable populations derived from larger supports over the same region but still maintain the same mean. If corrections for support are not applied to the semi-variogram and covariance functions they do not correctly represent any random function defined on anything other than point support. The process of attributing a value over a region of space, by considering a set of averaged point values, to a single point value is known as *regularisation*. The mean value $z_v(\mathbf{u}_\alpha)$ is said to be the regularisation of a point variable $z(\mathbf{u}_\alpha)$ over the volume $v(\mathbf{u}_\alpha)$ and is expressed as the integral

$$z_v(\mathbf{u}_\alpha) = \frac{1}{v}\int_{v(\mathbf{u}_\alpha)} z(\mathbf{u}_\alpha)\, d\mathbf{u}_\alpha \qquad (2.37)$$

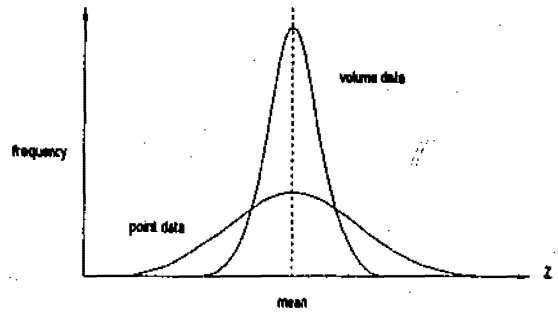

Figure. 2.10. Point and volume data histograms.

The change of support has two opposite effects that need to be considered. The first occurs when volume data is to be treated as a point value and the second is when point values are used to represent volumes. In the first case, if the 'size' of the volume is small in relation to the average distance between samples then the values may be considered as quasi-point data and do not require any correction. This is what we will assume for all examples and the case study in chapter five. We will not encounter the second case in our examples and case study and will not go into any great detail here except to mention one simple correction method. If we already have some measure of the difference in variance between two distributions defined on different supports and we know their mean we can use an *affine correction* to transform the values of one to the other.

$$z' = \sqrt{f}(z-m)+m \tag{2.38}$$

where f is the ratio of the variances

$$\sigma^2(V|R)/\sigma^2(v|R), \tag{2.39}$$

V is the larger support and v is the smaller support. This, in effect, compresses the distribution reducing its variance but leaves the mean unchanged (see figure 5.1). For more detailed theory on support correction see Journel & Huijbregts (1978)

2.5 Kriging

Simple kriging is a minimum error variance estimation algorithm based on linear regression and is the basis for all other types of kriging. It requires knowledge of the means of the random variables under consideration and in its non-stationary form is expressed as

$$Z^*_{SK}(\mathbf{u}_i) - m(\mathbf{u}_i) = \sum_{\alpha=1}^{n} \lambda_\alpha (Z(\mathbf{u}_\alpha) - m(\mathbf{u}_\alpha)) \tag{2.40}$$

where $\mathbf{u}_i$ is the location of the random variable to be estimated, $Z^*_{SK}(\mathbf{u}_i)$ is the simple kriging estimate and $\lambda_\alpha \quad \alpha = 1, \ldots, n$ is the set of kriging weights. In its stationary form, with a constant mean m it reduces to

$$Z^*_{SK}(\mathbf{u}_i) = \sum_{\alpha=1}^{n} \lambda_\alpha Z(\mathbf{u}_\alpha) + (1 - \sum_{\alpha=1}^{n} \lambda_\alpha)\, m. \tag{2.41}$$

The simple kriging weights for equation 2.41 are given by

$$\sum_{\beta=1}^{n} \lambda_\beta C(\mathbf{u}_\alpha, \mathbf{u}_\beta) = C(\mathbf{u}_\alpha, \mathbf{u}_i) \quad \alpha = 1, \ldots, n \tag{2.42}$$

The simple kriging estimation error variance is given by,

$$\sigma^2_{SK} = C(0) - \sum_{\alpha=1}^{n} \lambda_\alpha C(\mathbf{u}_\alpha, \mathbf{u}_i). \tag{2.43}$$

Ordinary kriging is a linear system of equations that eliminates the need to know the means of the random variables. The ordinary kriging estimator $Z^*_{OK}(\mathbf{u}_i)$ is a linear combination of n weighted surrounding random variables,

$$Z^*_{OK}(\mathbf{u}_i) = \sum_{\alpha=1}^{n} \lambda_\alpha Z(\mathbf{u}_\alpha) \tag{2.44}$$

where $\lambda_\alpha \quad \alpha = 1, \ldots, n$ is a set of weights whose sum is equal to one and whose ordinary kriging estimation variance $\sigma^2_{OK}(\mathbf{u}_i)$ is a minimum. Ordinary kriging is an *unbiased* estimator meaning that the average estimation error is zero as shown by equations 2.45 to 2.47. With the condition

$$\sum_{\alpha=1}^{n} \lambda_\alpha = 1 \tag{2.45}$$

we have

$$E[Z^*_{OK}(\mathbf{u}_i)] = \sum_{\alpha=1}^{n} \lambda_\alpha E[Z(\mathbf{u}_\alpha)] = m \sum_{\alpha=1}^{n} \lambda_\alpha = m = E[Z(\mathbf{u}_i)] \tag{2.46}$$

and hence

$$E[Z(\mathbf{u}_i) - Z^*_{OK}(\mathbf{u}_i)] = 0. \tag{2.47}$$

The estimation error variance for ordinary kriging is,

$$\sigma^2_{OK}(\mathbf{u}_i) = E[(Z(\mathbf{u}_i) - Z^*_{OK}(\mathbf{u}_i))^2]. \tag{2.48}$$

The estimation error variance can be expanded (for full details see Journel & Huijbregts 1978) to

$$\sigma^2_{OK}(\mathbf{u}_i) = C(\mathbf{u}_\alpha, \mathbf{u}_\alpha) - 2\sum_{\alpha=1}^{n} \lambda_\alpha C(\mathbf{u}_\alpha, \mathbf{u}_i) + \sum_{\alpha=1}^{n}\sum_{\beta=1}^{n} \lambda_\beta \lambda_\alpha C(\mathbf{u}_\alpha, \mathbf{u}_\beta). \tag{2.49}$$

The equations are now in a quadratic form in λ_α and λ_β and $\sigma^2_{OK}(\mathbf{u}_i)$ can be minimised using the method of Lagrange multipliers by setting each of the n partial derivatives to zero

$$\frac{\partial(\sigma^2_{OK} + 2\mu \sum_{\alpha=1}^{n} \lambda_\alpha)}{\partial \lambda_\alpha} = 0 \tag{2.50}$$

where μ is the Lagrange parameter and where the condition $\sum_{\alpha=1}^{n} \lambda_\alpha = 1$ is met. This then provides a system of $n + 1$ equations with $n + 1$ unknowns, which are the n weights λ_α and the Lagrange parameter μ. This system of equations is called the *ordinary kriging system* and is written,

$$\left\{ \begin{array}{l} \sum_{\beta=1}^{n} \lambda_\beta C(\mathbf{u}_\alpha, \mathbf{u}_\beta) + \mu = C(\mathbf{u}_\alpha, \mathbf{u}_i), \qquad \forall \alpha = 1, \ldots, n \\ \sum_{\beta=1}^{n} \lambda_\beta = 1 \end{array} \right\} \tag{2.51}$$

with the minimised estimation variance or *kriging variance* written as

$$\sigma^2_{OK}(\mathbf{u}_i) = C(\mathbf{u}_\alpha, \mathbf{u}_\alpha) - \mu - \sum_{\alpha=1}^{n} \lambda_\alpha C(\mathbf{u}_\alpha, \mathbf{u}_i). \tag{2.52}$$

We mentioned in section 2.2 that in practice most structural modelling is done using the semi-variogram. However the ordinary kriging equations written in terms of the covariance function are more efficient to program on a computer. In practice the final ordinary kriging equations are usually converted from semi-variogram terms in which the structure was modelled to covariance function terms as follows. When the covariance function exists, the relationship between the semi-variogram function and the covariance function is as in equation 2.18, namely $\gamma(\mathbf{h}) = C(0) - C(\mathbf{h})$. When only the semi-variogram exists it is possible to define the *pseudo-covariance function* $C(\mathbf{h})$ such that $\gamma(\mathbf{h}) = A - C(\mathbf{h})$ where A is a constant greater than the greatest $\gamma(\mathbf{h})$ used in the kriging system. This constant A is then eliminated in the equation reduction process. The kriging systems can be expressed in matrix form as follows

$$\mathbf{C}_{\alpha\beta}\,\lambda = \mathbf{C}_{\alpha i} \tag{2.53}$$

where $\mathbf{C}_{\alpha\beta}$ is the matrix of variances and covariances which includes the Lagrange parameter terms and is obtained from our nested semi-variogram model equation, λ is the column matrix of unknown weights, and $\mathbf{C}_{\alpha i}$ is the column matrix of covariances with the estimation location which we also know from our nested semi-variogram model equation. Using the covariance function the unknown weights then become

$$\lambda = \mathbf{C}_{\alpha\beta}^{-1}\,\mathbf{C}_{\alpha i} \tag{2.54}$$

and the ordinary kriging variance becomes

$$\sigma_{OK}^2(\mathbf{u}_i) = C(0) - \lambda^T\mathbf{C}_{\alpha i} \tag{2.55}$$

where σ^2 is the variance of the random function under consideration. The general structure of the matrices is as follows.

$$\mathbf{C}_{\alpha\beta} = \begin{bmatrix} C(\mathbf{u}_1, \mathbf{u}_1) & \cdots & C(\mathbf{u}_1, \mathbf{u}_\beta) & \cdots & C(\mathbf{u}_1, \mathbf{u}_n) & 1 \\ \vdots & & \vdots & & \vdots & \vdots \\ C(\mathbf{u}_\beta, \mathbf{u}_1) & \cdots & C(\mathbf{u}_\beta, \mathbf{u}_\beta) & \cdots & C(\mathbf{u}_\beta, \mathbf{u}_n) & 1 \\ \vdots & & \vdots & & \vdots & \vdots \\ C(\mathbf{u}_n, \mathbf{u}_1) & \cdots & C(\mathbf{u}_n, \mathbf{u}_\beta) & \cdots & C(\mathbf{u}_n, \mathbf{u}_n) & 1 \\ 1 & \cdots & 1 & \cdots & 1 & 0 \end{bmatrix}$$

Note that the main diagonal contains the variance σ^2 and that the matrix is symmetric since $C(\mathbf{u}_\alpha, \mathbf{u}_\beta) = C(\mathbf{u}_\beta, \mathbf{u}_\alpha)$.

$$\lambda = \begin{bmatrix} \lambda_1 \\ \vdots \\ \lambda_\alpha \\ \vdots \\ \lambda_n \\ \mu \end{bmatrix}, \qquad \mathbf{C}_{\alpha i} = \begin{bmatrix} C(\mathbf{u}_\alpha, \mathbf{u}_i) \\ \vdots \\ C(\mathbf{u}_\alpha, \mathbf{u}_i) \\ \vdots \\ C(\mathbf{u}_\alpha, \mathbf{u}_i) \\ 1 \end{bmatrix}$$

Referring back to equation 2.44, we do not need to know the mean m of the random function $Z(\mathbf{u})$ to carry out ordinary kriging. It is enough to know that the random function is second order stationary or intrinsic stationary and has a constant mean. The final nested theoretical model that is fitted to the experimental semi-variogram is actually composed of $Y(\mathbf{u})$ and e, where e includes the nugget effect, and this combination of $Y(\mathbf{u})$ and e is what is used to find the values for matrices $\mathbf{C}_{\alpha\beta}$ and $\mathbf{C}_{\alpha i}$ in the kriging system equations. Note that ordinary kriging can be used as a moving neighbourhood estimation method with a random function whose mean is globally non-stationary but has a stationary covariance (Brownian motion behaves this way) if the local mean within each neighbourhood can be considered constant. This is because ordinary kriging re-calculates the mean at each new location to be estimated.

In the geostatistical literature there are now many variations on the kriging system which we will not be using and which are too detailed to be discussed at this point. Some of there are: block kriging (Goovaerts 1997), indicator kriging (Deutsch & Journel 1996), cokriging (Deutsch & Journel 1996), dual kriging (Galli et. al. 1984), disjunctive kriging (Rivoirard 1990), factorial kriging and co-kriging (Goovaerts 1997), rank order kriging (Journel & Deutsch 1996), median indicator kriging, (Gomez-Hernandez & Srivastava 1990) and constrained kriging (Cressie 1993).

2.6 Examples-Ordinary Kriging Estimation

For all the examples here and in chapters three and four we will use two data sets for which we know the complete spatial distributions. These are the *True* data set and the *Berea* data set. We will use subsets of these data sets to mimic experimentally sampled data for input into estimation and simulation procedures. We will use the *True* data to show detailed examples and the *Berea* data to show only the handling of anisotropy, throughout chapters two, three and four.

The *True* data comes with the GSLIB software (Journel & Deutsch 1992). It is a two dimensional set of 2500 points which was created by simulated annealing (Chu 1996, Gomez-Hernandez & Srivastiva 1990) where the first lag of a low nugget isotropic semi-variogram was matched. The sample data subset, which we will call *Gslib97*, is also provided with GSLIB and consists of 97 non-clustered points that were sampled from the *True* data on a pseudo regular grid. The *True* data set has some of the characteristics of a gold bearing ore body with a similar range of values and a highly skewed distribution but it should be emphasised that it is itself a simulation and not an

actual gold mineralisation data set. It is used here because both sample and complete populations are available thus enabling us to compare the estimations and simulations to reality and because it has been used in other fractal simulation studies. Costa & Dimitrakopoulos (1997) used another subset of the *True* data for fractal simulation which, in addition to the 97 values in *Gslib97,* also contained additional data clustered around the higher values making a total of 140 points. We will not use the clustered data as we do not want to introduce the complications involved in determining declustering weights. Figures 2.11 and 2.12 and table 2.1 give details of the *Gslib97* data.

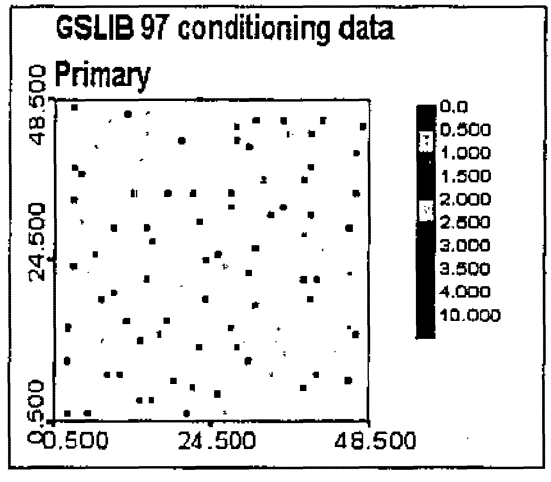

Figure 2.11. *Gslib97* data set plot.

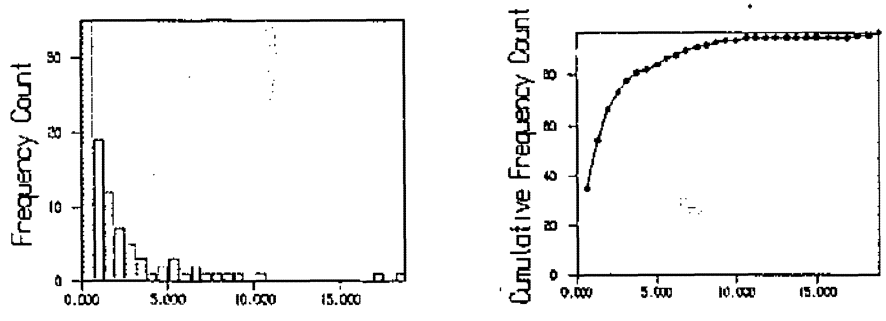

Figure 2.12. *Gslib97* data histogram and cumulative frequency plot.

Histogram Statistics		
Description = GSLIB 97 sample data		
Tot. Population= 97	No. of Samples <= 0	= 0
Minimum Cutoff = 0.05990	Minimum Histogram Value	= 0.05990
Maximum Cutoff = 18.76010	Maximum Histogram Value	= 18.76010
No. of Samples Used = 97		
	Ungrouped Data	Data Grouped to Class Intervals
Mean	2.21113	2.26073
Median	N/A	1.12607
Geometric Mean	0.98063	1.19510
Natural LOG Mean	-0.01956	0.17823
Standard Deviation	3.17454	3.13694
Variance	10.07772	9.84037
Log Variance	1.83468	1.17580
Coefficient of Variation	1.43571	1.38758
Moment 1 about Arithmetic Mean	0.00000	0.00000
Moment 2 about Arithmetic Mean	10.07772	9.84037
Moment 3 about Arithmetic Mean	96.46899	93.09951
Moment 4 about Arithmetic Mean	1411.893	1337.798
Moment Coefficient of Skewness	3.01540	3.01599
Moment Coefficient of Kurtosis	13.90200	13.81555

Table 2.1. *Gslib97* data set summary statistics.

The *Berea* data is a real two dimensional data set consisting of 1600 points derived from air permeability measurements taken on a slab of Berea sandstone (Giordano et. al. 1985). It is used because of its distinctive anisotropic properties, because it has a close to normal distribution and because it has been used in other geostatistical and fractal simulation studies (Journel & Alabert 1989, Chu & Journel 1994). Chu & Journel used a random sample of 64 points from the *Berea* data and we will do the same. However we do not know the random selection details which they used and our randomly selected points will not necessarily be the same as theirs. Our sample data set will be called *Berea64*.

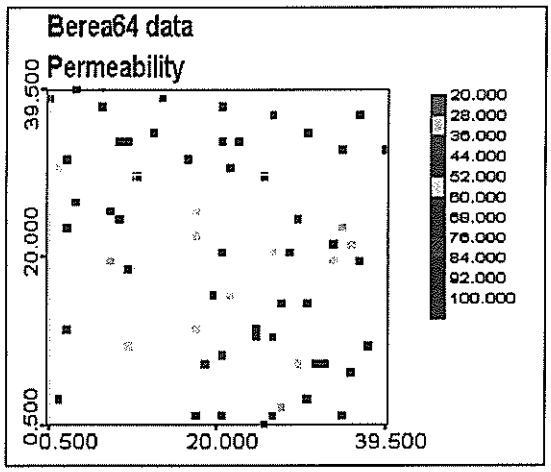

Figure 2.13. *Berea64* data plot.

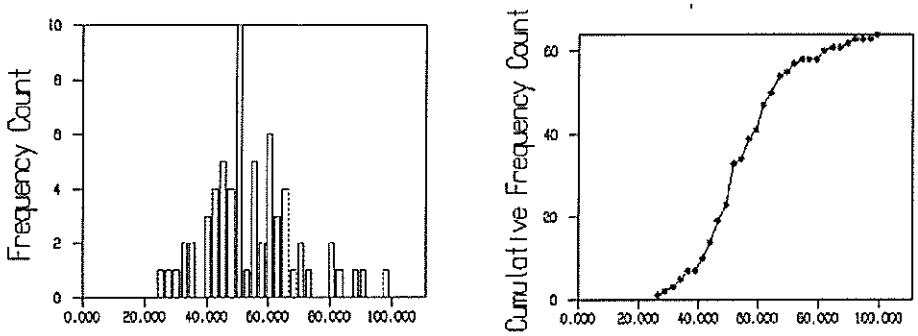

Figure 2.14. *Berea64* data histogram and cumulative frequency plot.

Histogram Statistics		
Description = Berea64 data		
Tot. Population= 64	No. of Samples <= 0	= 0
Minimum Cutoff = 24.00000	Minimum Histogram Value	= 24.00000
Maximum Cutoff = 99.50010	Maximum Histogram Value	= 99.50010
No. of Samples Used = 64		
	Ungrouped Data	Data Grouped to Class Intervals
Mean	54.51563	54.67228
Median	N/A	51.43203
Geometric Mean	52.52312	52.67184
Natural LOG Mean	3.96125	3.96408
Standard Deviation	14.89310	14.92800
Variance	221.804	222.845
Log Variance	0.07607	0.07607
Coefficient of Variation	0.27319	0.27305
Moment 1 about Arithmetic Mean	0.00000	0.00000
Moment 2 about Arithmetic Mean	221.804	222.845
Moment 3 about Arithmetic Mean	2215.056	2088.908
Moment 4 about Arithmetic Mean	180891.3	173084.8
Moment Coefficient of Skewness	0.67055	0.62794
Moment Coefficient of Kurtosis	3.67686	3.48540

Table 2.2. *Berea64* data set statistics.

The first task in any geostatistical modelling process is that of exploratory data analysis. This involves becoming familiar with the data and looking for any characteristics that need to be taken into account during the modelling process such as irregularities in the sampling pattern, outliers, skewed distributions and clustering. Exploratory data analysis is a large topic in itself and will not be covered here except to show what was done in each case. See Cressie (1991), Isaaks & Srivastava (1989) and Tukey (1977) for more detail. It should be remembered that in practice the complete spatial distribution is never known and inferences are made from the experimentally sampled data.

From figures 2.11 and 2.13 it can be seen that, for both *Gslib97* and *Berea64* the sample point locations are irregularly spaced but are reasonably well spread over the region and do not show any significant clustering. Looking at the histograms in figures 2.12 and 2.14 and the summary statistics in tables 2.1 and 2.2 the main feature to note is that *Gslib97* is a highly skewed distribution and that *Berea64* is near normal. This will become important when simulating in chapter three but will simply be noted here. Neither of the histograms or data plots shows any values that could be considered as outliers. From all these observations we conclude that the sample data sets can be used for estimation without alteration.

The next step in preparation for ordinary kriging estimation is that of modelling the spatial structure or variography. Any anisotropy that may be present must first be determined. This is done via an iso-semi-variogram diagram and/or via a series of directional semi-variograms. Once the anisotropy is determined then a semi-variogram

model or nested semi-variogram model must be fitted to the experimental semi-variogram. We will examine the *Gslib97* data first.

The iso-semi-variogram (see section 2.3), shown in figure 2.15, and directional semi-variograms, shown in figure 2.16, were all calculated using a lag spacing of 3 units, an angular tolerance of 20^0 and no limit on the horizontal tolerance. The iso-semi-variogram does not show any anisotropy and the directional semi-variograms all have a similar range. Note that directions are specified with 0^0 equal to north, which is also the y axis direction and directions are measured clockwise from 0^0. Direction in this sense is often called *azimuth* in mining terminology. As there is no anisotropy present we will fit the model to an omni-directional experimental semi-variogram which is calculated from all possible pairs of values in all directions at all lags from zero to twenty four at a lag spacing of three units.

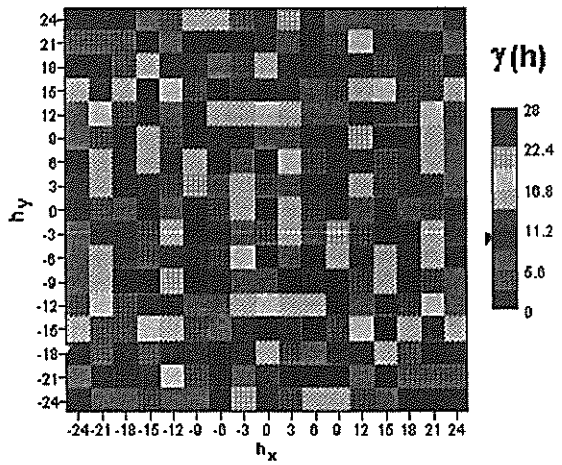

Figure 2.15. Iso-semi-variogram diagram for *Gslib97*. Lag spacing 3.0 units.

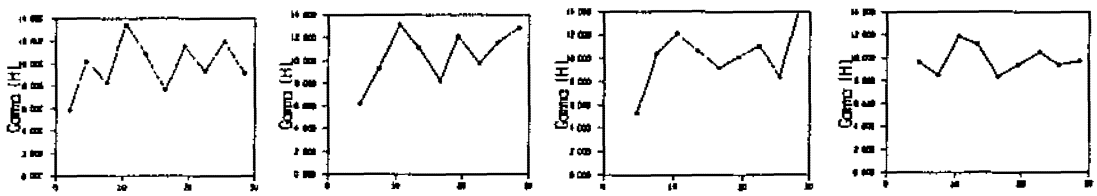

Figure 2.16. Four directional experimental semi-variograms, from left to right, $0^0, 45^0, 90^0$ and 135^0 from *Gslib97*.

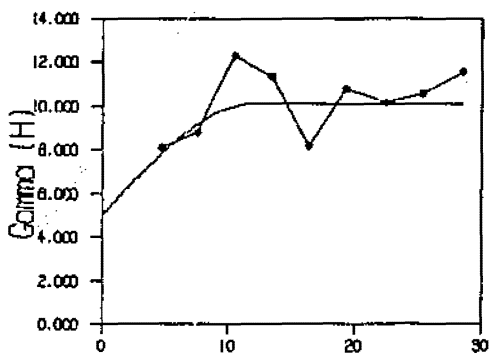

Figure 2.17. Omni directional semi-variogram from *Gslib97* and fitted nested model. Nugget model of 5.0 plus spherical model with range of 12 and partial sill of 5.1.

The fitted model is a nested nugget and spherical model expressed as,

$$\gamma(\mathbf{h}) = \left\{ \begin{array}{c} 5.0 + 5.1\left(\frac{3|\mathbf{h}|}{24} - \frac{|\mathbf{h}|^3}{3456}\right), \quad 0 \le |\mathbf{h}| \le 12 \\ 10.1, \quad |\mathbf{h}| > 12 \end{array} \right\}$$

which is equal to a covariance model of,

$$C(\mathbf{h}) = \left\{ \begin{array}{c} 10.1 - (5.0 + 5.1\left(\frac{3|\mathbf{h}|}{24} - \frac{|\mathbf{h}|^3}{3456}\right)), \quad 0 \le |\mathbf{h}| \le 12 \\ 0, \quad |\mathbf{h}| > 12 \end{array} \right\}.$$

This covariance equation is used to obtain the kriging matrices in the following example calculation using the sixteen surrounding values as shown in figure 2.18. The ordinary kriging geometry, matrices, weights and estimate calculation for the location (20.5 x 25.5 y) are given.

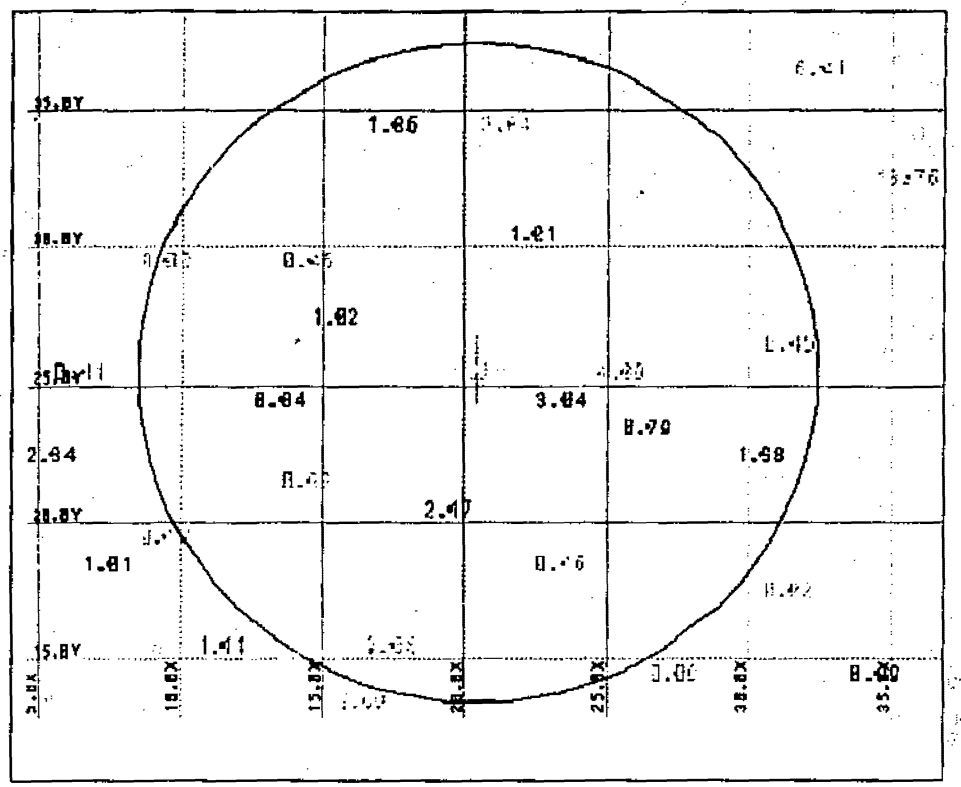

Figure 2.18. Search radius of 12 units and point values for estimation at (20.5 x 25.5 y).

The full matrix is a 17 by 17 symmetric matrix of all the possible covariance combinations from the sixteen closest surrounding data. However not all values are shown due to lack of space. The first and last four rows of lower half of the covariance matrix together with the coefficients of one used with the Lagrange parameter are

$$C_{\alpha\beta} = \begin{bmatrix} 10.1 & & & & & & & & & \\ 3.6910 & 10.1 & & & & & & & & \\ 1.7609 & 0.8240 & 10.1 & & & & & & & \\ 0.5736 & 0.1639 & 0.7336 & 10.1 & & & & & & \\ \vdots & \vdots & \vdots & \vdots & \ddots & & & & & \\ 0.4539 & 1.0283 & 0 & 0 & 1.8974 & \ddots & & & & \\ 1.0283 & 1.6753 & 0.0349 & 0 & 0.0245 & \cdots & 10.1 & & & \\ 0.0719 & 0 & 1.8974 & 0 & 0 & \cdots & 0 & 10.0 & & \\ 0.6705 & 1.5544 & 0 & 0 & 0.2311 & \cdots & 2.575 & 0 & 10.1 & \\ 1 & 1 & 1 & 1 & 1 & \cdots & 1 & 1 & 1 & 0 \end{bmatrix}$$

The first and last four rows of the covariance matrix of the sample locations with the estimate location together with the Lagrange parameter in the last row are

$$\mathbf{C}_{\alpha\beta} = \begin{bmatrix} 3.1307 \\ 2.0970 \\ 2.0450 \\ 1.8974 \\ \vdots \\ 0.2207 \\ 0.1236 \\ 0.1236 \\ 0.0471 \\ -0.0030 \end{bmatrix}.$$

The co-ordinates, regionalised value and kriging weight for each of the closest surrounding sample points in increasing order of distance |h| is shown below.

u_α^x	u_α^y	$z(u_\alpha)$	λ_α
23.5	24.5	3.04	0.229
25.5	25.5	4.89	0.101
19.5	20.5	2.17	0.144
15.5	27.5	1.02	0.136
22.5	30.5	1.21	0.138
26.5	23.5	0.79	0.040
13.5	24.5	0.84	0.053
14.5	21.5	0.33	0.056
14.5	29.5	1.46	0.051
23.5	18.5	0.16	0.031
21.5	34.5	2.84	0.019
17.5	34.5	1.36	0.014
27.5	32.5	1.71	0.001
30.5	22.5	1.38	-0.010
17.5	15.5	9.08	0.001
31.5	26.5	0.45	-0.004

The ordinary kriging estimate is given by,

$$z^*(\mathbf{u}_i) = \sum_{\alpha=1}^{16} \lambda_\alpha \, z(\mathbf{u}_\alpha)$$

$$= 2.00.$$

The kriging estimation variance is then,

$$\sigma_E^2(\mathbf{u}_i) = C(0) - \sum_{\alpha=1}^{16} \lambda_\alpha \, C(\mathbf{u}_\alpha, \mathbf{u}_i)$$

$$8.39 = 10.10 - 1.71.$$

The point ordinary kriging estimates and estimation variances for a 1 x 1 unit grid are shown in figures 2.19 and 2.20. The actual *True* data set values are shown in figure 2.21. Note the smoothing effect that is produced by kriging in comparison to the *True* data plot. Looking at the kriging estimation variances plot it can be seen that the variances at the sample point locations are zero (light blue) and that the estimated locations with fewer surrounding sample locations have the highest variance. The histogram and summary statistics for the full *True* data set are shown in figure 2.22 and table 2 3 for reference.

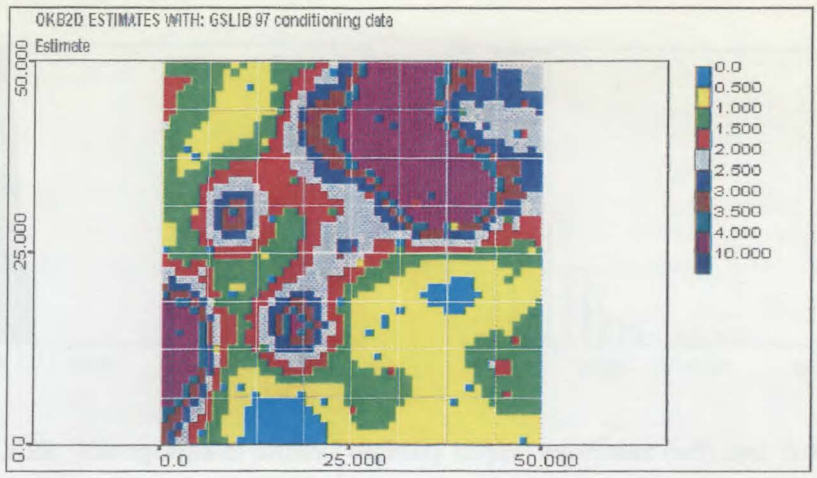

Figure 2.19. Plot of ordinary kriging estimates from *Gslib97*.

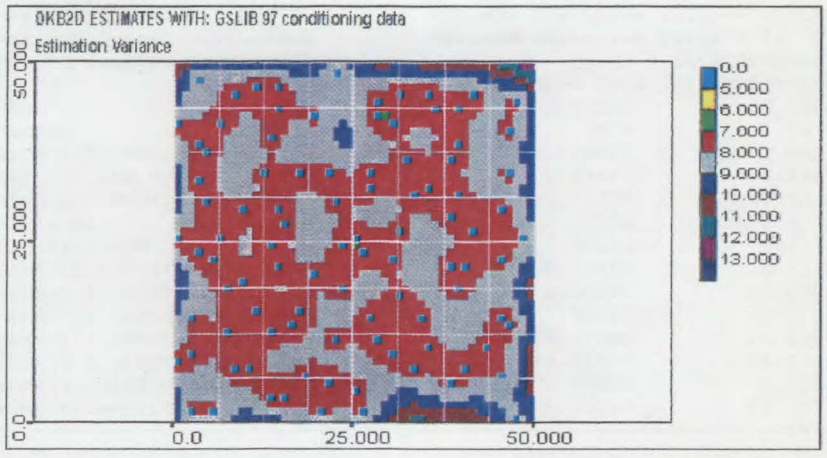

Figure 2.20. Plot of ordinary kriging estimation variances from *Gslib97*.

Figure 2.21. *True* data plot.

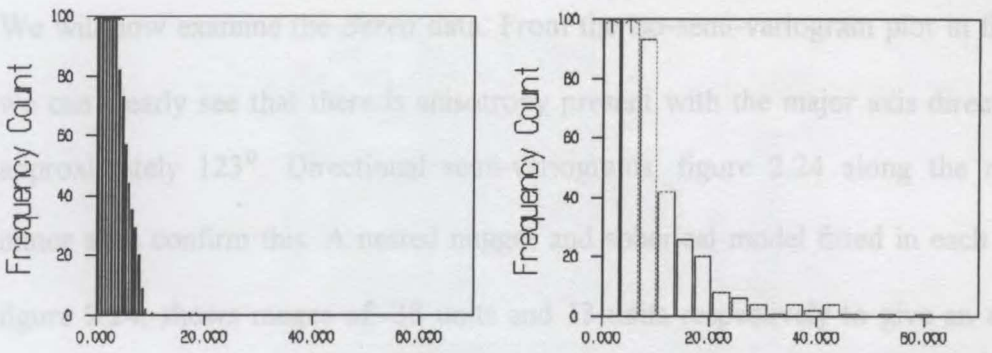

Figure 2.22. Histograms of *Clust97* ordinary kriging estimates (left) and *True* data (right).

Histogram Statistics		
Description = OK Clust97		
Tot. Population= 2500	No. of Samples <= 0	= 0
Minimum Cutoff = 0.05990	Minimum Histogram Value	= 0.05990
Maximum Cutoff = 18.76010	Maximum Histogram Value	= 18.76010
No. of Samples Used = 2500		Data Grouped to
	Ungrouped Data	Class Intervals
Mean	2.16407	2.16815
Median	N/A	1.64466
Geometric Mean	1.64669	1.64247
Natural LOG Mean	0.49877	0.49620
Standard Deviation	1.72234	1.72353
Variance	2.96645	2.97056
Log Variance	0.56533	0.57707
Coefficient of Variation	0.79588	0.79493
Moment 1 about Arithmetic Mean	0.00000	0.00000
Moment 2 about Arithmetic Mean	2.96645	2.97056
Moment 3 about Arithmetic Mean	10.32363	10.17608
Moment 4 about Arithmetic Mean	90.96906	88.83489
Moment Coefficient of Skewness	2.02058	1.98757
Moment Coefficient of Kurtosis	10.33757	10.06716

Histogram Statistics		
Description = True data		
Tot. Population= 2500	No. of Samples <= 0	= 0
Minimum Cutoff = 0.00990	Minimum Histogram Value	= 0.00990
Maximum Cutoff = 102.700	Maximum Histogram Value	= 102.700
No. of Samples Used = 2500		Data Grouped to
	Ungrouped Data	Class Intervals
Mean	2.58020	3.23300
Median	N/A	2.13546
Geometric Mean	0.95538	2.30609
Natural LOG Mean	-0.04564	0.83555
Standard Deviation	5.15090	4.89500
Variance	26.53180	23.96100
Log Variance	2.08155	0.41483
Coefficient of Variation	1.99632	1.51407
Moment 1 about Arithmetic Mean	0.00000	0.00000
Moment 2 about Arithmetic Mean	26.53180	23.96100
Moment 3 about Arithmetic Mean	933.611	871.730
Moment 4 about Arithmetic Mean	59434.937	54485.846
Moment Coefficient of Skewness	6.83150	7.43232
Moment Coefficient of Kurtosis	84.43227	94.90169

Table 2.3. *Clust97* ordinary kriged estimate statistics and *True* data set statistics.

We will now examine the *Berea* data. From the iso-semi-variogram plot in figure 2.23 we can clearly see that there is anisotropy present with the major axis direction being approximately 123^0. Directional semi-variograms, figure 2.24 along the major and minor axes confirm this. A nested nugget and spherical model fitted in each direction, figure 2.24, shows ranges of 38 units and 13 units respectively to give an anisotropy ratio of 0.34. Note that the fitted model at 123^0 does not reach its sill within the limits of the experimental semi-variogram and for the purpose of this model is effectivly unbounded. This is perfectly acceptable as the model does reach a sill at a range that is beyond our area of interest (at 38 units). We have not extended the experimental semi-variogram further as, in general, semi-variograms are not reliable at distances greater than half the width of the region of interest (Isaaks & Srivastava 1989). In this case the width at 123^0 is 48 units so the experimental semi-variogram is valid to approximately 24 units. The anisotropic nested model semi-variogram is

$$\gamma(\mathbf{h}) = \left\{ \begin{array}{c} 15 + 206.8\left(\frac{3|\mathbf{h}'|}{76} - \frac{|\mathbf{h}'|^3}{438976}\right), \quad 0 \le |\mathbf{h}'| \le 38 \\ 221.8, \quad |\mathbf{h}'| > 38 \end{array} \right\}$$

where

$$\mathbf{h}' = \begin{bmatrix} \cos(-123^0) & \sin(-123^0) \\ -\sin(-123^0) & \cos(-123^0) \end{bmatrix} \begin{bmatrix} 1 & 0 \\ 0 & \frac{13}{38} \end{bmatrix} \begin{bmatrix} \cos 123^0 & \sin 123^0 \\ -\sin 123^0 & \cos 123^0 \end{bmatrix} \mathbf{h}$$

The equivalent covariance model used for the kriging matrices is,

$$C(\mathbf{h}) = \left\{ \begin{array}{c} 221.8 - \left(15 + 206.8\left(\frac{3|\mathbf{h}'|}{76} - \frac{|\mathbf{h}'|^3}{438976}\right)\right), \quad 0 \le |\mathbf{h}'| \le 38 \\ 0, \quad |\mathbf{h}'| > 38 \end{array} \right\}$$

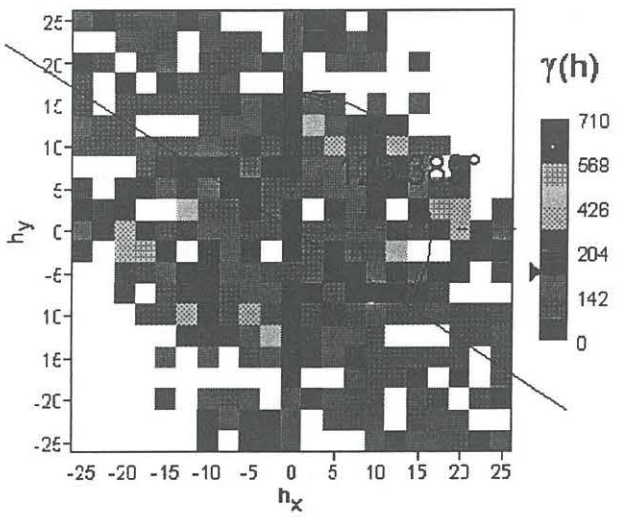

Figure 2.23. Iso-semi-variogram diagram from *Berea64* showing major axis of anisotropy at 123^0. Lag spacing 2.5 units.

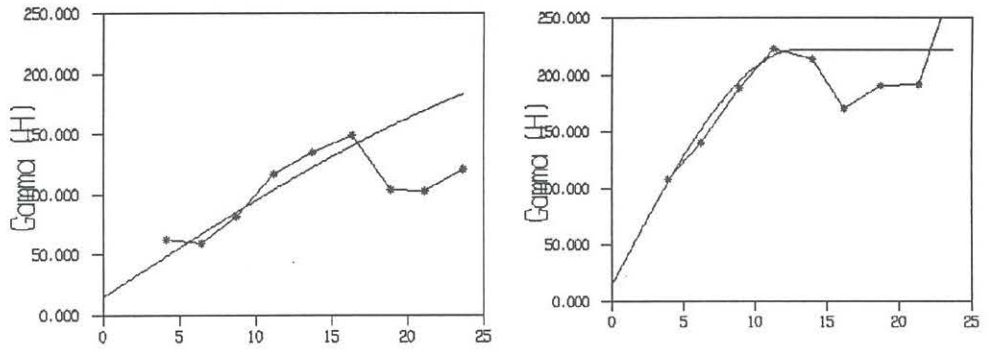

Figure 2.24. Directional semi-variograms. Major anisotropy axis at 123^0 and minor anisotropy axis at 33^0 from *Berea64*. Fitted nested models, nugget model of 15.0 for both, plus spherical models with ranges of 13 and 38 respectively and partial sill of 207 for both.

The point ordinary kriging estimates and estimation variances for a 1 x 1 unit grid are shown in figures 2.25 and 2.26. The actual *Berea* data set is shown in figure 2.7. Note

again the smoothing effect of kriging but note also the reproduction of anisotropy. Referring back to the *Berea64* sample data in figure 2.13 we see that the strength of the anisotropy in the top right hand corner of the kriging estimate plot is related to the geometry of the samples in that area and the weak anisotropy in the bottom left hand corner is related to a sparseness of sample data in that area. A comparison of the kriged data histogram to the actual *Berea* data histogram is given in figure 2.28 highlighting the reduction of variance produced by kriging. The summary statistics for the *Berea* data set are given in table 2.4 for reference.

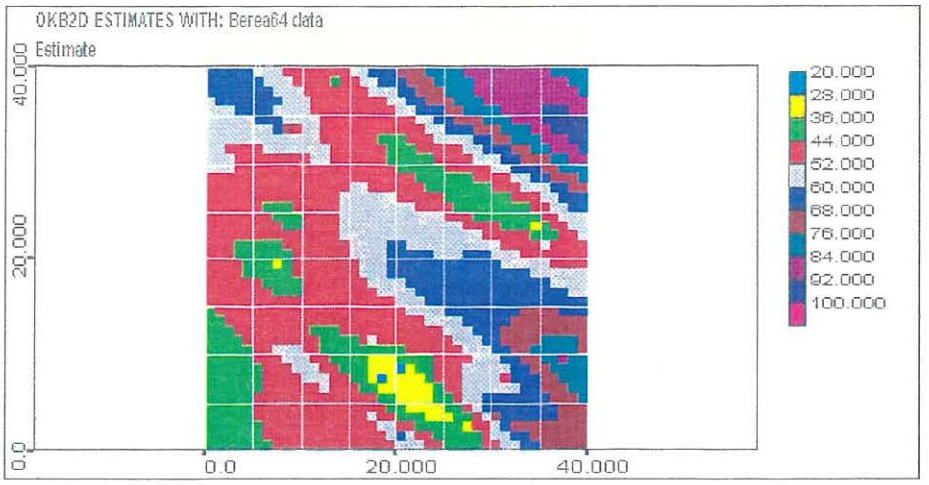

Figure 2.25. Ordinary kriging estimates from *Berea64*.

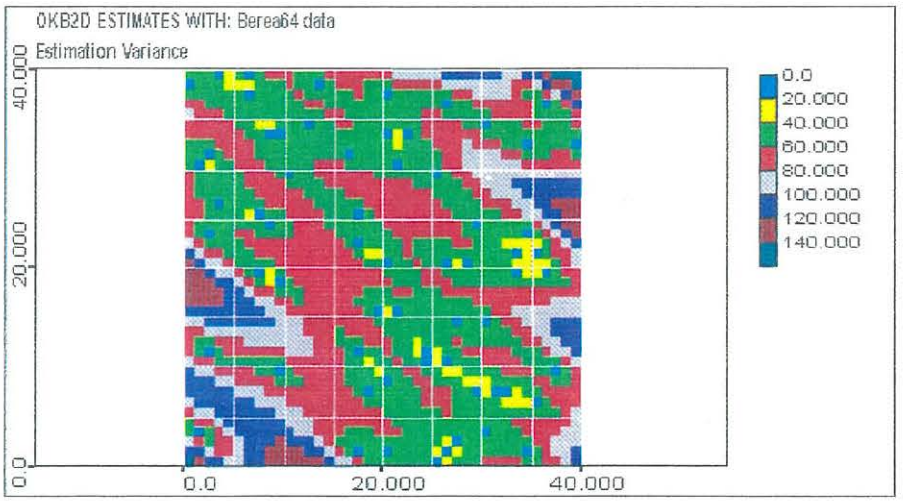

Figure 2.26. Ordinary kriging estimation variances from *Berea64*.

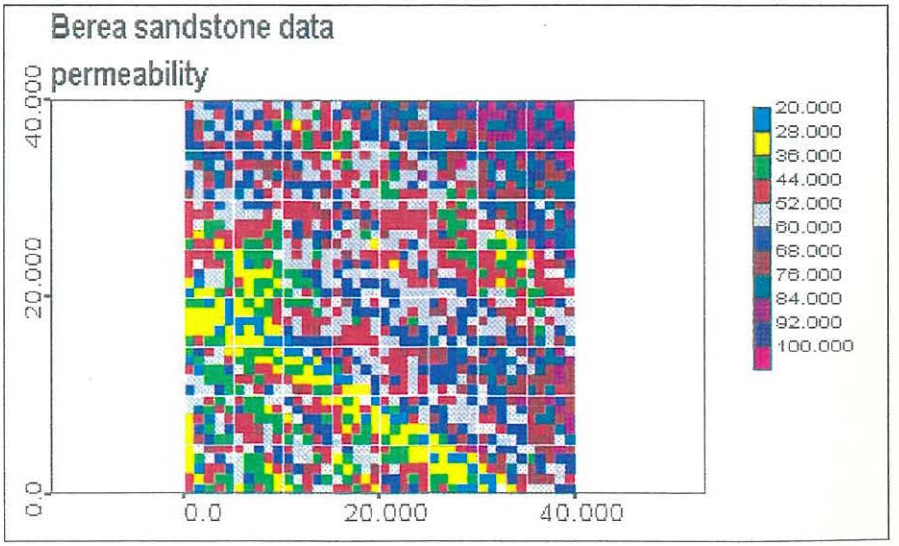

Figure 2.27. *Berea* data plot.

Histogram Statistics		
Description = OK Berea64		
Tot. Population= 1600	No. of Samples <= 0	= 0
Minimum Cutoff = 24.00000	Minimum Histogram Value	= 24.00000
Maximum Cutoff = 99.50010	Maximum Histogram Value	= 99.50010
No. of Samples Used = 1600		
	Ungrouped Data	Data Grouped to Class Intervals
Mean	54.92510	54.92081
Median	N/A	51.19161
Geometric Mean	53.54525	53.53076
Natural LOG Mean	3.98053	3.98026
Standard Deviation	12.94994	12.99469
Variance	167.701	168.862
Log Variance	0.04917	0.04955
Coefficient of Variation	0.23577	0.23661
Moment 1 about Arithmetic Mean	0.00000	0.00000
Moment 2 about Arithmetic Mean	167.701	168.862
Moment 3 about Arithmetic Mean	2269.372	2279.943
Moment 4 about Arithmetic Mean	104848.0	105730.3
Moment Coefficient of Skewness	1.04497	1.03902
Moment Coefficient of Kurtosis	3.72812	3.70796

Histogram Statistics		
Description = Berea sandstone data		
Tot. Population= 1600	No. of Samples <= 0	= 0
Minimum Cutoff = 19.50000	Minimum Histogram Value	= 19.50000
Maximum Cutoff = 111.500	Maximum Histogram Value	= 111.500
No. of Samples Used = 1600		
	Ungrouped Data	Data Grouped to Class Intervals
Mean	55.52594	55.52989
Median	N/A	54.41949
Geometric Mean	53.21521	53.22860
Natural LOG Mean	3.97434	3.97460
Standard Deviation	15.78203	15.77321
Variance	249.073	248.794
Log Variance	0.08913	0.08864
Coefficient of Variation	0.28423	0.28405
Moment 1 about Arithmetic Mean	0.00000	0.00000
Moment 2 about Arithmetic Mean	249.073	248.794
Moment 3 about Arithmetic Mean	1490.723	1550.376
Moment 4 about Arithmetic Mean	193962.7	194252.4
Moment Coefficient of Skewness	0.37923	0.39507
Moment Coefficient of Kurtosis	3.12656	3.13824

Table 2.4. *Berea64* ordinary kriging estimate statistics and *Berea* data set statistics.

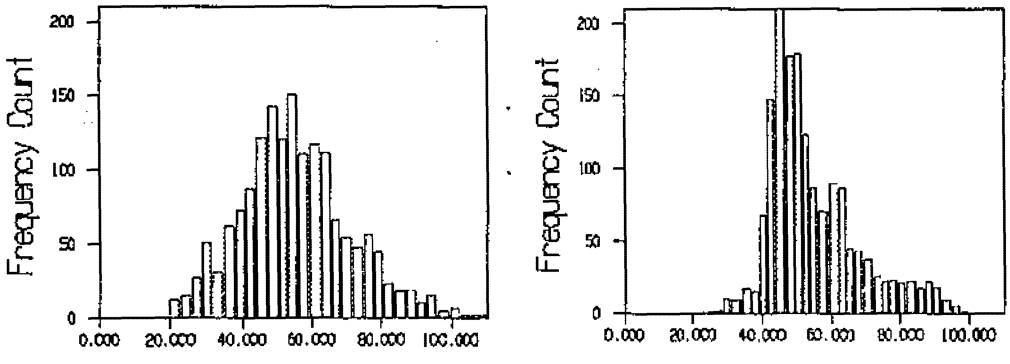

Figure 2.28. *Berea* data histogram (left) and *Berea64* ordinary kriging estimate histogram (right).

2.7 Summary

We have detailed the underlying theory of geostatistical estimation and shown two examples. It is obvious from comparisons of the kriging estimation plots with the full data plots that although kriging is a best linear unbiased estimator it does not provide the detailed variability that is exhibited in the full data sets. Simulation, which is the subject of chapter three addresses this problem.

3 Simulation

Much of the following material is based on Deutsch & Journel (1992,1996) and Goovaerts (1997). Geostatistical simulation aims to provide alternative, equally probable, numerical models of the spatial distribution of a regionalised variable $Z(\mathbf{u})$ that conform to certain characteristics of its joint spatial distribution. These characteristics are usually the histogram and semi-variogram function of the distribution. However this is not always the case as the aim of the simulation may be to reproduce other characteristics such as geometric properties of the distribution that relate to clustering and connectivity. The regionalised variable $Z(\mathbf{u})$ may be categorical or continuous and each simulated realisation of its set is denoted $\{z^{(l)}(\mathbf{u}), \mathbf{u} \in R\}$ where R is the region of interest and l is an index denoting a particular realisation. Geostatistical *conditional simulation* aims to provide alternative equally probable numerical models which as well as conforming to particular distribution characteristics also coincide with the actual sampled values

$$z_c^{(l)}(\mathbf{u}_\alpha) = z(\mathbf{u}_\alpha), \forall l \tag{3.1}$$

where the conditional simulation is denoted by $z_c^{(l)}(\mathbf{u})$. Unlike kriging, simulation (conditional or non-conditional) does not produce the best estimates at unsampled locations. It does produce a numerical model that, on average, conforms to the variability characteristics defined by the sample population of the random function under consideration. As we saw with the *Berea* data in chapter two, if a large number of unknown locations within a region are kriged and the histogram of the kriged points is plotted, it will not be the same as the histogram of the sampled values. The kriged histogram will have the same mean but will have a much smaller variance. Figure 3.1

shows the differences between kriging, simulation and reality for a theoretical one dimensional profile.

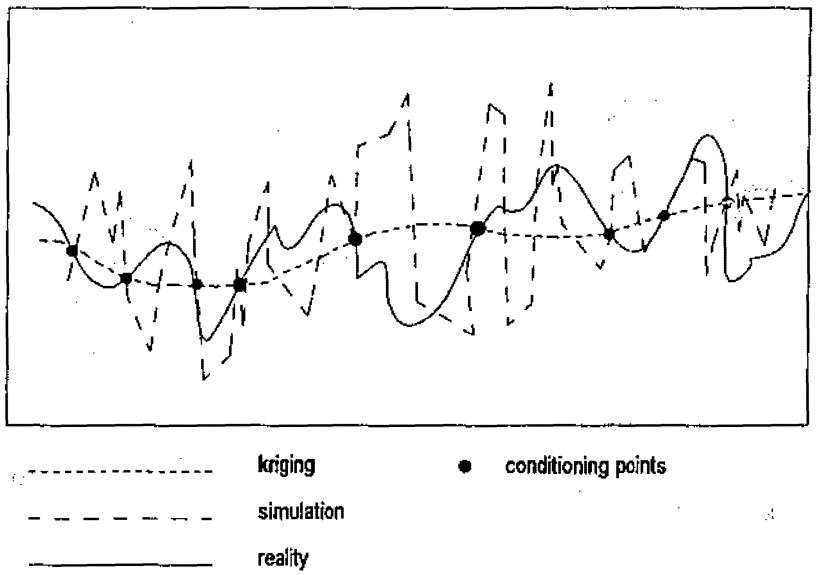

Fig. 3.1. Dispersion characteristics for 1 dimensional data. (From Journel & Huijbregts 1978)

Conditional simulations are useful for obtaining detailed numerical models from which calculations can be made for such things as grade tonnage curves, in the case of ore body modelling, and flow properties and rock porosity in the petroleum well modelling. A set of many alternative realisations of a certain conditional simulation provides a measure of uncertainty and averaging the values over a large number of alternative realisations will provide an estimated numerical model similar to that of kriging.

There are now many different algorithms available to carry out geostatistical simulation. The ones we shall examine in detail in this chapter are *sequential Gaussian* and *LU decomposition*. We will briefly describe a few of the other methods that are prominent in the literature of geostatistics at the moment. These are, *turning bands, sequential indicator simulation, p-field simulation, simulated annealing and spectral methods.*

3.1 Gaussian Methods

Sequential Gaussian simulation, as the name implies, and LU decomposition are both known as Gaussian simulation methods and must be used with standard normal data only. Gaussian simulation methods are based on what is known in geostatistical literature as the *multiGaussian random function* model. This is a standard statistical *multivariate normal* model that consists of many univariate distributions of the same attribute at different locations rather than many univariate distributions of different attributes regardless of location. In geostatistical situations where there is more than one attribute to be considered the spatial distribution is termed *multivariate multiGaussian*. We shall define the notation for a univariate normal distribution as $N(m, \sigma^2)$ and for a multivariate normal distribution as $N(\mathbf{m}, \mathbf{C})$.

Definition 3.14 A *multivariate normal* distribution is defined by its multivariate probability density function as,

$$f(z(\mathbf{u}_\alpha)) = \frac{1}{(2\pi)^{n/2}|\mathbf{C}_{\alpha\beta}|^{1/2}} e^{-(z(\mathbf{u}_\alpha)-m(\mathbf{u}_\alpha))^T \mathbf{C}_{\alpha\beta}^{-1}(z(\mathbf{u}_\alpha)-m(\mathbf{u}_\alpha))/2}$$

where $\quad -\infty < z(\mathbf{u}_\alpha) < \infty, \ \alpha = 1, \cdots, n \qquad (3.2)$

Definition 3.15 A *multiGaussian random function*, $Y(\mathbf{u}) = \{Y(\mathbf{u}), \mathbf{u} \in R\}$, is defined via its characteristic properties (Deutsch & Journel 1996) as listed below.

(a) All subsets of the random function are multivariate normal, i.e.

$$\{Y(\mathbf{u}), \mathbf{u} \in B \subset A\} \quad \text{are} \quad N(\mathbf{m}, \mathbf{C})$$

(b) All linear combinations of the random variable components of the random function are normally distributed, i.e.

$$X = \sum_{\alpha=1}^{n} \omega_\alpha Y(\mathbf{u}_\alpha) \quad \text{is } N(m, \sigma^2), \ \forall \ \omega_\alpha \text{ where } u_\alpha \in A .$$

(c) Two random variables are independent if $C[Y(\mathbf{u}), Y(\mathbf{u}')] = 0$.

(d) All conditional distributions of any subset of the random function $Y(\mathbf{u})$, given realisations of any other subset, are multivariate normal.

When dealing with a conditional simulation we need to infer the conditional distribution of the random variables within a random function. *The conditional cumulative distribution function* is defined by ,

$$F(\mathbf{u}_i; z|(n)) = P(Z(\mathbf{u}_i) \leq z|(n)) \tag{3.3}$$

where there are $\alpha = 1, \ldots, n$ conditioning values available. Under the multiGaussian model the mean and variance of the conditional cumulative distribution functions at locations $\mathbf{u}_\alpha$ are respectively equal to the simple kriging estimate $y^*_{SK}(\mathbf{u})$ and the simple kriging variance σ^2_{SK} from the n data $y(\mathbf{u}_\alpha)$ (Deutsch & Journel 1992). These two parameters, the simple kriging estimator and the simple kriging variance, define a conditional cumulative distribution function $N(z^*_{SK}(\mathbf{u}_i), \sigma^2_{SK})$ at each successive unknown location. For example where the random variable $Y(\mathbf{u}_i)$ models the uncertainty about a specific unsampled value $y(\mathbf{u}_i)$ given n data y_α,

$$\begin{aligned} y^*_{SK}(\mathbf{u}_i) &\equiv E[Y(\mathbf{u}_i)|y(\mathbf{u}_\alpha) = y_\alpha, \alpha = 1, \ldots, n] \\ &= m(\mathbf{u}_i) + \sum_{\alpha=1}^{n} \lambda_\alpha (y_\alpha - m(\mathbf{u}_i)) \end{aligned} \tag{3.4}$$

$$\begin{aligned} \sigma^2_{SK} &\equiv Var[Y(\mathbf{u}_i)|y(\mathbf{u}_\alpha) = y_\alpha, \alpha = 1, \ldots, n] \\ &= C(\mathbf{u}_i, \mathbf{u}_i) - \sum_{\alpha=1}^{n} \lambda_\alpha C(\mathbf{u}_i, \mathbf{u}_\alpha) \end{aligned} \tag{3.5}$$

Note that the random function $Y(\mathbf{u})$ is not necessarily stationary. The multiGaussian random function model is extremely useful as it allows the determination of a sequence of successive conditional cumulative distribution functions to be reduced to solving a corresponding sequence of simple kriging systems. However with many real data sets

their spatial distribution is not multiGaussian and the usual method in geostatistics of handling this is to apply a *normal score transformation* to the data before processing.

Normal score transforms essentially compare cumulative probabilities of the ranked actual data to those of the normal distribution with some sort of *continuity correction* to allow for the fact that we are dealing with discrete values. Different continuity corrections allow handling of values that are larger than the maximum experimental data and smaller than the minimum experimental data. An approximation to the inverse of the quantiles of a normal cumulative density function is then used to transform each ranked data value (original quantile) to that of a standard normal distribution N(0,1).

Definition 3.16 Let $Y(\mathbf{y})$ be a standard normal random function and $G(y) = P[Y(\mathbf{y}) \leq y]$ be its cumulative distribution function. Any random variable $Z(\mathbf{u})$ and its corresponding cumulative distribution $F_Z(z) = P[Z(\mathbf{u}) \leq z]$ can be transformed to standard normal by a *normal score transform,*

$$y_i = G^{-1}(F_Z(z_i)). \tag{3.6}$$

In practice the n data are ranked $z^{(1)} \leq z^{(2)} \leq z^{(3)} \leq \ldots \leq z^{(n)}$ and their respective cumulative distribution frequencies, without continuity correction, are given by $F_Z(z^{(k)}) = \frac{k}{n}$ where k is the rank of the unclustered data. Various continuity corrections exist in the literature and different software packages (in capitals below) use different ones. Some of these continuity corrections are listed below.

$F_Z(z^{(k)}) = \frac{k-\frac{1}{2}}{n}$ Johnson & Wichern (1992)

$F_Z(z^{(k)}) = \frac{k-\frac{3}{8}}{n+\frac{1}{4}}$ Walpole & Myers (1993) (MINITAB)

$F_Z(z^{(k)}) = \frac{k}{n+1}$ Journel & Huijbregts (1978) (GSLIB)

Other factors that need to be taken into consideration are declustering weights, which can change the cumulative probabilities, and some criterion for ordering tied ranked values (see, for example, Goovaerts 1996). An expression for the inverse function G^{-1} is very complicated and various approximations are used for example,

$$G^{-1}(f) = \frac{1}{4.19(f^{0.14}-(1-f)^{0.14})} \text{ where } f = F_Z(z^{(k)}) \qquad \text{Walpole \& Myers (1993)}$$

$$G^{-1}(f) = \begin{cases} \varphi + \frac{(((\varphi e+d)\varphi+c)\varphi+b)\varphi+a)}{(((\varphi j+i)\varphi+h)\varphi+g)\varphi+f)} & 0 < f < 0.5 \\ -\left(\phi + \frac{(((\phi e+d)\phi+c)\phi+b)\phi+a)}{(((\phi j+i)\phi+h)\phi+g)\phi+f)}\right) & 0.5 < f < 1 \end{cases} \qquad \text{Kennedy \& Gentle (1980)}$$

where

$$\varphi = \sqrt{\ln(\frac{1}{f^2})} \quad \text{and} \quad \phi = \sqrt{\ln\frac{1}{(1-f)^2}} \qquad \text{(GSLIB)}$$

and
a = -0.322232431088
b = -1.0
c = -0.342242088547
d = -0.0204231201245
e = -0.0000453642210148
f = 0.0993484626060
g = 0.588581570495
h = 0.531103462366
i = 0.103537752850
j = 0.0038560700634.

A normal score transform can also be done graphically and an example of this, figure 3.2, gives a clearer picture of the process in general.

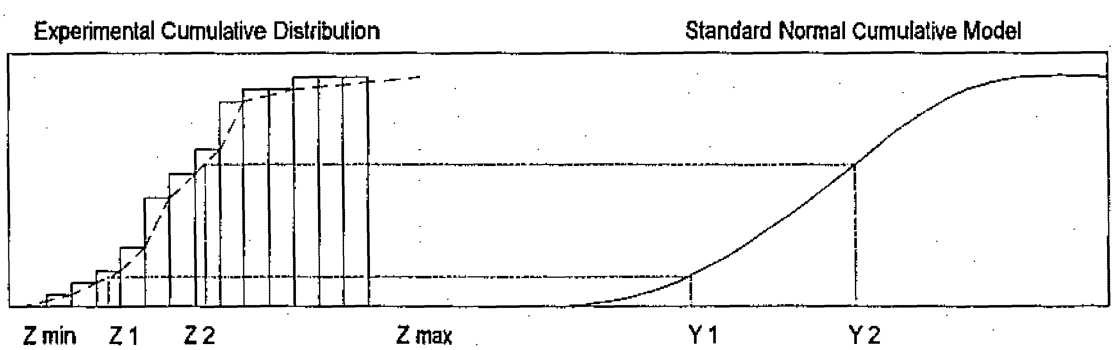

Figure 3.2. Graphical normal score transform.

Having transformed a random function to normality still does not guarantee that it is multiGaussian normal. Strictly, all n dimensional cumulative distribution functions must be multivariate normal, however it is sufficient to check the bivariate distribution to adopt or reject the multiGaussian model. There are various ways in which this can be done, two of which are, squared generalised distances (Johnson & Wichern 1992) and semi-variogram comparison (Goovaerts 1997). We shall not examine the details here. In practice these checks are rarely carried out and many simulations are done under the assumption of being multiGaussian. There are other ways to transform to a normal distribution such as fitting Hermite polynomials (Journel & Huijbregts 1978, p472) and various approximations such as log transforms and power transforms. However these approximate methods often do not reproduce normality well in the tails of the distributions (see specifically, Goovaerts 1996, p276) which is where the critical high values of a distribution occur.

Once a simulation is completed a back transform of the form

$$z_i = F^{-1}(G(y_i)) \qquad (3.7)$$

is necessary to reproduce the simulation with the original, non-Gaussian, distribution characteristics. Generally F^{-1} is impossible to determine directly and the back transform is accomplished by the use of a table created during the forward transform. Given that simulations generate much more data than the original sample values there will often be cases where some of the simulated values are lower than the smallest sample value and higher than the largest sample value in the transformation table.

In order to back transform from a normal distribution to the original distribution it is necessary to have some model of the behaviour of the original distribution in the upper

and lower tails beyond existing sample data. If the data is sparse it may also be desirable to model the distribution as something other than linear between two consecutive quantiles. Deutsch & Journel (1992) and Goovaerts (1997) both suggest linear and power models for lower and upper tail extrapolation and include a hyperbolic model for upper tail as well. These tail extrapolation models are given as options in the GSLIB suite of Gaussian related simulation routines.

Definition 3.17 The *lower tail power model* is defined as,

$$F(z) = \left(\frac{z - z_{\min}}{z_1 - z_{\min}}\right)^{\omega} F(z_1) \quad \forall z \in (z_{\min}, z_1) \tag{3.8}$$

where z_1 is the smallest sample value and $z_{\min}$ is a minimum possible allowable z value.

When $\omega = 1$ this corresponds to a linear model. Where $0 < \omega < 1$ the tail is positively skewed and where $\omega > 1$ the tail is negatively skewed.

Definition 3.18 The *upper tail power model* is defined as,

$$F(z) = F^*(z_K) + \left(\frac{z - z_K}{z_{\max} - z_K}\right)^{\omega} (1 - F(z_K)) \quad \forall z \in (z_{\min}, z_1) \tag{3.9}$$

where $\omega < 1$, z_K is the largest sample value and $z_{\max}$ is the maximum allowable z value.

Definition 3.19 The *hyperbolic tail model* is written

$$F(z) = 1 - \frac{\lambda}{z^{\omega}} \quad \forall z > z_K \tag{3.10}$$

where

$$\lambda = z_K^{\omega}(1 - F^*(z_K))$$

and $\omega \geq 1$.

The hyperbolic model should only be used for the upper tail of a positively skewed distribution. Setting $\omega = 1$ corresponds to a very long tail and the larger the value ω is the shorter the tail is. Deutsch & Journel (1992) suggest that $\omega = 1.5$ is a good general purpose value.

3.2 Sequential Gaussian Simulation

Sequential simulation methods were proposed by Journel & Alabert (1989, 1990) and are based on an application of Bayes theorem. The technique is similar to the generalised stochastic subdivision method in Lewis (1987). The *sequential simulation* theorem, as used by Journel & Alabert (1989), states that n dependent events A_i, $i = 1, \ldots, n$ can be simulated sequentially using the expression,

$$P(A_1, A_2, \ldots, A_n) = P(A_n | A_1, \ldots, A_{n-1}) \cdot P(A_{n-1} | A_1, \ldots, A_{n-2}) \cdot \ldots \cdot P(A_2 | A_1) \cdot P(A_1) \ .$$

This requires the inference of the successive $n-1$ conditional probability distributions which can be obtained by simple kriging as explained in section 3.1. The general sequential Gaussian procedure is as follows.

(a) Ensure that the data is, or is transformed to be, multiGaussian.

(b) Randomly order all the locations to be simulated.

(c) Estimate a value using simple kriging at the first/next randomly ordered location using all the original data as well as any previously simulated points. Take the simple kriging estimate and the associated simple kriging variance as the parameters of the conditional distribution $N(z^*_{SK}, \sigma^2_{SK})$ at that particular location.

(d) Randomly select a value from this distribution to become the conditionally simulated value at that location. (For details of random number generation see Press et. al. 1986.)

(e) Repeat the procedure from step (c) until all values at unknown locations have been simulated.

(f) Inverse transform the set of simulated values to conform to the original distribution if necessary.

The computational scheme is as follows,

$$z_c^{(l)}(\mathbf{u}) = \left\{ \begin{array}{c} F^{-1}(z^*_{SK(NS)}(\mathbf{u}_i) + (w_i\ \sigma_{SK(NS)})), \quad i = 1, \ldots, N \\ z(\mathbf{u}_\alpha) \quad \alpha = 1, \ldots, n \end{array} \right\} \qquad (3.11)$$

where the subscript (NS) indicates the normal score values and w_i is a random number drawn from a Gaussian distribution..

Note that the conditioning is inherent in this process. If a non-conditional simulation is required, no original values would be included and the first value simulated would be randomly drawn from the marginal distribution of the transformed random function. Anisotropies are also handled automatically. Strictly, simple kriging is required to be used with sequential Gaussian simulation because of the assumption of second order stationarity over the entire region, however ordinary kriging can be used if the situation allows for reliable estimation of the local means within a local search area defined for the estimation of each simulation point. For applications of sequential Gaussian simulation see Nowak & Srivastava (1996) and Ravenscroft (1994).

3.3 LU Decomposition

LU decomposition is a very simple conditional simulation method but can currently handle only small data sets, Deutsch & Journel (1996) suggest 'a few hundred', because of computer memory requirements for large matrices. It was first introduced, in a geostatistical form, by Davis (1987) and by Alabert (1987) and is based on the lower upper triangular decomposition of the covariance matrix,

$$\mathbf{C} = \mathbf{LU} \quad \text{where} \quad \mathbf{L}^T = \mathbf{U}. \qquad (3.12)$$

In the special case where **C** is a symmetric positive definite matrix (as is the covariance matrix) the factorisation can be achieved by Cholesky decomposition. The simulation scheme is outlined as follows.

Consider the linear system

$$\mathbf{C}\lambda = (\mathbf{LU})\lambda = \mathbf{L}(\mathbf{U}\lambda) = \mathbf{y} \qquad (3.13)$$

where the vector **y** is defined as

$$\mathbf{y} = \mathbf{Lw},$$

C is the covariance matrix of a set of spatially distributed points and **w** is a vector of independent random numbers with distribution $N(0, 1)$. The expectation of $\mathbf{y}\,\mathbf{y}^T$ is then given by,

$$\begin{aligned} E[\mathbf{y}\,\mathbf{y}^T] &= E[(\mathbf{Lw})(\mathbf{Lw})^T] \\ &= E[\mathbf{L}\mathbf{w}\mathbf{w}^T\mathbf{U}] \\ &= \mathbf{L}\mathbf{U}E[\mathbf{w}\mathbf{w}^T] \\ &= \mathbf{LUI} \\ &= \mathbf{C}. \end{aligned} \qquad (3.14)$$

The covariance matrix of a stationary random function model $Y(\mathbf{u})$ with mean zero and sample locations $\mathbf{u}_\alpha$ is,

$$\mathbf{C}_{\alpha\beta} = E[Z(\mathbf{u}_\alpha)\, Z(\mathbf{u}_\beta)], \quad \forall\alpha = 1, \ldots, n; \beta = 1, \ldots, n. \qquad (3.15)$$

From equations 3.12 and 3.13 it follows that **Lw** forms an unconditional simulation as it reproduces the covariance model. i.e.

$$z^{(l)}(\mathbf{u}_\alpha) = \mathbf{Lw}, \quad \forall\alpha = 1, \ldots, n. \qquad (3.16)$$

For conditional simulation let $\mathbf{u}_\alpha$, $\alpha = 1, \ldots, n$ be the locations of the conditioning data and $\mathbf{u}_i, i = 1, \ldots, N$ be the locations of the points to be simulated. To enable us to follow

the sub matrices subscripts have been used to distinguish them. The original covariance matrix is then made up of four submatrices,

$$\mathbf{C}_{(n+N)(n+N)} = \begin{bmatrix} [C(\mathbf{u}_\alpha - \mathbf{u}_\beta)]_{nn} & [C(\mathbf{u}_\alpha - \mathbf{u}_j)]_{nN} \\ [C(\mathbf{u}_i - \mathbf{u}_\beta)]_{Nn} & [C(\mathbf{u}_i - \mathbf{u}_j)]_{NN} \end{bmatrix}. \tag{3.17}$$

A conditional simulation $z_c^{(l)}(\mathbf{u})$ is obtained by

$$z_c^{(l)}(\mathbf{u}) = \begin{bmatrix} [z(\mathbf{u}_\alpha)]_{n1} \\ [z^{(l)}(\mathbf{u}_i)]_{N1} \end{bmatrix} = \mathbf{L}\mathbf{w} = \begin{bmatrix} \mathbf{L}_{nn} & 0 \\ \mathbf{L}_{Nn} & \mathbf{L}_{NN} \end{bmatrix} \begin{bmatrix} \mathbf{w}_{n1} \\ \mathbf{w}_{N1} \end{bmatrix}. \tag{3.18}$$

where

$$\mathbf{w}_{n1} = \mathbf{L}_{nn}^{-1} [z(\mathbf{u}_\alpha)]_{n1}$$

and $\mathbf{w}_{N1}$ is a column matrix of independent N(0,1) distributed random numbers. This leads to an expression for the simulated values,

$$z^{(l)}(\mathbf{u}_i) = \mathbf{L}_{Nn}\mathbf{L}_{nn}^{-1}[z(\mathbf{u}_\alpha)]_{n1} + \mathbf{L}_{NN}\mathbf{w}_{N1}. \tag{3.19}$$

It can be seen from this that other realisations of the simulated values can be easily calculated as they only require a fresh set of random numbers $\mathbf{w}_{N1}$ and do not require recalculation of the decomposition. LU decomposition also handles anisotropy automatically. The parallels of this method to simple kriging and corrections for bias introduced by ordinary kriging are outlined in Alabert (1987). For applications see Dowd & Sarac (1994) and Glacken (1996).

3.4 Other Simulation Methods

Turning Bands

Turning bands methods are based on the construction of a one dimensional simulation of a random function $Y(\mathbf{u})$, by any method, which is then rotated in space a number of times n to uniformly cover the space under consideration (see figure 3.3). Each rotation is given a different realisation of the one dimensional simulation. The point at which a

value is to be simulated is then projected onto each of these n lines to obtain a series of values $z_i(\mathbf{u}), i = 1$ to n which are then averaged to give the simulated value in a higher dimension.

$$z^{(l)}(\mathbf{u}) = \frac{1}{n}\sum_{i=1}^{n} z_i(\mathbf{u}) \qquad (3.20)$$

This results in an isotropic Gaussian non-conditional simulation. If the simulation is to be conditioned this is then carried out as a separate step after non-conditional simulation but before the final values are re-transformed to conform to the original joint distribution. The methods of simulating one dimensional random functions used with turning bands are, in the general case, spectral and in specific cases based on moving average methods. For applications see also Journel & Huijbregts (1978) and Brooker (1985).

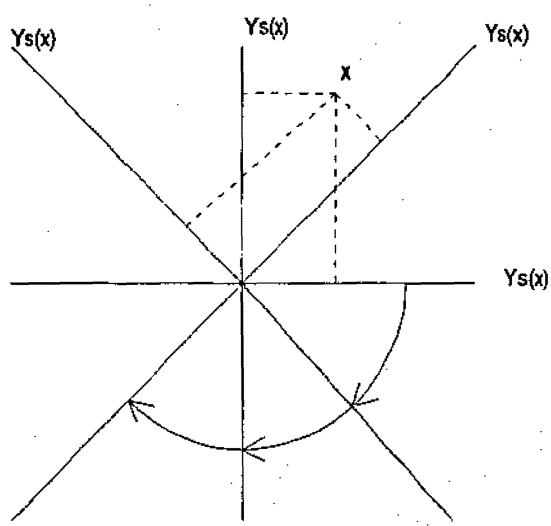

Fig. 3.3. Turning bands in two dimensions. Y(u) is a simulated random function.

Sequential Indicator Simulation

Sequential indicator simulation seeks to avoid the transformation to a Gaussian distribution by using indicators (see Deutsch & Journel 1996). It follows a similar

procedure to sequential Gaussian simulation except that at each location where a value is to be simulated the conditional distribution is estimated directly by kriging the indicator transformed values defined for each specific threshold. Instead of the simple kriging value and simple kriging variance being used to define a normal distribution, an estimated conditional probability distribution function F^* at each location is built up by indicator kriging for each threshold resulting in a distribution whose detail reflects the number and relative spacing of the thresholds used. For applications see Chu (1996) and Gomez-Hernandez & Srivastava (1990).

Simulated Annealing

Geostatistical simulated annealing is really an optimisation procedure rather than a true simulation. It is based on an analogy with the physical process of annealing by which a material (usually a metal) undergoes heating and is then slowly cooled. The slow cooling allows the molecules of the material to reorder themselves into a highly structured state or a 'low energy' state. Simulated annealing does not require any reference to a random function model. It works by gradually perturbing an initial numerical model so that changes are accepted if they bring the model closer to the target constraints which are usually to reproduce the semi-variogram and histogram. The conditioning is done by not allowing the original data at their locations to change. The initial numerical model is usually some sort of geostatistical simulation that already has some of the required properties but needs to be constrained further. The process of geostatistical simulated annealing is still called a simulation because there are usually many approximate solutions to the optimisation problem and hence a range of different but equally probable final numerical models can be generated by the annealing process.

An even greater range of final models can be produced if different equally probable initial images are used. Further details can be found in Deutsch & Cockerham (1994), Deutsch & Journel (1992,1996) and Goovaerts (1997).

p-field simulation

This method is based on the idea of using autocorrelated random numbers that conform to the desired covariance function to sample from conditional cumulative distribution functions at each location where a value is to be to be simulated. For a detailed examination of this method see Froidevaux (1993), Goovaerts (1997) and Srivastava (1992).

Spectral analysis

Fourier analysis, spectral analysis and power spectra are not examined in detail here as they are rather more complex and less easy to implement. However they are relevant to spatial statistics and also to stochastic fractals and some relationships will be briefly described. Fourier analysis can be applied to any quantity that fluctuates in time or space and involves fitting sine and cosine series of various amplitudes frequencies and phases to approximate the data. The *Fourier transform* equation relates the *time (or distance) domain* to the *frequency domain* and is written

$$Z(\mathbf{f}) = \iint_{-\infty}^{\infty} Z(\mathbf{u}) e^{2\pi i \mathbf{f}\mathbf{u}} d\mathbf{u} \qquad (3.21)$$

where **f** is the frequency vector. The *spectral density* is then written as

$$S(\mathbf{f}) = |Z(\mathbf{f})|^2. \qquad (3.22)$$

The covariance of a random function is related to its spectral density by the Wiener-Khintchine theory as follows

$$C(\mathbf{h}) = \iiint_{-\infty}^{\infty} S(\mathbf{f}) e^{2\pi i \mathbf{f}\mathbf{u}} d\mathbf{f}. \qquad (3.23)$$

Spectral methods are also related to fractal simulations which we will deal with in chapter four. For more details and spectral applications see Chiles & Delfiner (1996), Fox (1987), Peitgen & Saupe (1988) and Turcotte (1992).

3.5 Examples

We will illustrate sequential Gaussian simulation using the two sample data sets *Gslib97* and *Berea64* that were used in chapter 2. The GSLIB suite of programs is used for the normal score transformations, sequential Gaussian simulation and back transformation. Note that the normal score and back transformation parameters in the examples used here are taken from the probability density function inferred from the sample data alone. We will examine the *Gslib97* data first.

The variography needs to be assessed using standard normal scores. We would expect it to have similar anisotropy and range values to that of the original data but the semi-variogram models must be expressed in terms of the normal score values for input into the simulation routine. A direct translation of the semi-variogram model used in chapter one gives a nugget of 0.495, a range of 12 and a partial sill of 0.505. The experimental semi-variogram given by the normal scores is noticeably smoother than that given by the original data and models with a nugget effect lower of 0.3, range 12 and partial sill 0.7. The omni-directional normal score semi-variogram and fitted nested nugget and spherical mode are shown in figure 3.4 and the fitted model is,

$$\gamma(\mathbf{h}) = \left\{ \begin{array}{ll} 0.3 + 0.7\left(\frac{3|\mathbf{h}|}{24} - \frac{|\mathbf{h}|^3}{3456}\right), & 0 \le |\mathbf{h}| \le 12 \\ 1, & |\mathbf{h}| > 12 \end{array} \right\}$$

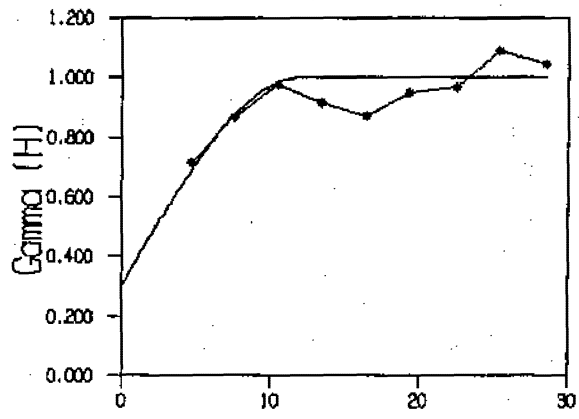

Figure 3.4 Normal score semi-variogram and fitted model for Gslib97.

An example calculation using the node $\mathbf{u}_i$ = (20x, 25y) follows. The estimate is a simple kriging estimate derived from sixteen surrounding values, however these are not the same sixteen values used in the example in chapter two. This is because some of the other nearby points have already been simulated and the sixteen values used for simple kriging are made up of the closest sixteen points regardless of whether they are original conditioning points or previously simulated points.

$$z^*_{SK(NS)}(\mathbf{u}_i) = 0.7727 \sim z^*_{SK}(\mathbf{u}_i) = 2.87$$

$$\sigma^2_{SK(NS)} = 0.5507$$

$$w_i = -0.0391$$

$$z^{(l)}_{c(NS)}(\mathbf{u}_i) = 0.7727 + (-0.0391 \cdot \sqrt{0.5507}) = 0.7434 \sim z^{(l)}_c(\mathbf{u}_i) = 2.79$$

As *Gslib97* is a highly skewed data set the back transform uses a linear lower tail cumulative frequency distribution extension with a minimum value of zero and an hyperbolic upper tail extension with a flattening parameter of 1.5. The resulting

full simulation is shown in figure 3.5. Note that this is a much more realistic looking plot than the plot of the kriged data in figure 2.19.

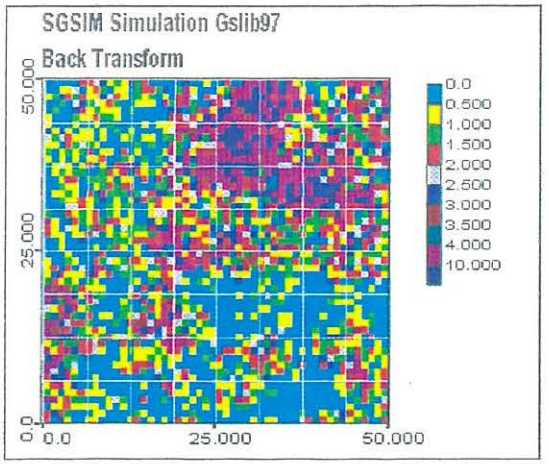

Figure 3.5. One realisation of a sequential Gaussian simulation from *Gslib97*.

Looking at the *Berea64* data we find that the experimental normal score directional semi-variograms model slightly differently from a direct translation of the original data models. In this case the nugget effect is higher and the range in the 33^0 direction models marginally lower at 12 units rather than 13 units. The fitted model is,

$$\gamma(\mathbf{h}) = \left\{ \begin{array}{ll} 0.2 + 0.8\left(\frac{3|\mathbf{h}'|}{76} - \frac{|\mathbf{h}'|^3}{438976}\right), & 0 \le |\mathbf{h}'| \le 12 \\ 1.0, & |\mathbf{h}'| > 12 \end{array} \right\}$$

where $|\mathbf{h}'|$ is the isotropic transformed lag distance and the anisotropy ratio is 0.3158.

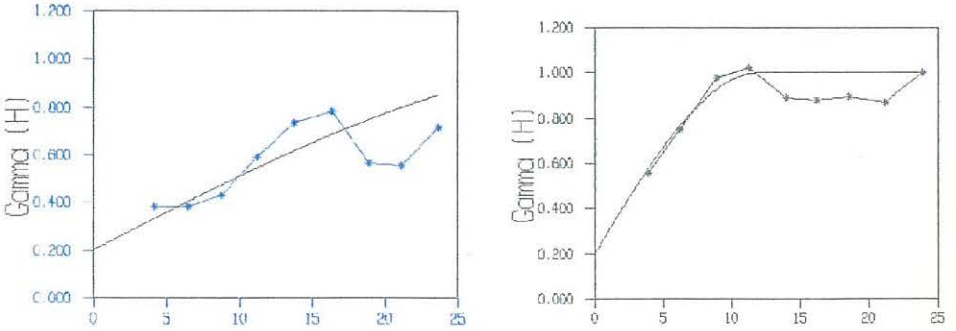

Figure 3.6. Directional normal score semi-variograms for *Berea64* at 123^0 (left) and 33^0 (right).

The back transformation was done with a linear lower and upper cumulative distribution tail extension with a minimum of zero and a maximum of 120. The resulting simulation is shown in figure 3.7. Note that the simulated plot looks more like the actual Berea data than the kriging plot in figure 2.25.

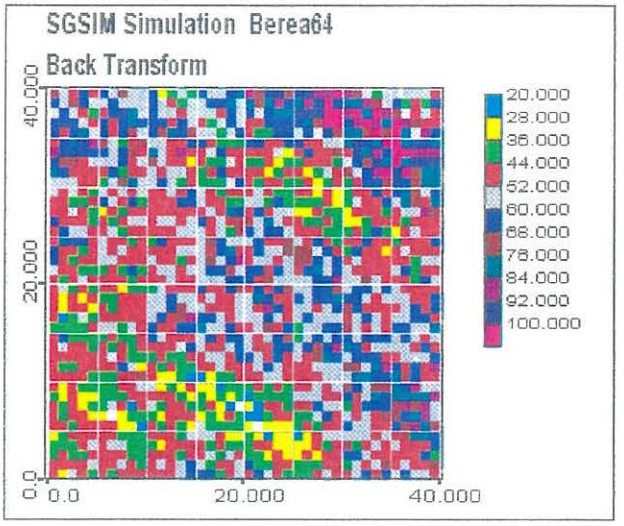

Figure 3.7. One realisation of a sequential Gaussian simulation from *Berea64*.

3.6 Summary

We have given an overview of geostatistical simulation in general and have looked specifically at sequential simulations to see how they can provide a better model than kriging of the overall variability of a random function. In the next chapter we will examine fractal concepts and simulation methods and show how they can be incorporated into and enhance geostatistical Gaussian simulation methods.

4 Fractals

Fractal geometry deals with the concept of self similiarity at different scales and has been found to apply to a wide range of natural phenomena. Examples (Burrough 1981) include tree ring indices, annual precipitation, river flows, ground water levels and land forms. The basic characteristic of fractals is that detail at one scale remains similar at all other scales. The classic example of a natural feature exhibiting fractal characteristics is that of a coastline where decreasing scale and increasing resolution continue to reveal detail that is similar in shape and statistical variability to that at each previous scale. A geometric example which is simpler to visualise is that of a Koch curve (see figure 4.1).

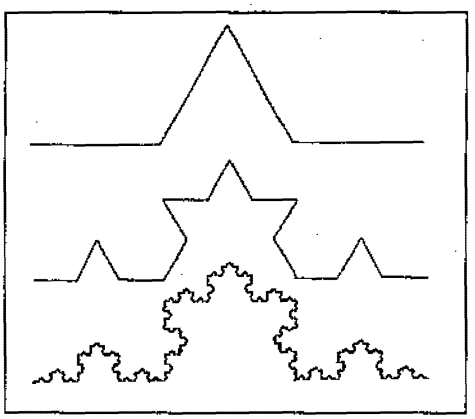

Figure. 4.1 Koch curve showing increasing levels of detail with increasing resolution.

In this chapter we will examine stochastic fractal theory and the model of *fractional Brownian motion* and show how it is linked to the power model in geostatistics. We then propose a new fractal simulation scheme, SGFRACT, and test it using the data from chapters two and three.

4.1 Fractal Theory

The strict definition of a fractal set requires it to have a Hausdorff dimension that is greater than or equal to its topological dimension. For a formal definition of *fractal dimension, Hausdorff dimension* and *topological dimension* see James & James (1992). A more general definition is that a fractal is a shape made of parts that are similar to the whole in some way (Mandelbrot 1983). We will explain this in terms of *self similarity* and *self affinity*. The following definitions of self similarity and self affinity are based on Voss (1988 & 1985) with notation changes to conform to previous sections.

Definition 4.1 Let the set Ω be a bounded subset of Euclidean space of dimension E where each location $\mathbf{u}$ is made up of co-ordinates $u_1, \ldots, u_E$. Using a similarity transform with $0 < r < 1$, Ω becomes $r\Omega$ with locations $r\mathbf{u} = (ru_1, \ldots, ru_E)$. The set Ω is *self similar* if it is the union of N disjoint subsets each of which is congruent to $r\Omega$ where congruent here means identical under translation and rotation.

Definition 4.2 The *fractal dimension* D of Ω is defined by

$$1 = Nr^D \quad \text{or} \quad D = \frac{\ln N}{\ln \frac{1}{r}} \tag{4.1}$$

Definition 4.3 A set Ω is *statistically self similar* if it is the union of N disjoint subsets each of whose distributions are unchanged by the similarity transform $0 < r < 1$.

In practice the statistical aspects are usually limited to the first few moments of the distribution of Ω. The fractal dimension D also characterises the covering of the set Ω by E dimensional 'boxes' of linear size L (see figure 4.2).

If the entire set is contained within one box of size L_{max} then each of the $N = 1/r^D$ subsets will fall within one box of size $L = rL_{max}$. Thus the number of boxes $N(L)$ of size L needed to cover the set Ω is then

$$N(L)/N(L_{max}) = \frac{1}{r^D} = (L_{max}/L)^D \text{ or } N(L) \propto 1/L^D. \quad (4.2)$$

Definition 4.4 A set Ω is *self affine* when it is the union of N disjoint subsets each of which is identical under translation and rotation to $\mathbf{r}\Omega$ where $\mathbf{r} = (r_1, \ldots, r_E)$ and $0 < r_i < 1,\ i = 1, \ldots, E$.

Therefore each co-ordinate may be scaled by a different ratio r_i and the set Ω is transformed to $\mathbf{r}\Omega$ with location co-ordinates $r_1 u_1, \ldots, r_E u_E$.

Definition 4.5 The set Ω is *statistically self affine* if it is the union of N disjoint subsets each of whose distributions are unchanged by the affine transform $\mathbf{r}$ where $0 < r_i < 1,\ i = 1, \ldots, E$.

It is not such a simple matter to obtain the fractal dimension from this definition of self affinity and we shall introduce the concept of the *fractal co-dimension H,* also known as the Hurst exponent or intermittency exponent. To do this we will look at *fractional Brownian motion* which is an extension of the traditional *Brownian motion* stochastic process or random walk. Usually Brownian motion $B(t)$ is expressed in one dimensional time however we will express it in terms of spatial co-ordinates $\mathbf{u}$.

Definition 4.6 *Brownian motion* $B(\mathbf{u})$ is the sum of a sequence of independent Gaussian random variables

$$B(\mathbf{u}) = \Sigma W(\mathbf{u}) \quad (4.3)$$

where $W(\mathbf{u})$ represents the Gaussian random function also known as white noise.

Brownian motion is extended to *fractional Brownian motion* $B_H(\mathbf{u})$ by re-scaling. The *fractal co-dimension H* relates the typical change $\Delta B_H(\mathbf{u})$ in $B_H(\mathbf{u})$ to the change

$\Delta\mathbf{u} = \mathbf{h}$ in $\mathbf{u}$ by the scaling law

$$\Delta B_H(\mathbf{u}) \propto \mathbf{h}^H. \tag{4.4}$$

The parameter H is a measure of spatial similarity of $B_H(\mathbf{u})$ and its values fall into three distinct categories. When $0 < H < 0.5$ the increments of $B_H(\mathbf{u})$ are negatively correlated, for $H = 0.5$ the increments are uncorrelated Gaussian white noise and for $0.5 < H < 1$ the increments are positively correlated. A value of $H = 1$ means that the function is deterministic, differentiable and smooth.

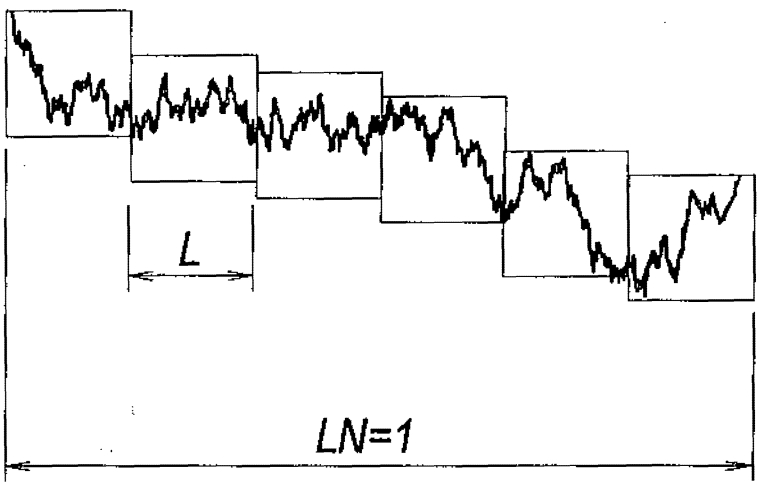

Figure 4.2. Box counting method of determining H.

The relationship between the fractal dimension D and *fractal co-dimension* H is illustrated by considering a one dimensional trace of fractional Brownian motion covering $|\mathbf{h}| = 1$ in the horizontal direction and $\Delta B_H(\mathbf{u}) = 1$ in the vertical direction (figure 4.2). Here $|\mathbf{h}|$ represents a particular distance increment or lag. $B_H(\mathbf{u})$ is statistically self affine since when $\mathbf{h}$ is scaled by $\boldsymbol{r}$ and $B_H(\mathbf{u})$ is scaled by $\mathbf{r}^H$ a re-scaled fraction of the trace is obtained identical in distribution to the original trace. Dividing the horizontal interval into N equal subintervals gives

$$|\mathbf{h}| = 1/N \text{ and } \Delta B_H(\mathbf{u}) = |\mathbf{h}|^H = 1/N^H. \tag{4.5}$$

If we use the box coverage method as in equation 4.2 to determine D each interval will be covered by $\Delta B_H(\mathbf{u})/|\mathbf{h}| = (1/N^H)/(1/N) = N/N^H$ square boxes of linear scale $L=1/N$. The total number of boxes becomes

$$N(L) = N\,(N/N^H) = N^{2-H} = 1/L^{2-H} \quad . \tag{4.6}$$

By comparison with equation. 4.2 noting that now $N(L_{\max}) = 1$,

$$D = 2 - H$$

and this can be generalised to higher dimensions to give the general rule

$$D = E + 1 - H \tag{4.7}$$

where E is the Euclidean dimension of the space in which the set is contained.

Definition 4.7 The *fractal co-dimension* H is defined by

$$H = E + 1 - D$$

where E is the Euclidean dimension and D is the fractal dimension.

We now examine the properties of fractional Brownian motion. The following discussion is based on Mandelbrot & Wallis (1969, part 3) with appropriate notation changes. Brownian motion is a self affine process in that if $\mathbf{u} = \mathbf{r}(\mathbf{u}+\mathbf{h})$ then $B(\mathbf{u}) - B(0) = B(\mathbf{r}(\mathbf{u}+\mathbf{h})) - B(0)$ is statistically the same as $\mathbf{r}^{0.5}(B(\mathbf{u}+\mathbf{h}) - B(0))$. It follows from this and equation 4.4 that

$$Var[\tfrac{B(\mathbf{u}+\mathbf{h})-B(\mathbf{u})}{\mathbf{h}^{0.5}}] = 1 \text{ or } E[(B(\mathbf{u}+\mathbf{h}) - B(\mathbf{u}))^2] = (\mathbf{h}^{0.5})^2 \tag{4.8}$$

It can now be seen that the increments of Brownian motion have a variance proportional to the absolute location difference.

$$E[|B(\mathbf{u}_\alpha) - B(\mathbf{u}_\beta)|^2] \propto |\mathbf{u}_\alpha - \mathbf{u}_\beta| \tag{4.9}$$

Similarly the increments of fractional Brownian motion $B_H(\mathbf{u}_\alpha) - B_H(\mathbf{u}_\beta)$ (in any Euclidean dimension) have a Gaussian distribution with variance

$$E[|B_H(\mathbf{u}_\alpha) - B_H(\mathbf{u}_\beta)|^2] = V_H|\mathbf{u}_\alpha - \mathbf{u}_\beta|^{2H} \tag{4.10}$$

where V_H is a constant of proportionality and $0 < H < 1$. Note that $H = 0.5$ gives the traditional Brownian motion with $\Delta B(\mathbf{u})^2 \propto |\mathbf{h}|$. Equation 4.10 is equivalent to a variogram function as it is a variance of increments hence,

$$2\gamma(\mathbf{h}) = V_H |\mathbf{h}|^{2H} \tag{4.11}$$

and V_H is therefore the total variance at the reference unit scale $|\mathbf{h}|=1$.

Brownian motion has no derivative as it shows irregular behaviour at all scales. However if some amount of smoothing is accepted this lack of derivative can be overcome. The derivatives of smoothed fractional Brownian motion with H values other than 0.5 are referred to as *fractional Gaussian noises* represented by $W_H(\mathbf{u})$ and have a covariance given by

$$C(\mathbf{h}, \delta) = \tfrac{1}{2} V_H \, \delta^{2H-2} \left(\left|\tfrac{\mathbf{h}}{\delta} + 1\right|^{2H} - 2\left|\tfrac{\mathbf{h}}{\delta}\right|^{2H} + \left|\tfrac{\mathbf{h}}{\delta} - 1\right|^{2H} \right) \tag{4.12}$$

where δ is an arbitrarily small interval over which smoothing has taken place. For more detail on the derivation of this covariance see Mandelbrot & Van Ness (1968). Fractional Brownian motion and fractional Gaussian noise with $0 < H < 1$ and their associated semi-variogram and covariance functions (equations 4.11 and 4.12 respectively) are the two types of model used in all stochastic fractal simulations.

4.2 Determining The Fractal Dimension

A useful property of fractal sets is that, like Euclidean sets, they typically reduce their dimension by one under intersection with a plane. Often the intersection of a self affine fractal object with the plane will result in a fractal set that is then self-similar but, as with topographic profiles, this may only be true for particular directions. (Voss 1988,

Klinkenberg 1994, Bruno & Raspa 1989). Most methods of determining the fractal dimension of an object are based on measurements carried out on one dimensional curves or profiles. The most widely used methods of determining D are *box counting, divider, spectral analysis, line scaling, area methods, area perimeter* and *DTM triangles*. A good review of these can be found in Klinkenberg (1994), however we will not examine them in detail here as two and three dimensional distributions can be examined in more detail using semi-variogram methods which use all the data at once rather than examining a series of sections or profiles. Other reasons for using the semi-variogram are that it is already a key tool in geostatistics and is well understood, it is simple to use, and it appears to have properties that make it preferable to such methods as spectral analysis (Carr & Benzer 1991, Klinkenberg & Goodchild 1992). Semi-variogram methods have been criticised by Lovejoy & Schertzer (1987) for the fact that they only explore the nature of the self affine value fluctuations (the values at the locations and their separation distance as opposed to the geometric arrangement of the locations) but this is of no concern in geostatistics as it is precisely these value fluctuations in which we are interested. The value fluctuations are self affine because we are dealing with a different quantity, for example mineral grade, in that 'direction' as opposed to some standard distance measure in all of the co-ordinate directions.

Equation 4.11 is the same as the power model of definition 2.13 with $b = \frac{1}{2}V_H$ and $\theta = 2H$. Distributions that conform to equation 4.11 are statistically self affine since variations over any scale $r|\boldsymbol{h}|$ are related to the variations over scale $|\mathbf{h}|$ by

$$\gamma(r\mathbf{h}) = r^{2H}\gamma(\mathbf{h}). \qquad (4.13)$$

This implies that the variance at any scale can be determined by the variance measured at any other scale (Hewett 1986). In practice the experimental semi-variogram is determined from the available data using equation 2.24. If the experimental semi-variogram is plotted with log scales on both axes the slope of the fitted line is equal to $2H$ and the anti-log of the $\gamma(\mathbf{h})$ axis intercept is $\frac{1}{2}V_H$, i.e.

$$2H = \Delta \ln \gamma(\mathbf{h}) / \Delta \ln |\mathbf{h}| \tag{4.14}$$

and

$$\frac{1}{2}V_H = e^{\gamma(0)}. \tag{4.15}$$

The same precautions that would be used in semi-variogram model fitting apply to finding H (i.e. choice of lag spacing, maximum lag, number of pairs etc.). There is some disagreement in the literature (Isaaks & Srivastava 1989, Journel 1996, Cressie 1991, Shibli 1996) as to whether automatic or manual curve (line) fitting should be used for both semi-variogram models and determination of D from log-log plots. We will use linear regression to find the slope of log-log experimental semi-variograms and thus to determine $2H$. A power model with the appropriate power $2H$ can then be fitted to the experimental semi-variograms in order to determine $\frac{1}{2}V_H$. Other methods of determining D using semi-variograms are *semi-variogram integrals* (Shibli 1996) and *graded normalised sequences* (Hewett 1986).

4.3 Stochastic Fractal Simulations

There are two basic categories of fractal simulation algorithms for creation of two dimensional surfaces and two dimensional random fields. One category is based on midpoint displacement methods and the other on Fourier transform techniques. The methods in the midpoint displacement category are *basic midpoint displacement* (Voss

1988), *successive random additions* (Voss 1988), *generalised stochastic subdivision* (Lewis 1987), *modified successive random additions* (Prasad 1991) and the method of Rümelin (1990 & 1992) which we shall call the *covariance of increments* method. The methods in the Fourier transform category are the *fast Fourier transform* (Voss 1988) and the *Weierstrass-Mandelbrot function* (Voss 1988 Chu & Journel 1992). Although all of these methods and their variants maintain the fractal co-dimension of the field they do not always maintain the covariance structure and are not necessarily conditional. In addition most variants of the midpoint displacement method do not handle irregularly spaced conditioning data well. We will focus on the *covariance of increments* method as it does reproduce both the fractal co-dimension and the covariance structure and we will propose an adaptation of it to carry out geostatistical simulation with sparse irregularly spaced data in two dimensions.

Rümelin (1992) suggests how sparse irregular data might be handled but he does not provide examples or details of this. We will show that the *covariance of increments* algorithm, with some adaptations, can be used in a geostatistical framework with sequential Gaussian and/or LU decomposition conditional simulations in order to handle sparse irregularly spaced data. Within the geostatistical fractal framework we aim to reproduce a specified histogram, population mean, population variance, fractal co-dimension and spatial correlation (discussed by means of a power law semi-variogram model). The covariance of increments method allows generation of an arbitrary number of values of fractional Brownian motion in one step and simplifies if only a single value is to be simulated. It follows similar logic to the (non-fractal) LU decomposition method described by Davis (1987) and Alabert (1987) discussed in

section 3.3 but also isolates one of the conditioning values to use as an arbitrary fixed reference value. This reference value is then used to calculate increments and as a benchmark against which to gauge the scaling parameter required to implement use of the fractal co-dimension H. This allows the use of the fractal co-dimension H in a stationary structure function to determine the variance of the conditional distribution at each location to be simulated instead of using the simple kriging variance derived from geostatistical structure functions such as spherical and exponential semi-variogram models. A summary of the covariance of increments method is given below.

Consider the scheme

$$[z^{(l)}_{\alpha(NS)}(\mathbf{u}_i)] = \lambda[\, z_{(NS)}(\mathbf{u}_\alpha)] + \mathbf{Sw} \quad \alpha = 1, \ldots, n \quad i = 1, \ldots, N \qquad (4.16)$$

where $\mathbf{w}$ is a vector of independent random variables with normal distribution N(0,1), λ is an N x n matrix of weights that maintains the spatial structure of the field while estimating $z(\mathbf{u}_i)$ and $\mathbf{S}$ is an N x N standard error matrix controlling the rate of random variation necessary for each simulated value. If we now arbitrarily choose a specific conditioning value $z(\mathbf{u}_\eta)$ and reformulate equation 4.16 in terms of increments with respect to $\mathbf{u}_\eta$ we obtain

$$[z^{(l)}_{\alpha(NS)}(\mathbf{u}_i) - z_{(NS)}(\mathbf{u}_\eta)] =$$

$$\lambda'[\, z_{(NS)}(\mathbf{u}_\alpha) - z_{(NS)}(\mathbf{u}_\eta)] + \mathbf{Sw} \quad \alpha = 1, \ldots, n-1 \quad i = 1, \ldots N \qquad (4.17)$$

where λ' is an N x n-1 matrix (λ without the $\mathbf{u}_\eta$ terms). Multiplying both sides of equation 4.17 from the right by $[z_{(NS)}(\mathbf{u}_\beta) - z_{(NS)}(\mathbf{u}_\eta)]^T$ and taking expectations reduces this to

$$[C(\mathbf{u}_i - \mathbf{u}_\alpha)] = \lambda' [C(\mathbf{u}_\alpha - \mathbf{u}_\beta)] \qquad (4.18)$$

This linear system is similar to a kriging system and can be solved for λ' by Cholesky decomposition in the same fashion as the LU decomposition in section 3.3, if the two covariance matrices are known. Rümelin (1990) has shown that

$$C[(\mathbf{u}_\alpha - \mathbf{u}_\beta)] = E[(z(\mathbf{u}_\alpha) - z(\mathbf{u}_\eta))\,(z(\mathbf{u}_\beta) - z(\mathbf{u}_\eta))]$$

$$= 0.5V_H[|\mathbf{u}_\alpha - \mathbf{u}_\eta|^{2H} - |\mathbf{u}_\alpha - \mathbf{u}_\beta|^{2H} + |\mathbf{u}_\eta - \mathbf{u}_\beta|^{2H}] \qquad (4.19)$$

and this applies for any covariance matrix of the increments between any paired combination $\mathbf{u}_\alpha, \mathbf{u}_\beta, \mathbf{u}_i$ and $\mathbf{u}_j$. Note that Rümelin (1990) did not include the proportionality constant V_H as we have here (see equation 4.10 and proof in appendix D). The important thing about the covariance function in equation 4.19 is that it is intrinsic second order stationary. Having solved for λ' we can then be find λ by the inclusion of

$$\lambda_{i\eta} = 1 - \sum_{j=1}^{n-1} \lambda_{ij} \quad i = 1, \ldots, N. \qquad (4.20)$$

To obtain matrix **S** we multiply both sides of equation 4.17 from the right by $\mathbf{w}^T$ and take expectations giving

$$E[(z^{(l)}_{c(NS)}(\mathbf{u}_i) - z_{(NS)}(\mathbf{u}_\eta))\mathbf{w}^T] = \mathbf{S}. \qquad (4.21)$$

Again we multiply both sides of equation 4.17 from the right by $[z^{(l)}_{c(NS)}(\mathbf{u}_j) - z_{(NS)}(\mathbf{u}_\eta)]^T$ and take expectations and using equation 4.21 as well we arrive at

$$\mathbf{S}\,\mathbf{S}^T = [C(\mathbf{u}_i - \mathbf{u}_j)] - \lambda'\,[C(\mathbf{u}_i - \mathbf{u}_\alpha)]^T. \qquad (4.22)$$

Now **S** can be computed by Cholesky decomposition. We now have all that is required to calculate the simulation values as in equation 4.16. The notation for this computational scheme can be reduced to what is essentially a set of kriging and error variance equations where λ' is the matrix of weights without the weight of the closest point $\mathbf{u}_\eta$, i.e.

$$\mathbf{C}_{\alpha,\beta|\eta}\,\lambda' = \mathbf{C}_{i,\alpha|\eta} \qquad (4.23)$$

$$\mathbf{SS}^T = \mathbf{C}_{i,j|\eta} - \boldsymbol{\lambda}'\mathbf{C}^T_{i,\alpha|\eta} \tag{4.24}$$

Equation 4.22 reduces to

$$s^2 = C_{i,j|\eta} - \boldsymbol{\lambda}'\mathbf{C}^T_{i,\alpha|\eta} \tag{4.25}$$

when only one point at a time is being simulated. The weight for point $\mathbf{u}_\eta$ is then found by equation 4.20. From here the point estimate and variance factor can be computed. If we introduce $|\mathbf{h}|$ as a unit increment value it can be seen from equation 4.19 that $\mathbf{C}_{\alpha,\beta|\eta}$, $\mathbf{C}_{i,\alpha|\eta}$ and $\mathbf{C}_{i,j|\eta}$ are all proportional to $|\mathbf{h}|^{2H}$. Therefore the calculation of $\boldsymbol{\lambda}$ from equation 4.23 is independent of $|\mathbf{h}|$. However $\mathbf{SS}^T$ is proportional to $\mathbf{C}_{i,j|\eta}$ therefore $\mathbf{SS}^T$, or s^2, is proportional to $|\mathbf{h}|^{2H}$. Thus for any system that uses the same geometry, calculation of the variance factor at any scale r only requires $\mathbf{S}$ or s to be scaled by a factor r^H and does not require recalculation of the entire system.

This method still has the current restrictions that apply to LU decomposition, that is the number of points that can be simulated at any one time is limited to several hundred because of the size of the covariance matrices. If applied on a regular grid with conditioning data also on a regular grid, the same data location configuration exists at every simulation point (disregarding edge effects) and hence only one linear system needs to be solved. This makes a moving window implementation very fast for simulating large numbers of nodes providing regular conditioning data exists. It can with some care be applied to conditioning data that is not on a regular grid but then a different location geometry occurs for every new simulation location and a different linear system must be solved each time. Computationally this is very time consuming if we follow an LU approach simulating many points at one time.

4.4 SGFRACT

It is proposed here that a sequential approach as described previously in section 3.2 utilising an adaptation of the covariance of increments method, simulating only one value at a time, can be used to compute a geostatistical simulation when used with a sufficient number of local irregularly spaced conditioning data. Computationally solving a linear system involving only one simulation point with up to 30 conditioning values is still fast and it is reasonable to recalculate at every individual simulation point. We will call this new simulation algorithm *sequential Gaussian fractal simulation* and call the resulting computer program SGFRACT. The implementation of the scheme parallels that of sequential Gaussian simulation and is as follows.

(a) Ensure that the conditioning data is, or has been transformed to be, multiGaussian.

(b) Randomly order all locations to be simulated.

(c) Define a local anisotropic search routine to be used at every node to find a specified number of both conditioning data and previously simulated data. (Any previously simulated data become conditioning data also.)

(d) At the first (or next) randomly ordered location to be simulated, split off the closest conditioning point to act as a reference value $z_{(NS)}(\mathbf{u}_\eta)$.

(e) Calculate the fractal estimate and fractal variance to form the parameters of the conditional distribution $N(\lambda[z_{(NS)}(\mathbf{u}_\alpha)], s^2)$ at that location.

(f) Randomly select a value from this distribution to become the conditionally simulated value at that point.

(g) Repeat the procedure from step (d) until all locations have been simulated.

If at any stage the local search fails to find any conditioning data a simulated value is arrived at by an estimate of zero and a random variance between zero and one (Remember we are dealing with normal score data). If a minimum number of conditioning points is specified and at any stage the local search does not find this minimum number the node is not simulated. To overcome the potential for leaving gaps in this case an optional feedback loop can be used to check all nodes once the first random path is complete and to attempt to simulate any not assigned a value, as there should now be more previously simulated nodes to search. If after a specified number of cycles of the feedback loop a location still cannot be simulated then it is left blank.

The GSLIB FORTRAN routine SGSIM was adapted as outlined above to create SGFRACT for the implementation the following fractal simulation examples and to carry out the case study in chapter five. Points to note about SGFRACT are:

1. It does not use a covariance lookup table (although part of the subroutine *ctable* is retained as it is necessary for the search routines) as this unnecessarily complicates matters when applying the fractal algorithm.

2. A feedback loop is included so that nodes not simulated due to lack of close data can be re-examined after the first random path is completed.

3. An option is included to set the minimum number of data and/or simulated nodes that together will be used to simulate any point, thus allowing the option for nodes to be simulated entirely from previously simulated nodes without any original conditioning data.

4. A normalisation factor is applied to the square root of the fractal variance to bring the simulated population variance back to around one. This factor is not fixed and is

dependent on the geometry of the particular simulation. For example the normalisation factor changes with the model, the grid size and/or the overall field size. This normalisation factor is applied at each individual point simulation rather than at the completion of the simulation so that it does not displace the conditioning data values.

5. The option of using a two dimensional bounding polygon is also included to enable the simulation of non-rectangular fields.

6. Following Rümelin (1990) a Cholesky forward/backward substitution routine is used to solve the linear system, as opposed to the Gaussian elimination routine used in SGSIM.

7. The search radius is explicitly set by the model to equal the range and cannot be altered. This is because when trying to reproduce a sill the power model is only valid up to the range. Beyond that the structure is uncontrolled.

Fitting a power model for use with SGFRACT with bounded data involves fitting a *truncated power model*. When using normal score data the concept of range as applied to a power law model translates to be the distance at which the model semi-variance equals 1. In theory if a sill exists in the experimental semi-variogram it should occur at a semi-variance of 1. Therefore the first step when modelling a power law is to decide on the approximate lag at which the range or flattening occurs. The power $2H$ should then be determined (to one decimal place) from the slope of the linear regression of the log-log scaled experimental semi-variogram up to where the value of $|\mathbf{h}|$ equals the range. Using this value for $2H$ the power law model is fitted by eye to the data by adjusting the coefficient $\frac{1}{2}V_H$. The exact range can then be calculated by

$$a = e^{-\ln(\frac{1}{2}V_H)/2H} \qquad (4.26)$$

This range then serves as the search radius calculated by SGFRACT. The coefficient $\frac{1}{2}V_H$ could be taken directly from the regression but it is best to check the fit by eye as there may be other factors to be considered such as model fits in other directions or extremely erratic experimental semi-variogram data. If the semi-variogram being fitted has no sill then the regression and power model should be fitted up to the largest reliable lag, usually half the field size in any given direction. This system of determining the power model parameters applies unchanged for anisotropic modelling.

4.5 Examples and evaluation of SGFRACT

The aim of this example is to test the algorithm and to illustrate the working of SGFRACT rather than to check the degree of accuracy it achieves in a practical situation. In order to gauge how well SGFRACT works, the same data and parameters (where possible) were used to create a series of simulations using a modified version of GSLIB's SGSIM routine. The properties of the SGSIM(SK), where (SK) denotes simple kriging, simulations will provide benchmarks for SGFRACT. We will use the data sets *True* and *Berea* from chapters two and three.

In practice the *True* data is not known and variography and normal score transformation parameters are estimated from the sample data *Gslib97* as we have done in chapter three. In this case, in order to eliminate as many sources of variation as possible, we will use the variography and normal score transformation parameters that come from the *True* data set as input for our simulations. Note that in this case each of the sample

conditioning data will be located exactly on a simulation node. Cases where conditioning data are not located exactly on simulation nodes will be dealt with in the next chapter.

Calculation of the power $2H$ and hence the fractal co-dimension H, is shown in table 4.1 as linear regression fits on successive lags for the log-log normal score experimental semi-variogram. It should be remembered that with the power model in this situation we only want to fit the model up to the range or the lag at which the population variance of one is reached. In this case a power of 0.7 was chosen and used interactively to fit the best looking model. This gave a coefficient $\frac{1}{2}V_H$ of 0.22, in turn giving a calculated range of 8.70. A nested nugget and spherical model was fitted to the same semi-variogram for use with SGSIM(SK). The fitted models for both SGFRACT and SGSIM(SK) are shown in figure 4.3. Note that a nugget effect is not necessary when using fractal modelling in this case.

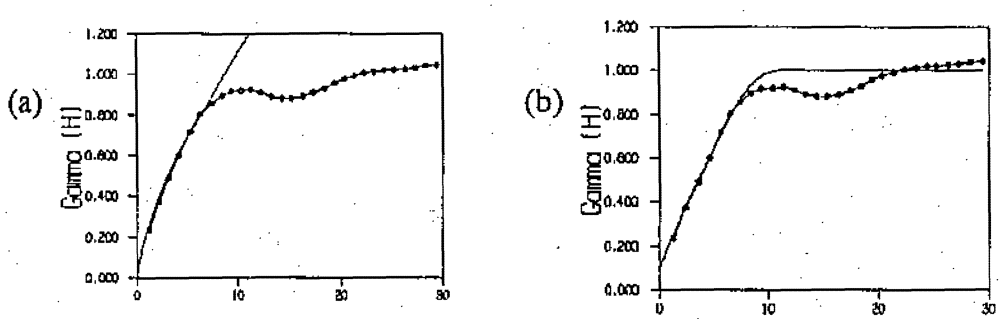

Figure. 4.3. Normal score experimental semi-variogram and fitted models. (a) Power model $\gamma(\mathbf{h}) = 0.22|\mathbf{h}|^{0.7}$. (b) Spherical model, nugget 0.01, range 11.0, partial sill 0.9.

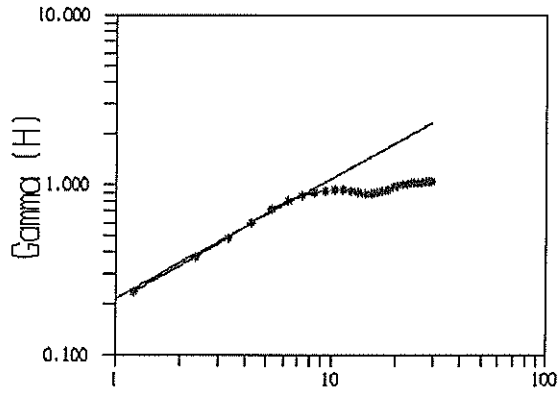

Figure. 4.4. Log-log experimental semi-variogram fitted up to lag 8.70 by power model $\gamma(\mathbf{h}) = 0.22|\mathbf{h}|^{0.7}$.

Lag	***2H***	$\mathbf{V}_H$
2.32	0.72	0.20
3.30	0.74	0.20
4.24	0.75	0.20
5.32	0.75	0.20
6.33	0.75	0.20
7.33	0.74	0.20
8.38	0.72	0.21
9.38	**0.69**	**0.21**
10.37	0.67	0.22
11.34	0.64	0.22
12.32	0.61	0.23

Table 4.1. Progressive linear regression fits to the *True* data log-log semi-variogram. Values closest to the range of 8.7 shown in bold

A sample SGFRACT calculation of the estimate, local variance and random addition will be shown below for the situation in figure 4.5. This figure shows the geometry for the first point to be simulated in the SGFRACT routine using a random seed of 112060. The ordinary kriging estimation and error variance are also given for this situation using the same power model.

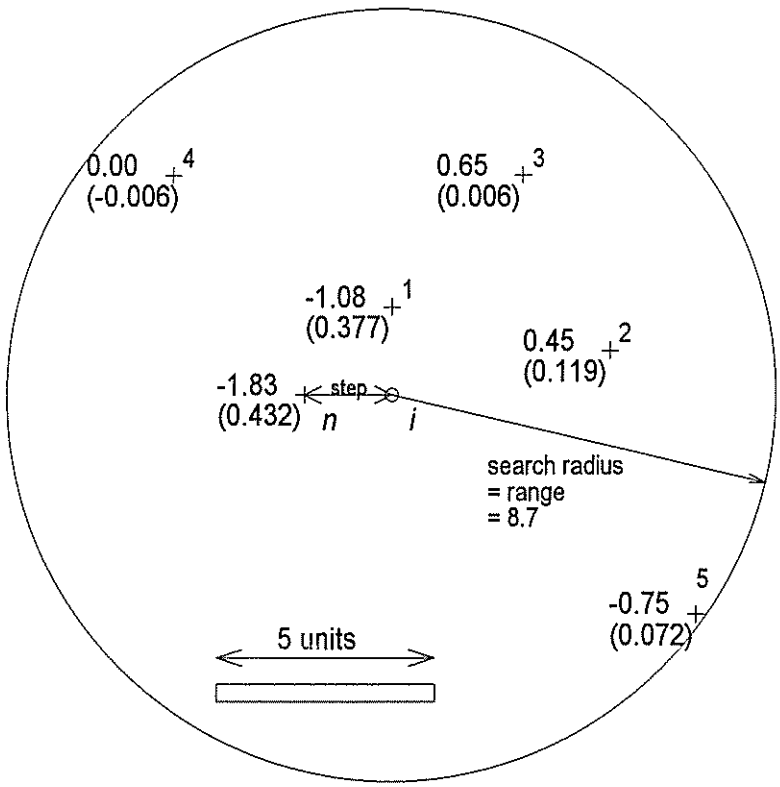

Figure 4.5. Layout of the conditioning data points used in the simulation at node (40.5x, 5.5y). Point values and (weights) are shown.

The closest conditioning point $\mathbf{u}_\eta$ is first split off to become the increment reference point. The covariance matrices $\mathbf{C}_{\alpha,\beta|\eta}$ and $\mathbf{C}_{i,\alpha|\eta}$ can then be calculated from equation 4.19. The linear system $\mathbf{C}_{\alpha,\beta|\eta}\,\lambda' = \mathbf{C}_{i,\alpha|\eta}$ can then be solved for λ' giving the following matrices (shown here rounded to 3 decimal places)

$$\underset{\mathbf{C}_{\alpha,\beta|\eta}}{\begin{bmatrix} 0.455 & 0.316 & 0.358 & 0.228 & 0.243 \\ 0.316 & 0.865 & 0.551 & 0.230 & 0.595 \\ 0.358 & 0.551 & 0.865 & 0.339 & 0.414 \\ 0.228 & 0.230 & 0.339 & 0.756 & 0.183 \\ 0.243 & 0.595 & 0.414 & 0.183 & 1.125 \end{bmatrix}} \underset{\lambda'}{\begin{bmatrix} 0.377 \\ 0.119 \\ 0.006 \\ -0.006 \\ 0.072 \end{bmatrix}} = \underset{\mathbf{C}_{i,\alpha|\eta}}{\begin{bmatrix} 0.228 \\ 0.267 \\ 0.233 \\ 0.124 \\ 0.245 \end{bmatrix}}$$

The weight for the increment reference point is simply one minus the sum of the other weights by equation 4.20. Hence the equivalence to ordinary kriging.

$$\lambda_\eta = 1-0.568=0.432$$

The estimate is then computed via $z^*(\mathbf{u}_l) = \lambda z(\mathbf{u}_\alpha),\ \alpha = \eta, 1, \ldots, 5$

$$z^*(\mathbf{u}_l) = -1.193.$$

The variance factor for this situation is then found by $s^2 = C_{l,l|\eta} - \lambda' C^T_{l,\alpha|\eta}$ which is

$$s^2 = 0.715-0.272=0.443.$$

With the inclusion of the normalisation factor of 1.13 applied to the standard deviation this becomes $s^2 = 0.567$ or s = 0.753. The random component w = -1.161 is generated and multiplied by the square root of the error variance together with the normalisation factor to give the appropriate random variation for this point. The final simulated value is then

$$z_c^{(l)}(\mathbf{u}_l) = -1.193 + 0.753(-1.161) = -2.067.$$

Using the same data, geometry and power model the ordinary kriging estimate and weights as calculated by GSLIB's OKB2D routine are exactly the same but the kriging error variance is 0.443 compared to SGFRACT's (normalised) variance factor of 0.567. Note that the fractal variance before normalisation is also exactly the same as the ordinary kriging variance.

The normalisation factor required for SGFRACT is established by starting with a value of 1.0 and running sets of ten simulations with each simulation using a different initial random seed. The normalisation factor was interactively adjusted until the set of ten simulations produced an average mean of close to zero for the simulated population and an average variance of close to one and this yielded a normalisation factor of 1.13. Ten simulations were then calculated using both SGFRACT and SGSIM(SK) and the

best three from each method were chosen as examples, where best is taken to be the closest to a population mean of zero and population variance of one as detailed in table 4.2.

	SGFRACT		SGSIM(SK)	
Seed	Variance	Mean	Variance	Mean
112060	**0.99**	**0.04**	0.86	0.03
112061	**1.00**	**-0.06**	0.86	-0.05
112062	1.08	-0.02	**0.93**	**-0.02**
112063	**0.95**	**0.03**	0.82	-0.03
112064	1.05	0.01	0.89	-0.01
112065	0.93	-0.03	0.81	-0.02
112066	0.89	0.05	0.77	0.04
112067	0.96	0.09	0.84	-0.08
112068	1.06	0.08	**0.91**	**-0.08**
112069	1.08	0.01	**0.94**	**-0.01**

Table 4.2. Population mean and variance from ten simulations with selected simulations shown in bold.

For each method a series of 100 simulations was calculated with all simulations being accepted regardless of how close they were to the desired mean and variance. These series were used to evaluate average grade tonnage curves. All simulations were then back transformed and, because the reference data set is highly skewed, a hyperbolic model was chosen for the upper tail extension with a tail length parameter of 1.5. The choice of the upper tail parameters can have a significant effect on the back transformation and care should be taken to establish a realistic tail length.

The resulting experimental semi-variograms for the three selected simulations from SGFRACT and SGSIM(SK), before and after back transformation, are shown in figures

4.6 and 4.7 together with the respective models used. Table 4.3 shows the summary statistics for the selected simulations in comparison to the *True* (Real) statistics and figures 4.8 and 4.9 show the simulation plots from SGFRACT and SGSIM(SK) respectively.

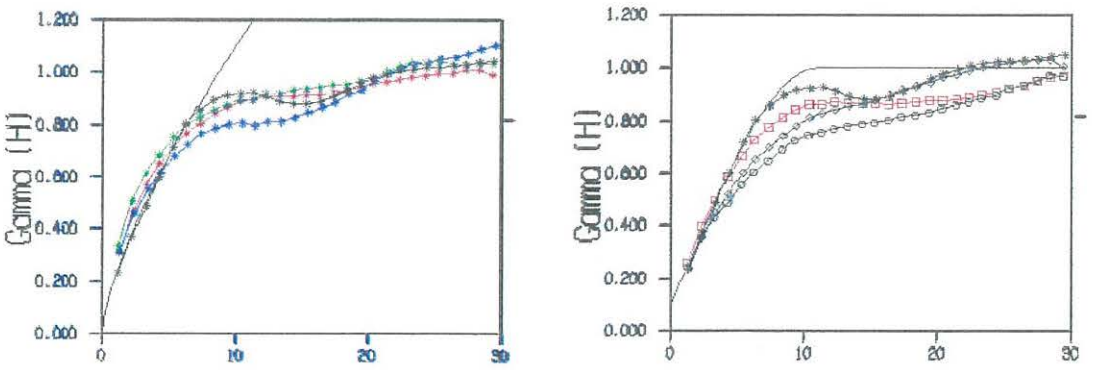

Figure 4.6. Experimental normal score semi-variograms for three example simulations, *True* data in black and model as full line, for SGFRACT (left) and SGSIM(SK) (right).

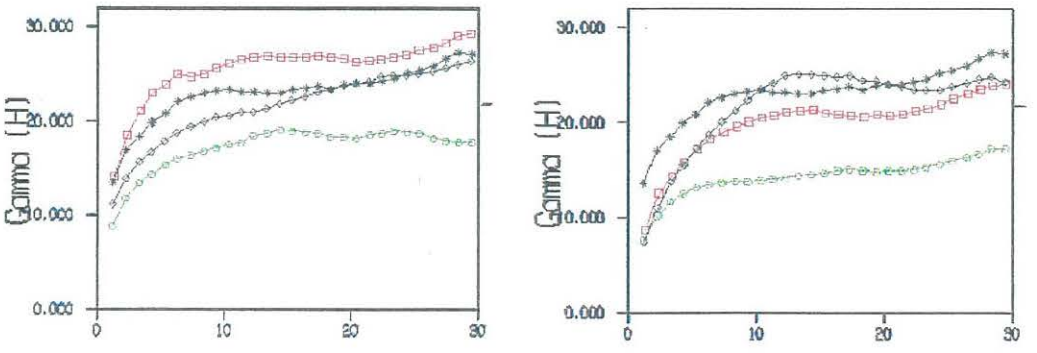

Figure 4.7. Experimental back transformed semi-variograms for three example simulations, *true* data in black for SGFRACT (left) and SGSIM(SK) (right).

	mean	variance	skewness	kurtosis	max	min
Real	0.00	1.00	0.00	3.00	3.56	-3.54
Fractal Sim. 1	0.04	0.99	0.00	2.83	3.30	-3.26
Fractal Sim. 2	-0.06	1.00	-0.09	2.91	2.94	-3.37
Fractal Sim. 3	0.04	0.95	0.06	2.94	3.57	-3.34
SG Sim. 1	-0.02	0.93	0.06	3.00	3.14	-3.39
SG Sim. 2	0.08	0.91	-0.06	2.59	3.17	-2.63
SG SIM. 3	0.00	0.94	-0.04	3.09	3.48	-3.11

BACKTRANSFORMED DATA

	mean	variance	skewness	kurtosis	max	min
Real	2.58	26.53	6.83	84.43	102.70	0.01
Fractal Sim. 1	2.68	24.57	5.02	39.60	66.51	0.01
Fractal Sim. 2	2.28	16.71	4.57	31.89	44.46	0.01
Fractal Sim. 3	2.66	28.54	6.90	84.84	107.03	0.01
SG Sim. 1	2.41	22.38	5.26	39.55	55.68	0.01
SG Sim. 2	2.55	16.19	4.36	39.65	56.52	0.03
SG SIM. 3	2.45	23.49	7.07	84.06	92.14	0.01

Table 4.3. Simulation population statistics and comparisons.

For SGFRACT the average normal score mean over 100 simulations was 0.024 and the average variance was 1.004. For SGSIM(SK) the average normal score mean was 0.029 and the average variance was 0.895. The average variance for SGSIM(SK) is unexpectedly low. The reason for this is not clear. A check set of 100 simulations was done using sample data that conformed exactly to mean 0.0 and variance 1.0 but this still returned a low value average variance of 0.922.

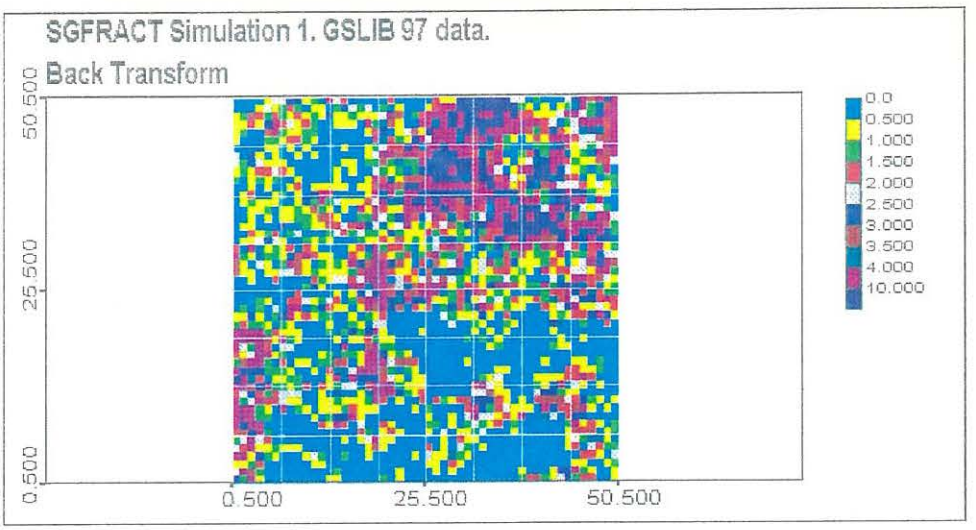

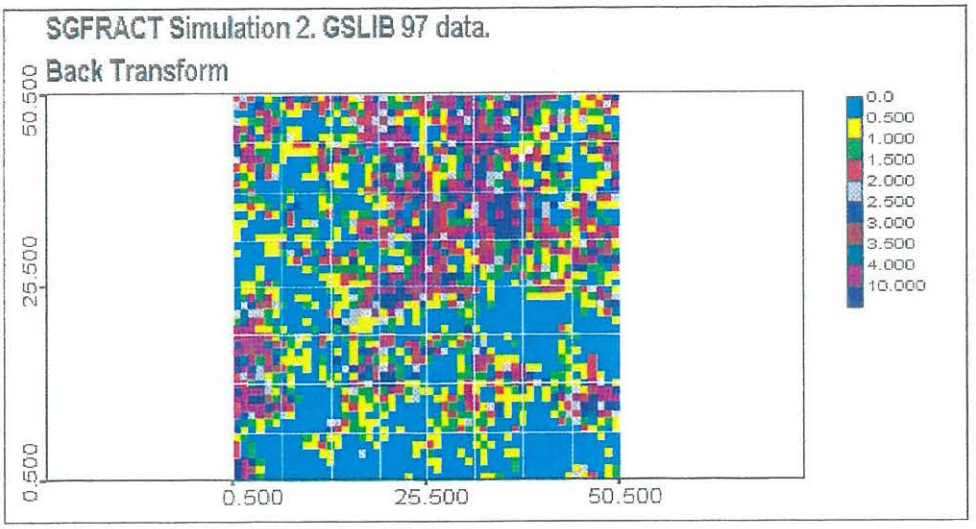

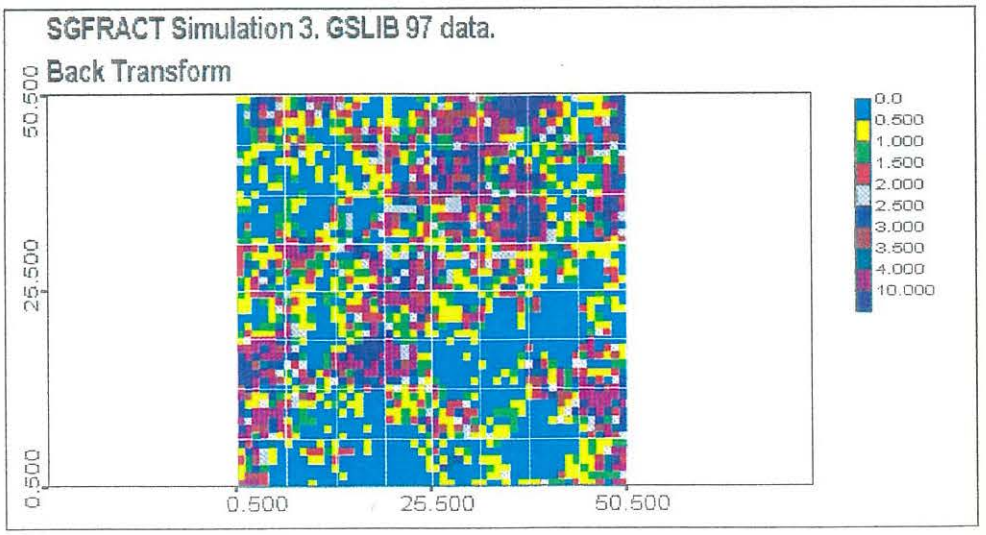

Figure 4.8. SGFRACT selected simulations.

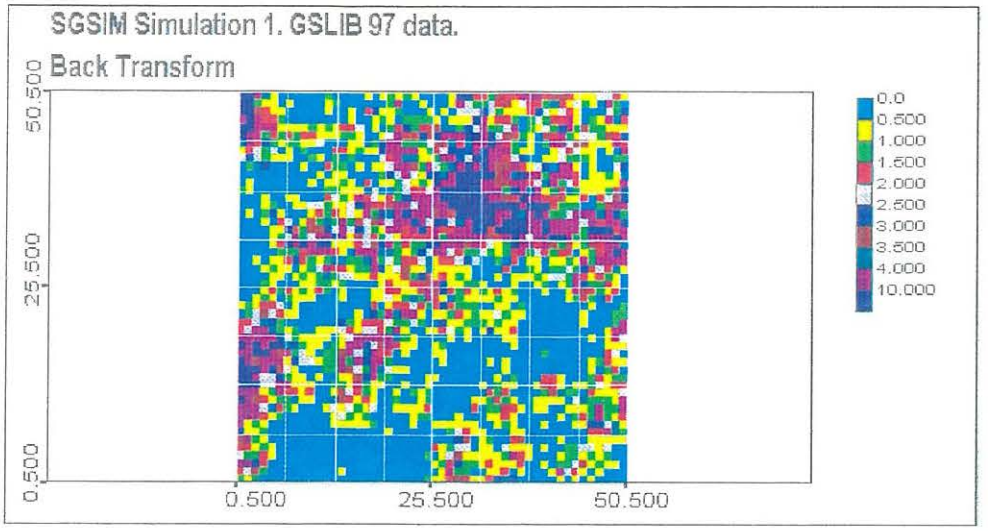

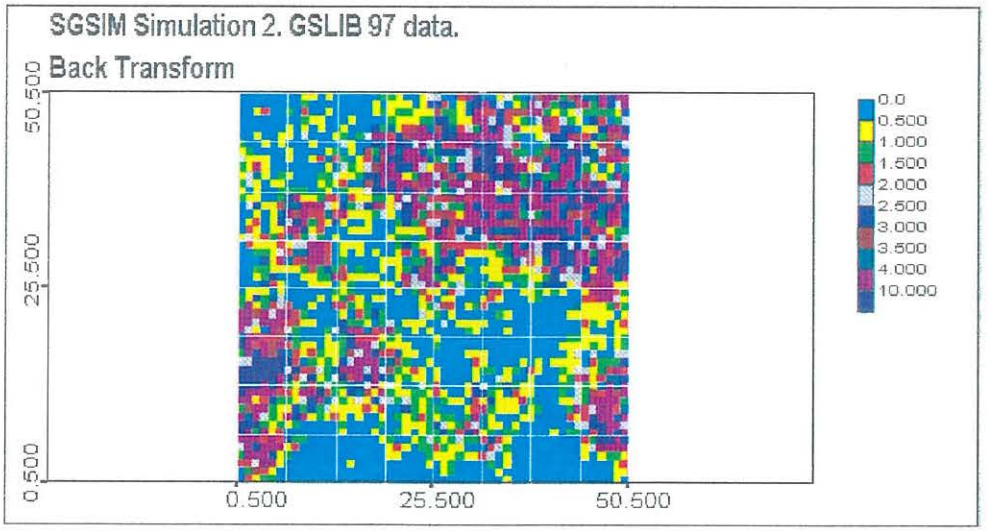

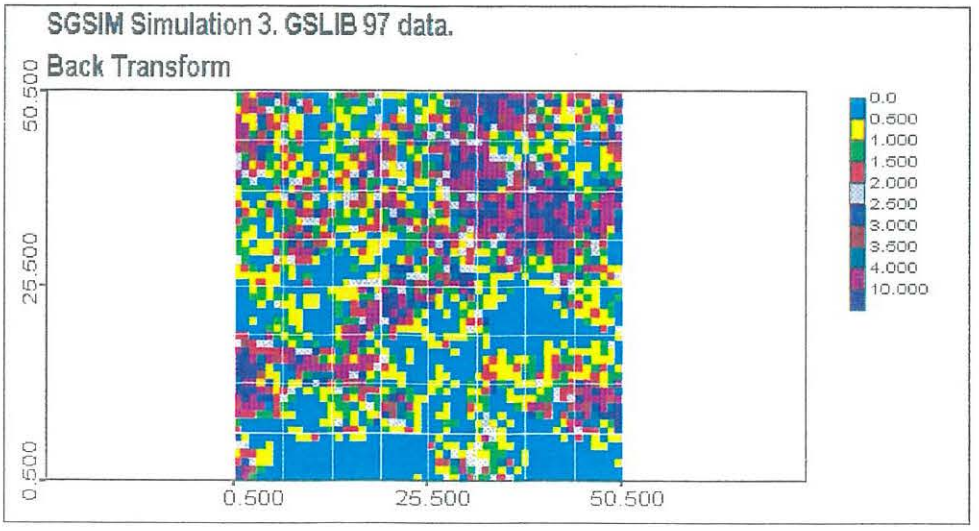

Figure 4.9. SGSIM(SK) selected simulations.

In mining operations *grade tonnage curves* are used in evaluating sample value cut offs to be used for particular areas of a deposit that will maintain a particular average grade and produce sufficient tonnage determined by the extraction and processing costs of a material. It is critical that the estimated grade tonnage curve is as close as possible to reality when evaluating an ore body and planning mining. Grade tonnage curves for this example were calculated by assuming that values are in grams per tonne and that each node represents a block of material 1m x 1m x 1m with a specific gravity of 2.5. This approximates values that would be found in a typical gold deposit. Note that in this case no correction for block support has been applied. The cut off values used in the plots below are from 0.5 g/t to 3.0 g/t. Each marker defines a 0.25g step from which can be read the average grade above that cut off and the total tonnage above that cut off. Figures 4.10 and 4.11 show the three selected simulation grade tonnage curves from SGFRACT and SGSIM(SK) respectively in comparison to the *True* (reference) curve. Figure 4.12 shows the averaged grade tonnage curves over 100 simulations for SGFRACT and SGSIM(SK) in comparison to the *True* curve.

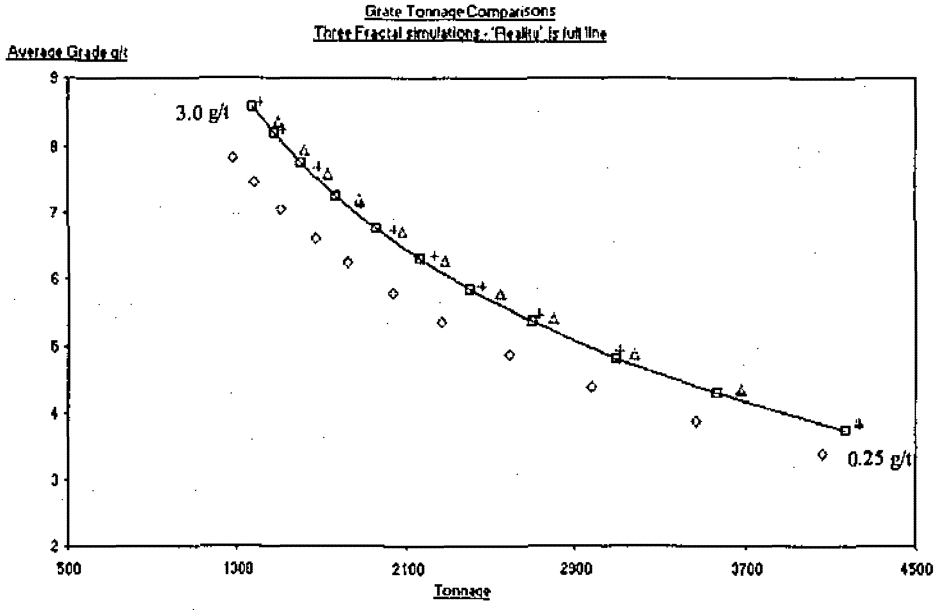

Figure 4.10. Grade tonnage curve showing three simulations from SGFRACT. The *True* reference data is full line.

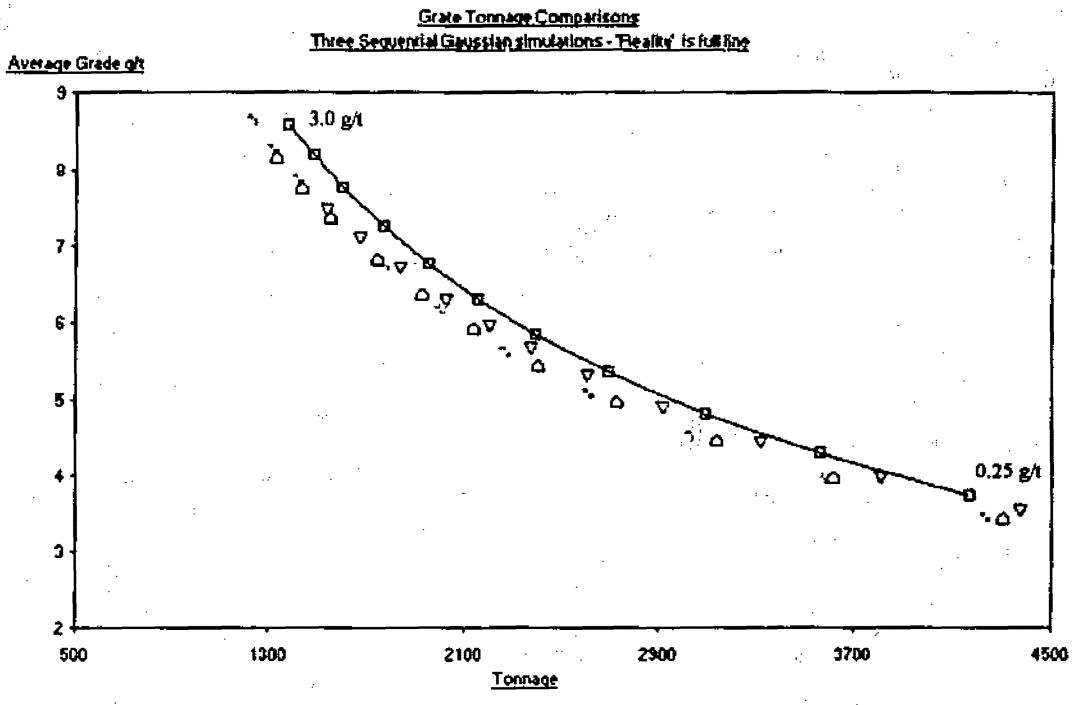

Figure 4.11. Grade tonnage curve showing three simulations from SGSIM(SK). The *True* reference data is full line.

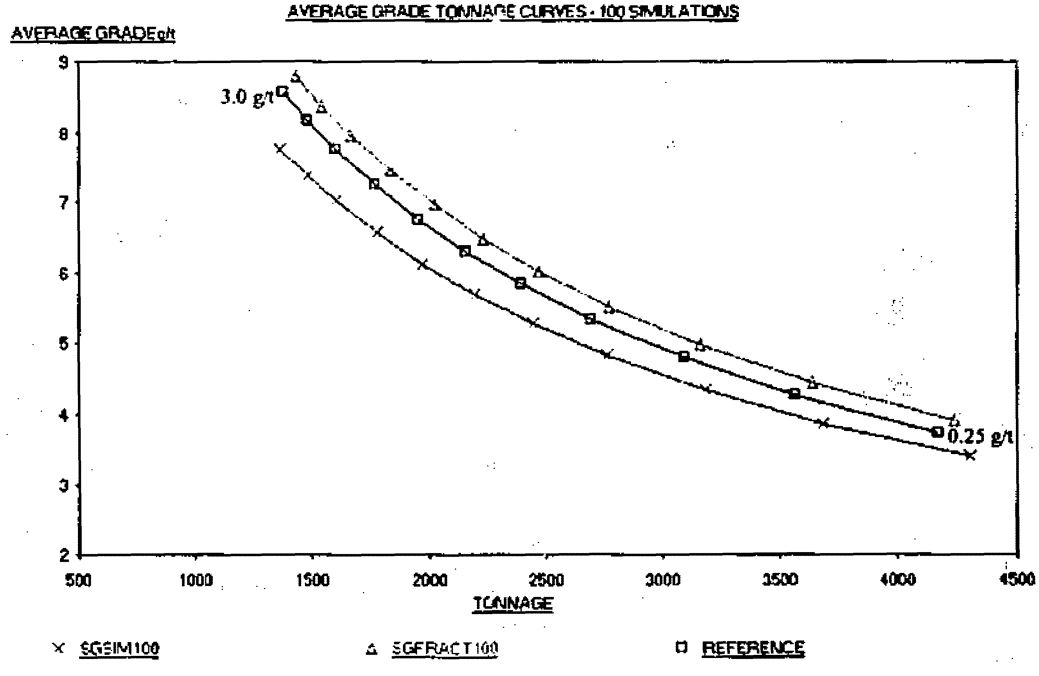

Figure 4.12. Average grade tonnage curves over 100 simulations. The *True* reference data is full line with square markers.

For the *Berea* data we will also use the variography and normal scores that are derived from the actual *Berea* data rather than the sample data in order to minimise uncertainties while testing SGFRACT. The anisotropic semi-variogram modelling with fractal power models is shown in figure 4.13. Note that use of a nugget effect is not necessary. We can calculate the anisotropy ratio τ in two ways, by simply taking the ratio of the directional ranges given by equation 4.26 as is usual, or by defining

$$\tau = \nu^{1/2H} \tag{4.27}$$

where $\nu = (\frac{1}{2}V_{H1})/(\frac{1}{2}V_{H2})$ and $\frac{1}{2}V_{H1}$ is the coefficient in the principal direction of anisotropy (Chu & Journel 1992).

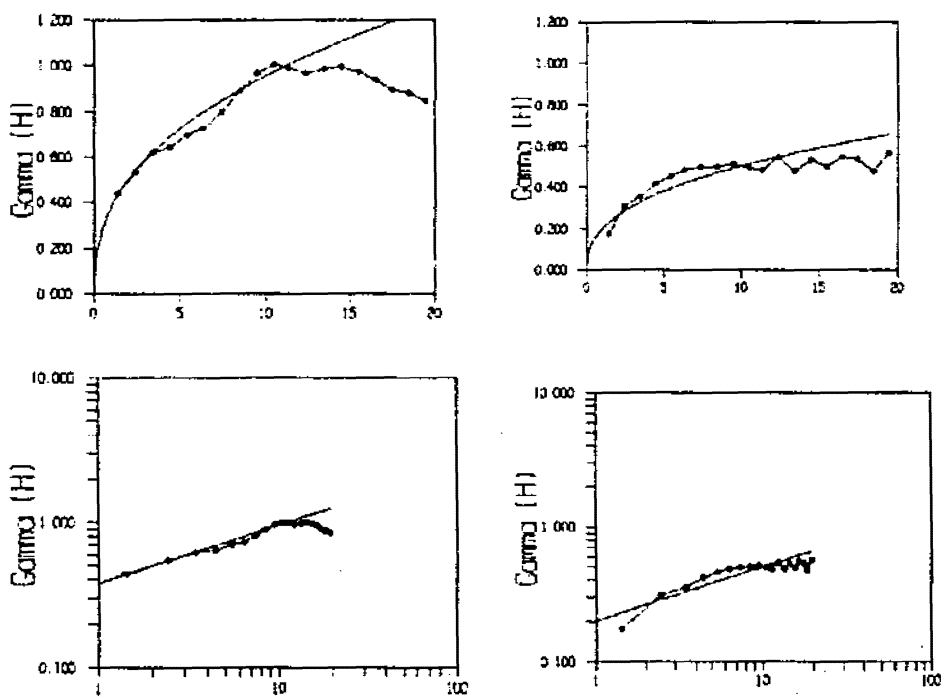

Figure 4.13. Actual directional semi-variograms from *Berea* and fitted fractal power models. At 33^0 the model is $\gamma(\mathbf{h}) = 0.38|\mathbf{h}|^{0.4}$ with a range of 11.2 (left). At 123^0 the model is $\gamma(\mathbf{h}) = 0.20|\mathbf{h}|^{0.4}$ with a range of 55.9 (right).

The same procedure as for the *Gslib97* data simulations was followed to give the simulations shown in figure 4.14.

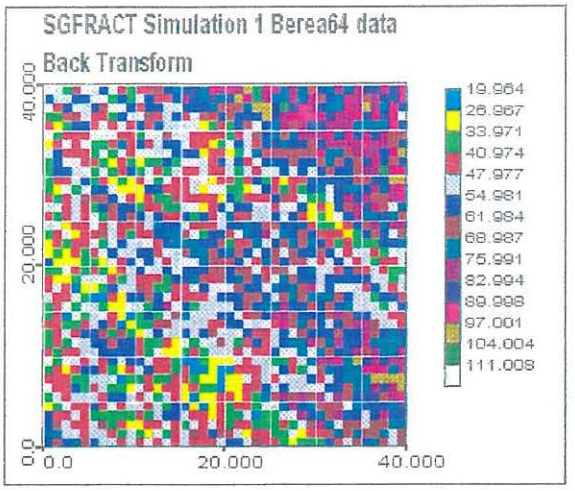

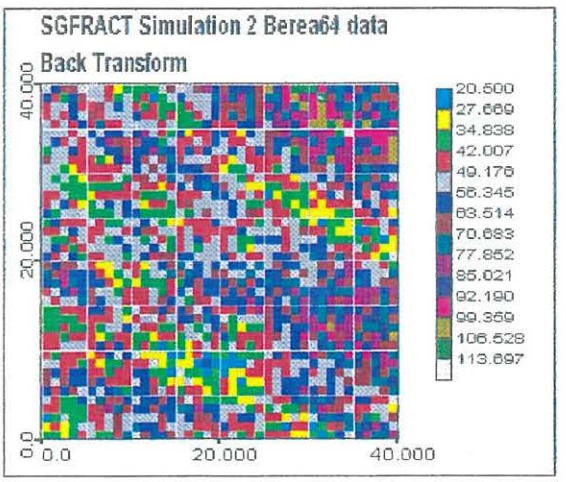

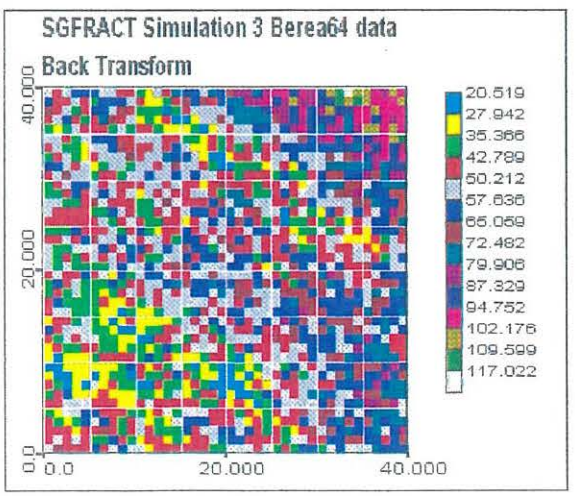

Figure 4.14. Three selected simulations from the *Berea64* data.

4.6 Summary

We have shown that SGFRACT provides estimates and error variances that are the same as ordinary kriging with a truncated power model but without having to resort to a pseudo-covariance function and without the use of the Lagrange parameter.

From examination of the three individual *True* simulations in figure 4.9 and the averaged statistics over 100 simulations it is clear that SGFRACT produces simulations that are broadly similar to those of SGSIM(SK) for this situation. Looking at the plots in figure 4.14 in comparison to the *Berea* simulation example in figure 3.7 we can see that the anisotropy is also reproduced well. Figure 4.12 shows that the average grade tonnage curve from SGFRACT is closer to the real curve than that from SGSIM(SK). We conclude that, for these two data sets, SGFRACT has, overall, performed well and that it can now be applied, and analysed in more detail, to an real industrial data set.

5 Application of SGFRACT to gold mineralisation

The aim of this case study is to evaluate how well SGFRACT reproduces grade control data from exploration data in an actual industrial example as compared to two current methods, sequential Gaussian simulation and ordinary kriging. There are many ways to evaluate the results depending on the intended use of the simulations. We will examine three selected individual simulations created by SGFRACT, SGSIM(SK) and SGSIM(OK) using exploration data and compare their individual population statistics (mean, variance, skewness, kurtosis, maximum and minimum), their normal score semi-variograms, their grade tonnage curves and their data plots with the grade control data and with ordinary kriged data. We shall also compare individual simulation averages from sets of one hundred simulations, for population mean and variance and grade tonnage curve, with grade control data. Finally we will compare the population of individual point averages over one hundred simulations with ordinary kriging estimates and data plots. The most important comparison from a mine planning point of view is that with the grade tonnage curve as, when calculated for an entire deposit, this defines the size and value of the deposit for different minimum grade scenarios. The grade tonnage curve comparisons in this case study can be viewed as an exploration to grade control reconciliation exercise. The case study will be carried out using real gold mineralisation data provided by Western Mining Corporation from the Goodall gold mine in the Northern Territory. First we give a brief summary of gold exploration and open pit mining procedures for deposits such as Goodall.

Once a mineralised target has been determined from surface mapping and sampling it will be further investigated by diamond drilling, which produces solid cores of rock, and some sort of percussion or reverse circulation drilling, which produces small chips of rock and rock dust. The diameter of these drill holes can vary from 100 millimetres to 400 millimetres depending in the type of drilling rig used. Typically one or more holes are drilled on vertical sections across the target area on section spacings of 100, 50 or 25 metres. These holes are sampled by one metre segments down the hole and may be up to 300 metres long. They are designed to intersect the potential ore body rather than to follow it in order to define its limits and are typically inclined at a dip of -60^0 to the horizontal. These holes are known as the exploration holes.

Once mining of the ore body begins, blast holes and/or grade control holes are drilled on each mining bench. A bench or level is a horizontal slice of rock that is mined at one time or one pass. These holes are typically drilled on a three to five metre grid or offset grid and are usually from 50 to 150 millimetres in diameter. They are usually drilled at between -60^0 and -90^0 from the horizontal and can be from one to 30 metres long depending on the mining method used.

In this chapter we will give a brief description of the geology of the Goodall deposit, describe the data sets we use, discuss the details of normal score transforms, variography and simulation parameters, then present and analyse the results.

5.1 Data set history and geology

The data acquired are from an area of the Goodall open cut gold mine in the Northern Territory know as A-Pod. Mining of A-Pod was completed in 1992 and all pre-mining exploration data and post mining grade control assays are available. A brief description of the geology is given below. A full description can be found in Quick (1991).

> "The mineralisation occurs on the eastern limb of an anticline in a well defined sub-vertical zone which measures up to 50m in width and 800m along strike, and up to 140m in depth. The folding is related to the F1 Howley anticline and is an open upright anticlinal fold slightly overturned to the west. Dykes have intruded after the main folding and cross-cut the fold axis. The gold mineralisation is epigenetic, structurally controlled, and is associated with thin (5 to 50 mm) vein arrays of quartz-sulphide veins which bulk to around five to 20 percent of the rock. The mineralisation occurs primarily within the sulphides. Grades are slightly higher along the eastern margin and lower in the centre of the mineralised zone."

We will use a small subset of the A-Pod data for the actual simulation examples but it is important, in the sense of potential industrial application, to have an understanding of the entire deposit, how it was formed and the implications this has when modelling the subset we are using. In effect we have a mineralised zone consisting of long narrow vertical structures which merge, separate and contain discontinuities. The subset of data we will use refers to a 2.5m thick horizontal slice through these structures.

5.2 Description of Data sets

Subsets from two raw data sets from the same region will be used in this study. The first raw data set will be called the *exploration* data set and comes from a mixture of diamond drilling core splits and percussion drilling samples taken as one metre down hole composites from holes drilled on 25 metre spaced vertical sections. The raw exploration data comprise approximately 19 000 samples. These holes are between 25 and 200 metres long. Because of the differences between diamond and percussion drilling there is potential for these two populations to exhibit different characteristics. However, the summary statistics calculated on both sets showed no great difference (see table 5.1).

EXPLORATION COMPOSITES SUMMARY STATISTICS

	mean	variance	skewness	kurtosis	max	min
Diamond split Composites	0.94	3.47	6.05	61.37	25.88	0.00
Percussion Composites	0.91	3.20	5.16	39.61	19.19	0.00

Table 5.1.

The second raw data set will be called the *blast hole* data set and consists of blast hole sampling taken as 1.5 metre down hole composites from bench by bench blast hole and grade control hole drilling on an approximate four metre by two metre spacing. These holes are between 1.5 and 12 metres deep. The raw blast hole data comprise approximately 126 000 samples. The two raw data sets need to be composited so that the samples represent the same vertical thickness and can be compared in similar regions

of space. Compositing involves calculating and assigning gold grade values to specified segment lengths located at specified positions down the hole that are different from the actual segments assayed. In this case we want to compare segments that are contained within each bench at a 2.5 metre vertical thickness. The volume of sample will be assumed to be the same for both *exploration* diamond split, *exploration* percussion, and *blast hole* data even though in reality they are all slightly different. The composited populations of the *exploration* data and the *blast hole* data sets will be called the *expcomp* data set and the *blastcomp* data set respectively (see figures 5.1 to 5.3).

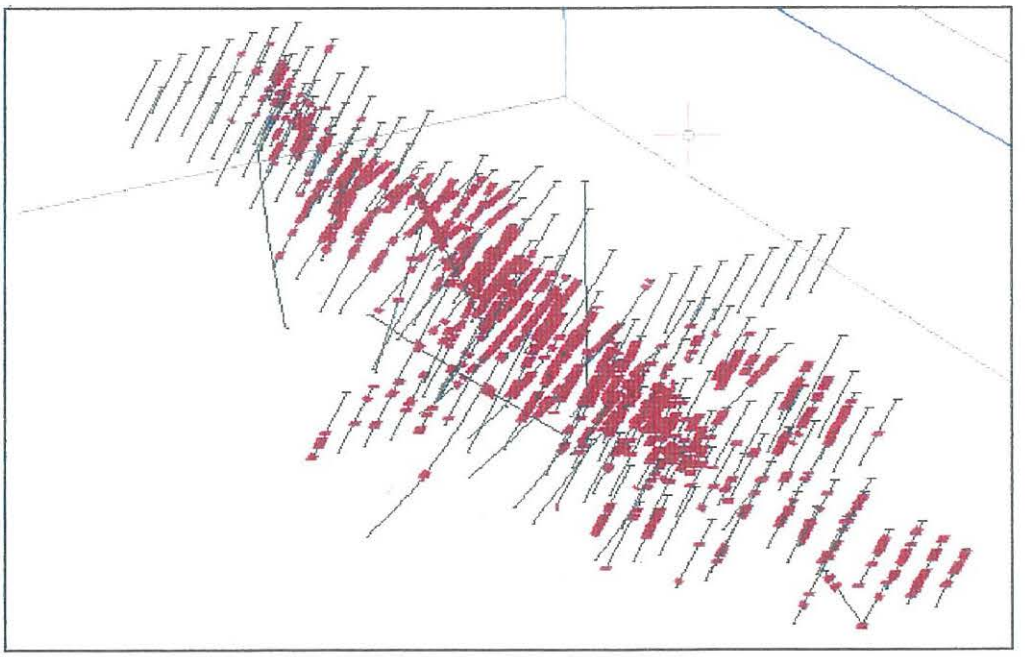

Figure 5.1. 3D perspective view of *expcomp* holes for A-Pod showing assay values above 0.5g/t in red.

Both data sets contain mineralised and non-mineralised populations and these need to be separated before processing. The separation was done by outlining the mineralised zones, in section for the exploration data and in plan for the blast hole data, determined by a 0.5 gram per tonne (g/t) gold assay cut off (figures 5.2 and 5.3). The choice of this

boundary is based on the interpretation of the zones done by the geologists at the mine as shown on the actual section plans used to determine the extent of the ore body. From the exploration sections an approximate three dimensional model was created from the section outlines in GS32 in order to visualise the approximate shape and extent of the mineralised zone.

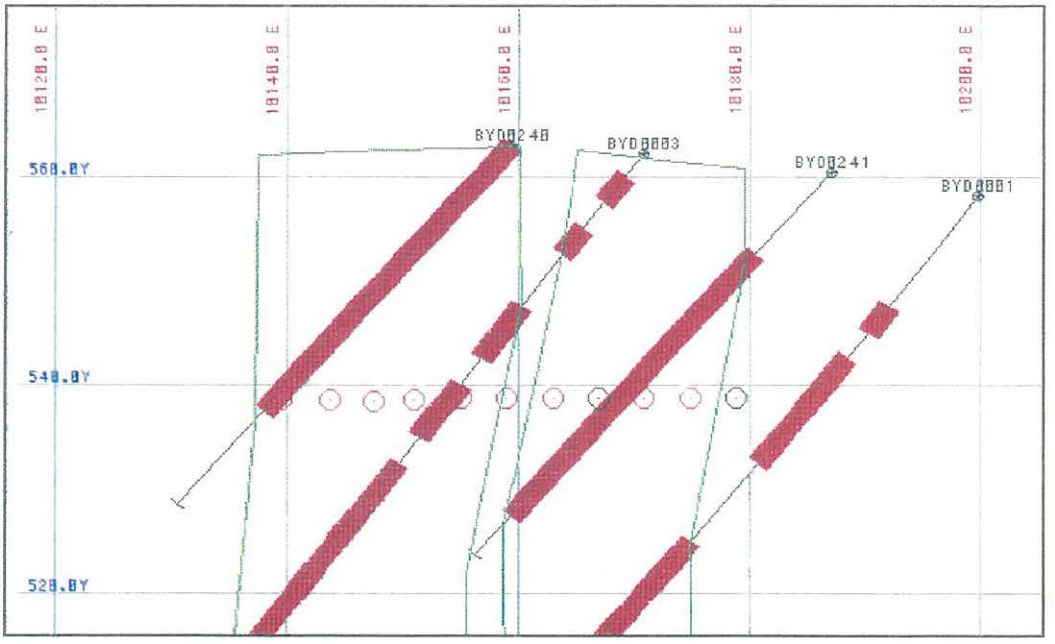

Figure 5.2. Cross section at 10900N showing mineralised zone outline (green), *expcomp* hole traces and *blastcomp* grade control for 540RL. Assays above 0.5g/t in red.

Modelling an entire three dimensional deposit would be a complicated and time consuming exercise and, in order to test SGFRACT, we will only be looking at a two dimensional subset of data from part of a single bench. The area we will examine is the mineralised zone that lies within the co-ordinates 10 800N - 11 100 N, 10 130E - 10 210E, 537.5RL - 540RL (see figure 5.3). Note that RL stands for reduced level or elevation.

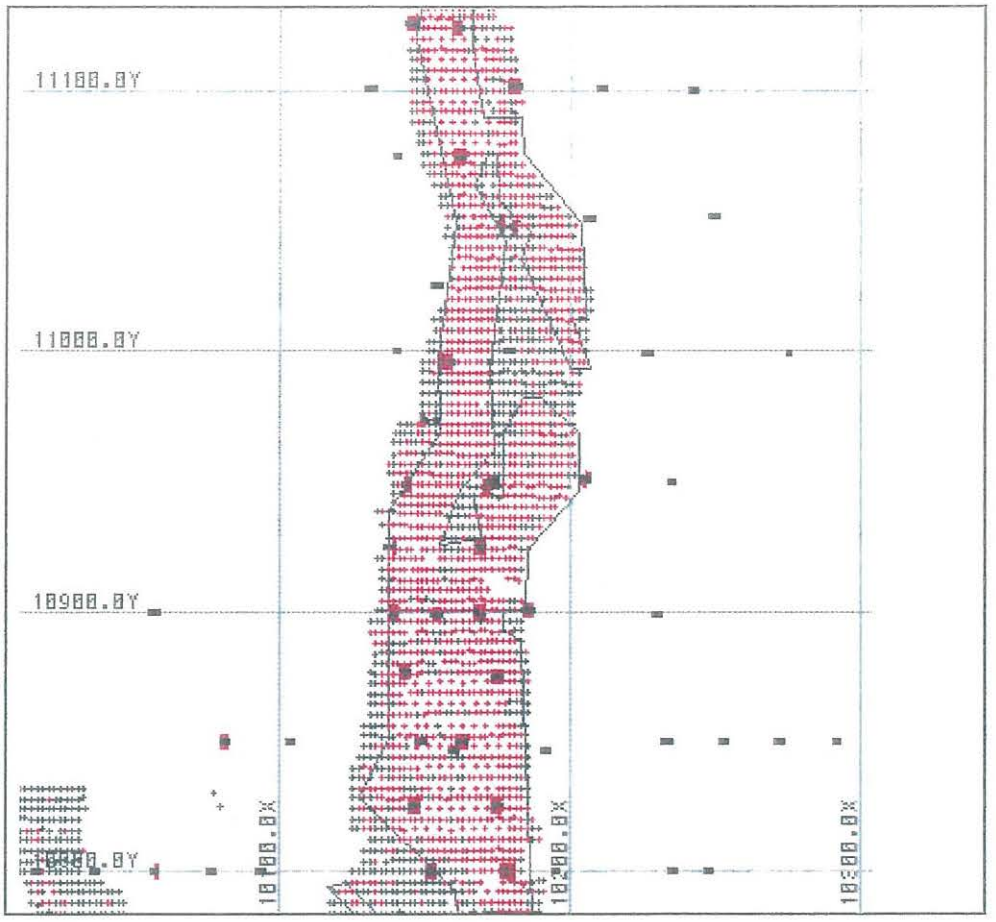

Figure 5.3. 540RL study area showing *expcomp* (large rectangles) and *blastcomp* (crosses) assays greater than 0.5g/t in red.

The subset of the *expcomp* data set that lies within this zone will be called the *exp540* data set and consists of 21 values (see figures 5.4 and 5.5 and table 5.2).

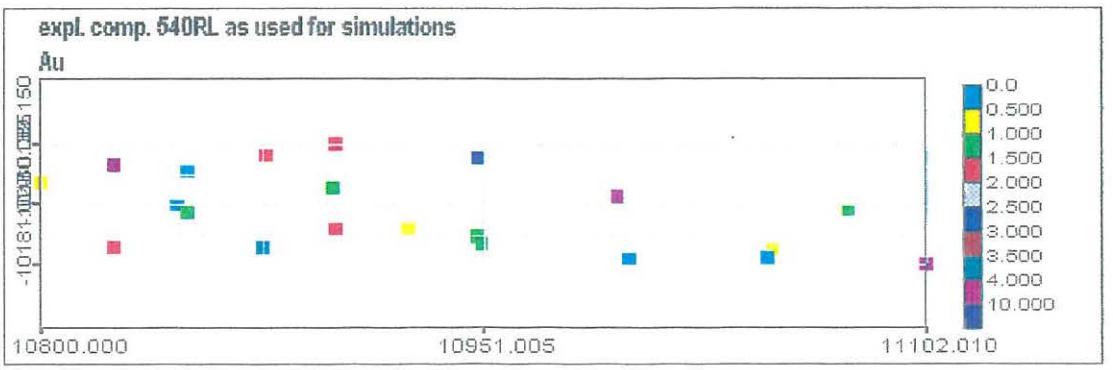

Figure 5.4. *Exp540* data plot.

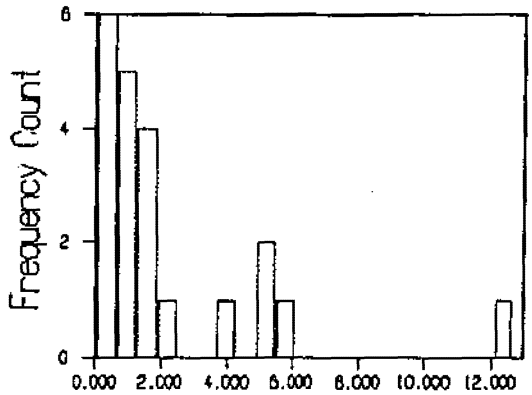

Figure 5.5. Histogram of *exp540.*

Histogram Statistics exp540		
Description = expl. comp. 540RL as used for simulations		
Tot. Population= 21	No. of Samples <= 0	= 0
Minimum Cutoff = 0.05150	Minimum Histogram Value	= 0.05150
Maximum Cutoff = 12.67830	Maximum Histogram Value	= 12.67830
No. of Samples Used = 21		
	Ungrouped Data	Data Grouped to Class Intervals
Mean	2.27361	2.27058
Median	N/A	1.19397
Geometric Mean	1.18635	1.26639
Natural LOG Mean	0.17088	0.23617
Standard Deviation	2.84947	2.81802
Variance	8.11947	7.94124
Log Variance	1.49402	1.11551
Coefficient of Variation	1.25328	1.24110
Moment 1 about Arithmetic Mean	0.00000	0.00000
Moment 2 about Arithmetic Mean	8.11947	7.94124
Moment 3 about Arithmetic Mean	55.05677	51.10401
Moment 4 about Arithmetic Mean	574.944	515.790
Moment Coefficient of Skewness	2.37968	2.28361
Moment Coefficient of Kurtosis	8.72108	8.17892

Table 5.2.

The subset of the *blastcomp* data set that lies within the mineralised zone will be called the *b5404x4* data set and, when thinned to eliminate holes that do not lie on the approximate 4m x 4m grid, contains 720 values (see figures 5.6 and 5.7 and table 5.3). Note that the *exp540* and *b5404x4* data sets are independent of each other in that the assays were collected at different times and with different methods.

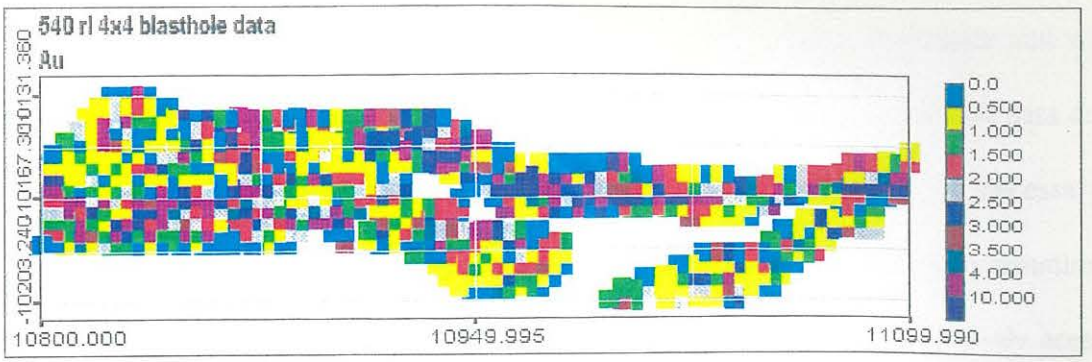

Figure 5.6. *b5404x4* data plot.

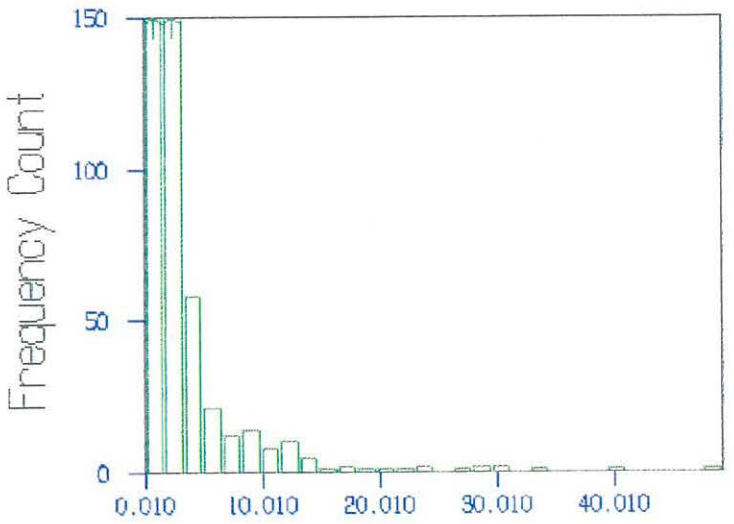

Figure 5.7. Histogram of b5404x4 data set.

Histogram Statistics b5404x4		
Description = 540 rl 4x4 ref.		
Tot. Population= 720	No. of Samples <= 0	= 0
Minimum Cutoff = 0.00990	Minimum Histogram Value	= 0.00990
Maximum Cutoff = 49.30000	Maximum Histogram Value	= 49.30000
No. of Samples Used = 720		Data Grouped to
	Ungrouped Data	Class Intervals
Mean	2.76546	2.83038
Median	N/A	1.46317
Geometric Mean	1.37625	1.65039
Natural LOG Mean	0.31936	0.50101
Standard Deviation	4.61701	4.56990
Variance	21.31682	20.88399
Log Variance	1.37523	0.80606
Coefficient of Variation	1.66953	1.61459
Moment 1 about Arithmetic Mean	0.00000	0.00000
Moment 2 about Arithmetic Mean	21.31682	20.88399
Moment 3 about Arithmetic Mean	471.432	462.493
Moment 4 about Arithmetic Mean	15233.456	14796.265
Moment Coefficient of Skewness	4.79000	4.34601
Moment Coefficient of Kurtosis	33.52382	33.92542

Table 5.3.

Normally we would not know the variography of the *b5404x4* data in advance and we would therefore have to estimate it from the sample data we have. The *exp540* data do not contain enough values to properly estimate the variography and it will be necessary to use a larger subset of the *expcomp* data set to do so. We will use extra information that is available at the *expcomp* data scale to infer the variography of the study area. The variography we infer at the scale of the *exp540* data may well be different from that at the scale of the *b5404x4* data but it is the best information we have at that stage, as in practice no blast hole data would yet be available. The subset of the *expcomp* data used to infer the variography will be that which is refers to the same horizontal slice and same bounding polygon as the *exp540* data set but also includes data that is 20m vertically above and below it. This subset will be a three dimensional subset called the *expvar* data set and contains 638 values (see figures 5.8 and table 5.4).

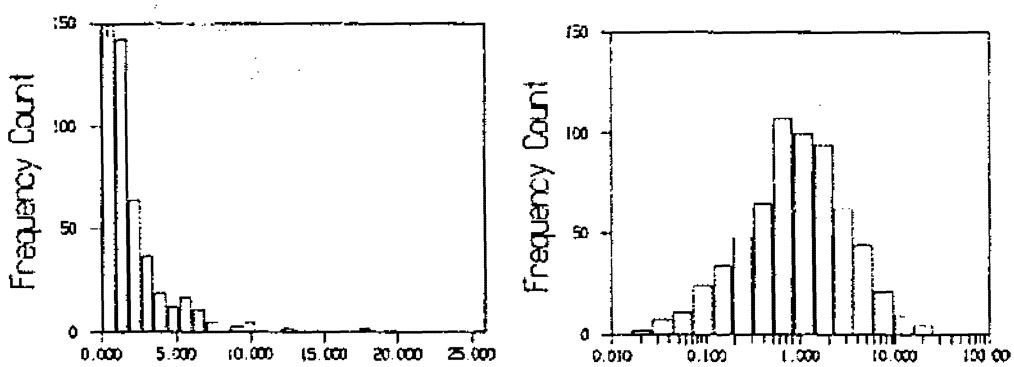

Figure 5.8. Histogram and lognormal histogram of expvar.

Histogram Statistics expvar

Description = expl. comp. 520-560RL min. zone at 540RL		
Tot. Population= 638	No. of Samples <= 0	= 6
Minimum Cutoff = 0.00000	Minimum Histogram Value	= 0.00000
Maximum Cutoff = 25.88350	Maximum Histogram Value	= 25.88350
No. of Samples Used = 638		
	Ungrouped Data	Data Grouped to Class Intervals
Mean	1.73573	1.77293
Median	N/A	0.89926
Geometric Mean	N/A	N/A
Natural LOG Mean	N/A	N/A
Standard Deviation	2.52437	2.50817
Variance	6.37243	6.29094
Log Variance	N/A	N/A
Coefficient of Variation	1.45436	1.41470
Moment 1 about Arithmetic Mean	0.00000	0.00000
Moment 2 about Arithmetic Mean	6.37243	6.29094
Moment 3 about Arithmetic Mean	64.25427	63.35739
Moment 4 about Arithmetic Mean	1074.249	1039.827
Moment Coefficient of Skewness	3.99433	4.01535
Moment Coefficient of Kurtosis	26.45418	26.27421

Table 5.4.

5.3 Normal score transforms

Both the *expvar* and *b540dx4* data sets are highly skewed and appear to approximate a log normal distribution (see figures 5.5 and 5.8). We will not use log normal transforms in our simulations but a log histogram is a useful way of viewing of a highly skewed population. The simulation algorithms SGFRACT and SGSIM require normal score data and normal score semi-variogram models as input. In this case using a normal score transform presents us with a number of problems as we have a small number of conditioning data points. If we use only the 21 conditioning data points in our *exp540* data set these will not provide enough information to model the semi-variogram and, as discussed in the previous section, they are unlikely to be a good representation of the global population and will provide poor transformation parameters. If, instead, we use the surrounding information as contained in our expanded set *expvar* to estimate

semi-variogram models and global population statistics, as we have, the subset of the normal score transform that contains the 21 sample point values will not be standard normal. In this case *exp540* has a mean of 0.29 and a variance of 0.87 rather than zero and one. The mean and variance of the back transformed population are very sensitive to the way in which values greater than the highest value in the transformation table are handled. Using a hyperbolic upper tail extension (see section 3.1) assists in reproducing a highly skewed distribution but only if the simulated normal score distribution is wider than the back transformation table used. Hence if the sample distribution has a variance less than one, few if any, of the simulation values produced with it will extend beyond the largest value in the transformation table, resulting in a lower back transform average and variance.

5.4 Modelling the spatial structure

All data will be treated as point data in two dimensional space rather than block data for the purposes of modelling simulation and estimation. Semi-variogram modelling and determination of *2H* was done using the normal score transform of *expvar*. To conform to our two dimensional sample data, the three dimensional search tolerances used were set with a small vertical bandwidth of plus or minus one metre, so that although the 638 variography data cover a 40m vertical extent, pairs are only calculated if they are in the same one metre thick horizontal slice as each other. This amounts to averaging a stacked series of 2 dimensional semi-variograms. The experimental semi-variograms were calculated with lags at intervals of four metres, angular tolerance of 30^{0} and horizontal tolerance of ten metres. The long thin nature of the layout of the data

suggests that the principal axis of any anisotropy will occur along strike in the north-south direction. The iso-semi-variogram plot is ambiguous due to the scarcity of east-west data, however semi-variograms at 0^0 and 90^0 confirm the presence of anisotropy. Note that the maximum reliable lag in the east west direction is only about 25m as the mineralised zone averages only 50m wide. Because of this, the east-west semi-variogram is very difficult to interpret and the value for *2H* as shown in table 5.5 has been calculated from the north-south direction only and then assumed for the east-west direction.

Lag	**2H**	$\mathbf{V_H}$
23.19	0.31	0.33
25.90	0.27	0.35
29.75	0.30	0.33
33.59	**0.30**	**0.33**
47.05	**0.30**	**0.33**
50.37	0.29	0.34
53.88	0.29	0.34
57.42	0.25	0.37

Table 5.5. Progressive linear regression fits to log-log normal score directional semi-variogram at 0^0 from *expvar*. Bold lettering indicates the lags either side of where the sill begins.

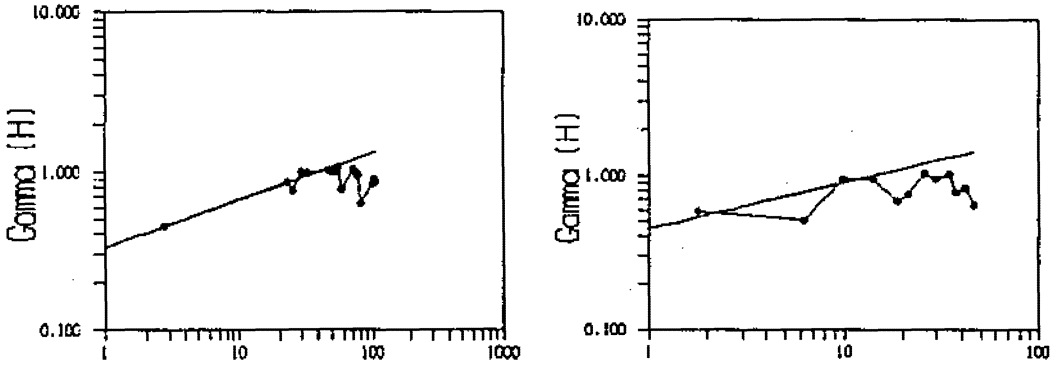

Figure 5.9. Directional log-log semi-variograms 0^0 and 90^0 fitted by $\gamma(\mathbf{h}) = 0.33|\mathbf{h}|^{0.3}$ and $\gamma(\mathbf{h}) = 0.45|\mathbf{h}|^{0.3}$ respectively.

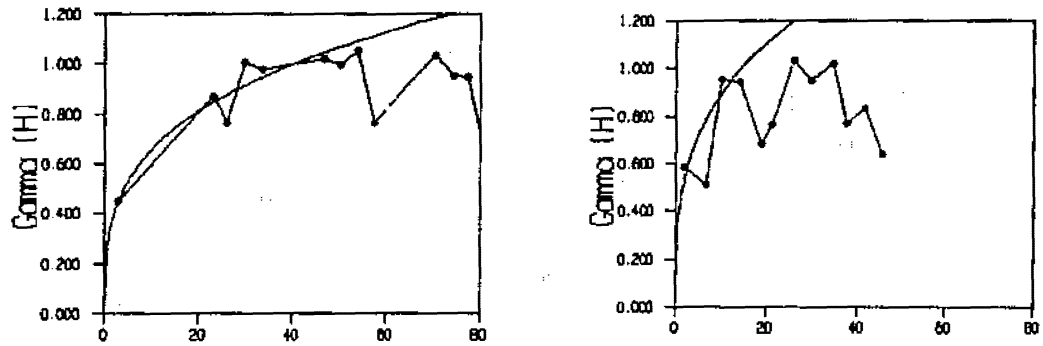

Figure 5.10. Directional normal score semi-variograms for expvar 0^0 and 90^0 fitted by $\gamma(\mathbf{h}) = 0.33\mathbf{h}^{0.3}$ and $\gamma(\mathbf{h}) = 0.45\mathbf{h}^{0.3}$ respectively.

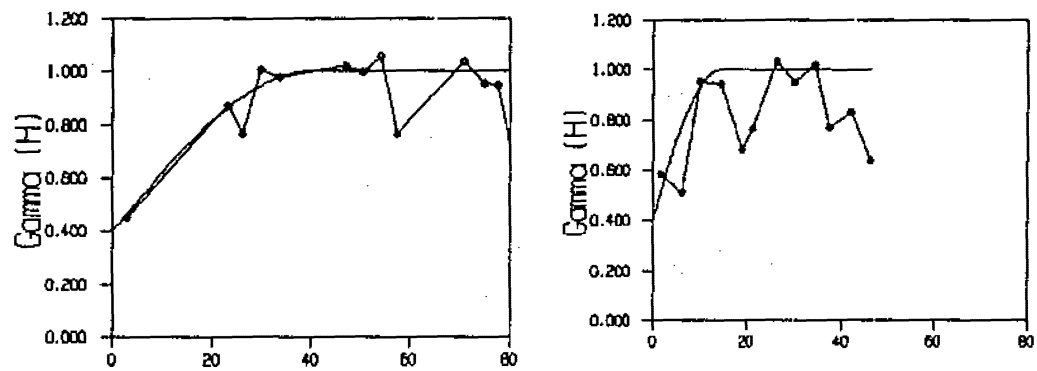

Figure 5.11. Normal score directional semi-variograms 0^0 and 90^0 fitted by nugget = 0.4, partial sill = 0.6 and ranges 40m and 14m respectively.

5.5 Simulation

The following list is an extract from the parameter file used for SGFRACT showing parameter groups (a) to (f). With the exception of the power model specification (d) and the normalisation factor (e) these parameter groups apply to SGSIM as well. Each groups will be explained in detail after the listing.

```
(a)   18   10131.3   4          \nx,xmn,xsiz
      74   10804.0   4          \ny,ymn,ysiz
(b)   0                         \0=two part search, 1=data-nodes
(c)   2                         \max per octant(0 -> not used)
      0.0 0.0 0.0 0.35 1.0      \sang1,sang2,sang3,sanis1,2
      1  16                     \min, max data for simulation
      16                        \number simulated nodes to use
      4 2                       \min data+sim nodes, fback loops
(d)   6 0.3 0.33                \it, Power=2H (aa),Constant=VH (cc)
```

```
      0.0  0.0   0.0  0.35  1.0          \ang1,ang2,ang3,anis1,anis2:
(e)   1.23                               \normalisation factor
(f)   1                                  \use bounding polygon? yes=1, no=0

Group (a)    18    10131.3    4         \nx,xmn,xsiz
             74    10804.0    4         \ny,ymn,ysiz
```

This defines the grid upon which grades will be simulated. The lower left hand corner is 10131.3E, 10804N. These co-ordinates correspond approximately to the alignment of the centres of the *b5404x4* blast hole pattern on the 540RL bench. The blast holes are usually within half a metre radius of any node on this grid. The grid is square with a four metre spacing in each direction and extends for eighteen nodes or 68 metres to the east and 74 nodes or 292 metres to the north.

```
Group (b)          0                  \0=two part search, 1=data-nodes
```

The *exp540* conditioning data are not aligned with the *b5404x4* data or with the simulation grid. This parameter gives the option to relocate the conditioning data to the closest grid node in order to speed up the search routine at the expense of a loss of accuracy. As the data set we are using is small and the conditioning data could be up to two metres away from the closest grid node we will not relocate the conditioning data.

```
Group (c)    2                        \max per octant(0 -> not used)
             0.0  0.0  0.0  0.35  1.0  \sang1,sang2,sang3,sanis1,2
             1    16                  \min, max data for simulation
             16                       \number simulated nodes to use
             4  2                     \min data+sim nodes, fback loops
```

These parameters define how the local search is carried out and which surrounding conditioning data and/or previously simulated points are used. The values of sang and sanis define the anisotropy parameters for an elliptical search in three dimensions. Here the principal axis of anisotropy is parallel to the north-south direction and no rotation on any of the three co-ordinate axes is required. The ratio of the minor and major axes

is defined by the range in their respective directions, namely 14/40=0.35. The elevation axis is not used and its ratio remains set at one. The search routine then finds all original values within this ellipse taking the closest two within each octant. It then finds all previously simulated values within this ellipse again taking the closest two within each octant. If there are more than sixteen original values plus simulated values returned then the total number is reduced to sixteen favouring the closest original values. If there is at least one original value and at least three other values simulation proceeds. If there are fewer than a total of four values found then the value at that node is not simulated on the first loop.

Group (d) 6 0.3 0.33 \it, Power = 2H (aa),Constant = $\frac{1}{2}V_H$ (cc)
0.0 0.0 0.0 0.35 1.0 \ang1,ang2,ang3,anis1,anis2:

The semi-variogram model is defined by its coefficient $\frac{1}{2}V_H$=0.33, its power 2H=0.3, and its anisotropy as described in (c). The anisotropy of the model may be different from that for the search ellipse. The value of six is a flag that tells the program that it is using a fBm model.

Group (e) 0.87 \normalisation factor

A normalisation factor of 0.87 was determined as described in section 4.4 .

Group (f) 1 \use bounding polygon? yes=1, no=0

The grid definition covers a rectangular region within which the irregularly shaped study area is contained. To restrict the simulation to only those grid nodes contained within the study area, a bounding polygon is defined as a separate file composed of vertex

co-ordinates. Note that the search routine can still find original data that is outside the bounding polygon. This may be desirable in some circumstances if only part of a simulation is required but in this study it is undesirable and is controlled by initially eliminating any original data outside the polygon.

The SGSIM program also has the option of using simple kriging or ordinary kriging for computation of the estimates. As we have very sparse data ordinary kriging is unlikely to estimate the local mean accurately and simple kriging should give a better result. However as SGFRACT produces ordinary kriging estimates only it is useful to also compare SGSIM's results with the ordinary kriging option. Both sets of results are presented.

Ordinary kriging with a power model was carried out with *exp540* in its original form (model $\gamma(\mathbf{h}) = 2.1|\mathbf{h}|^{0.3}$) and with its normal score form. These two kriged data sets will be known as *rawok* and *nsbtok*. The normal score kriging results were back transformed using the *expvar* transformation table and upper tail extension in the same way as the normal score simulations. In order to compare the different simulation methods to kriging each point in the study area for each simulation method was averaged over 100 simulations. These averaged simulations will be called *fractal100av*, *sgav100sk* and *sgav100ok*. (see figure 5.18). See also appendix E for the 'evolution' of the various Goodall data sets.

The grade tonnage curves were calculated by assuming that each value of *b5404x4* and each value of every simulated point is representative of a block 4m x 4m x 2.5m

centred on the value's location. No block support correction is applied because we are comparing point support simulations to point support grade control data. A full simulation includes all blocks whose centres lie within the bounding polygon and contains 722 blocks. The real *b5404x4* data set has 720 values. The missing values are due to the realistic imperfect nature of its grid. Because of the different random paths, some simulations contain situations where, even after feedback loops, some nodes could not be simulated due to lack of close data. These simulations have fewer than the full 722 values, the worst of the simulations having about two percent missing. When averaging each grade tonnage curve over 100 simulations this has very little effect on the results. Curves are also calculated for the point averaged sets over 100 simulations as distinct from the curve averages. Confidence limits for the average grade tonnage curves were calculated by finding the variance for each grade and tonnage above each cut off used from 100 simulations.

5.6 Analysis of results

From the first ten simulations of each method the three simulations with the best mean and variance were chosen for detailed examination. The results for these are shown in the following figures and tables. It is very encouraging to find that the fractal co-dimension in this case remains the same for the actual data and the normal score data. This was not the case with the *True* data used in chapter four, possibly because the *True* data is not real data but is itself simulated without regard to the fractal co-dimension. Table 5.6 shows that the model used and the three individual simulations examined provided a good estimate of the actual fractal co-dimension H of 0.1.

NS Semi-variogram	2H	V_H
b5404x4 (reality)	0.2	0.48
expvar (model)	0.3	0.33
Fractal Sim.1.	0.3	0.28
Fractal Sim.2.	0.3	0.27
Fractal Sim.3.	0.4	0.19
Semi-variogram		
b5404x4	0.2	11.80

Table 5.6. Reproduction of (twice) the fractal co-dimension, 2H at range = 40m.

Figures 5.12, 5.13 and 5.14 show the variography for the three selected simulations for each of the three methods, SGFRACT, SGSIM(SK) and SGSIM(OK) overlaid with the their respective models and with the *b5404x4* semi-variogram. The first chosen simulation is identified by diamond markers, the second chosen simulation is identified by circular markers and the third chosen simulation is identified by square markers. These figures show that the *b5404x4* data in the north-south (0^0) direction actually has a steeper semi-variogram in the first ten metres than any of the models or any of the simulations.

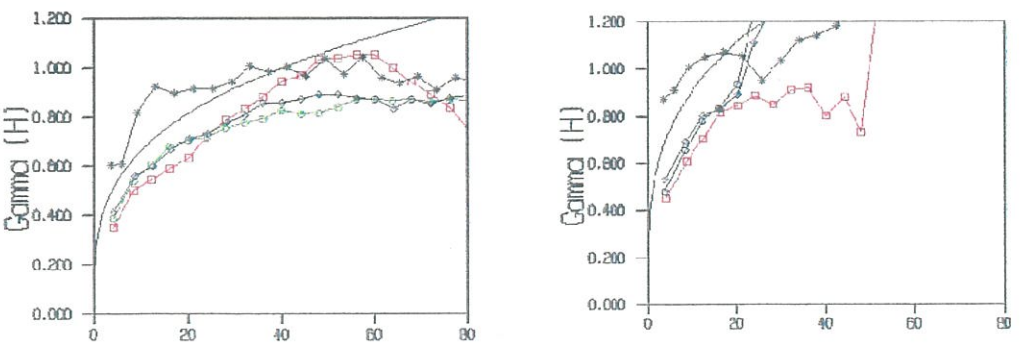

Figure 5.12. Experimental normal score semi-variograms for three example simulations from SGFRACT 0^0 and 90^0. B5404x4 in black and model as full line.

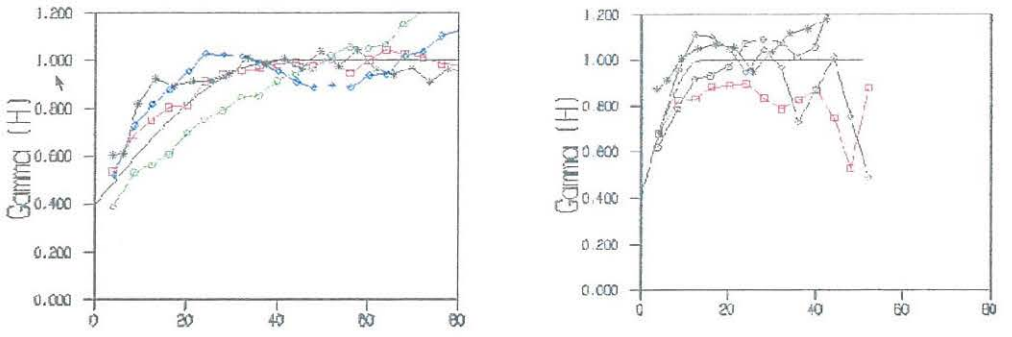

Figure 5.13. Experimental normal score semi-variograms for three example simulations from SGSIM(SK) 0^0 and 90^0. B5404x4 in black and model as full line.

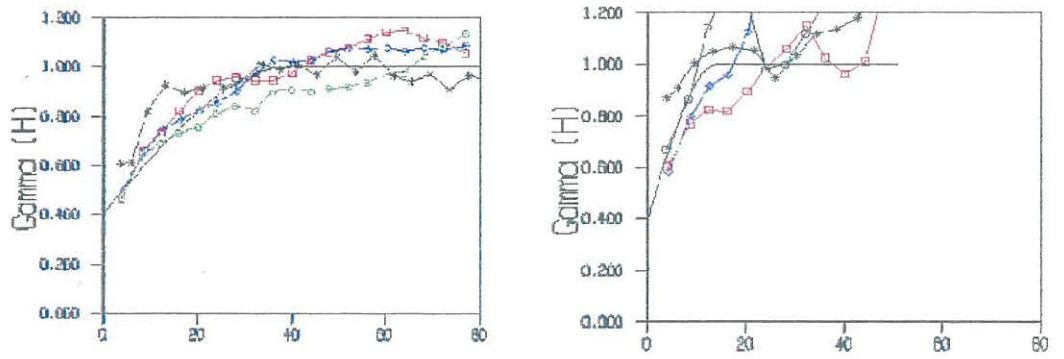

Figure 5.14. Experimental normal score semi-variograms for three example simulations from SGSIM(OK) 0^0 and 90^0. B5404x4 in black and model as full line.

It appears that the larger than expected normal score average mean obtained using SGFRACT shown in table 5.7 is due to the fact that it produces ordinary kriging type estimates rather than simple kriged estimates. Ordinary kriging with OKB2D also produces a similarly high mean when using the normal score sample data as does SGSIM(OK). SGSIM(SK), as strictly required by the theory, produces an average mean closer to the expected mean of zero.

Method	Mean	Variance
SGFRACT	0.23	1.08
SGSIM(SK)	0.08	0.96
SGSIM(OK)	0.19	1.39

Table 5.7. Average mean and average variance over 100 normal score simulations.

The larger than expected average means from SGFRACT and SGSIM(OK) indicate that *exp540* data are probably too sparse to support ordinary kriging and the use of ordinary kriging estimates may be inappropriate for reproduction of the global mean in this situation. We mentioned earlier that our input sample values were not perfectly normal with a mean of 0.29 and a variance of 0.87, and OK appears to be reproducing a mean closer to this. Subsequent simulations using the normal score transform of the 21 sample points only (giving perfect normality) gave an average mean over 100 simulations of - 0.07 and an average variance of 1.10 for SGFRACT and - 0.08 and 1.40 for SGSIM(OK). This gives a much better average mean but to back transform with this data would be inappropriate as discussed in section 5.3. In both sets of simulations with SGSIM(OK) the average variance is much larger than expected. The average variance from SGFRACT is approximately normalised to begin with so it is difficult to tell if it is being affected by the OK nature of its estimates.

Looking at the individual simulation summary statistics for both SGFRACT and SGSIM in tables 5.8 and 5.9 we see that although the normal score means and variances are reproduced reasonably, the back transformed means and variances are all considerably lower than expected. This is probably due to the input normal score samples being only quasi-normal. The lower sample variance of 0.87 leads to narrower normal score simulation distributions which do not allow as many values to fall in the sensitive upper tail region of the back transformation table. This effect can be shown in another way. If a top cut of 25g/t is applied to the 720 *b5404x4* data, with the loss of only 10 values, the mean and variance of this top cut reference data are now in more line with the individual simulations with a mean of 2.42 and a variance of 10.22.

ORIGINAL AND BACK TRANSFORMED STATISTICS

	mean	variance	skewness	kurtosis	max	min
exp540	2.27	8.11	2.37	8.72	12.67	0.05
b5404x4	2.76	21.31	4.79	33.52	49.30	0.01
Fractal Sim. 1	1.65	4.73	3.35	19.38	19.16	0.00
Fractal Sim. 2	1.92	10.81	5.86	55.08	42.64	0.00
Fractal Sim. 3	1.72	5.31	3.27	17.21	18.33	0.00
SG Sim. 1 (SK)	1.99	7.66	3.00	13.98	18.53	0.00
SG Sim. 2 (SK)	1.69	4.69	2.87	13.35	15.25	0.00
SG Sim. 3 (SK)	1.73	5.10	3.10	16.30	19.09	0.00
SG Sim. 1 (OK)	2.29	39.96	12.11	189.84	112.81	0.00
SG Sim. 2 (OK)	2.07	8.27	3.02	14.50	19.60	0.00
SG Slim.3 (OK)	1.90	7.18	3.25	16.88	22.30	0.00
NS BT OK	1.35	0.64	1.85	9.41	6.13	0.00
RAW OK	2.10	1.91	1.86	7.91	9.46	0.00
Fractal AV100	2.49	2.91	4.35	35.60	21.11	0.00
SG AV100 (SK)	1.89	0.36	2.86	21.68	8.05	0.00
SG AV100 (OK)	3.97	80.79	13.26	208.62	157.01	0.00

Table 5.8.

NORMAL SCORE STATISTICS

	mean	variance	skewness	kurtosis	max	min
exp540	0.29	0.87	-0.08	3.01	2.32	-1.87
b5404x4	0.00	1.00	0.00	2.96	3.20	-3.20
Fractal Sim. 1	-0.04	1.03	-0.19	2.99	2.82	-3.42
Fractal Sim. 2	-0.01	1.15	-0.03	3.04	3.38	-3.70
Fractal Sim. 3	0.01	0.98	-0.08	2.85	2.73	-2.95
SG Sim. 1 (SK)	0.10	1.03	0.07	2.69	2.75	-2.67
SG Sim. 2 (SK)	0.03	0.91	-0.05	2.84	2.48	-2.95
SG Sim. 3 (SK)	0.03	0.95	-0.08	3.01	2.81	-3.49
SG Sim. 1 (OK)	-0.05	1.38	-0.01	3.25	3.75	-4.16
SG Sim. 2 (OK)	0.12	1.06	0.07	2.65	2.85	-2.73
SG Slim.3 (OK)	0.06	1.03	0.01	2.98	2.98	-3.98
NS BT OK	0.20	28.00	-0.96	4.85	1.67	-1.87
RAW OK						
Fractal AV100	0.22	0.19	0.07	3.19	1.83	-0.78
SG AV100 (SK)	0.08	0.05	0.86	5.07	1.05	-0.54
SG AV100 (OK)	0.19	0.18	0.10	2.78	1.47	-0.78

Table 5.9.

Examination of the point averaged simulation sets in tables 5.9 shows an exceedingly high maximum *sgavok*. This is due to the back transformation. A few of individual simulations within the 100 produce very high point normal score values of around five. A value of five is unusual but theoretically acceptable. This did not affect the normal score point means as the few high values were absorbed by the averaging process. However, when the high values are back transformed to a highly skewed distribution using a tail length parameter of 1.5 (see section 3.2) a value of five back transforms to a value of 6890 which is unrealistic and influences the point mean considerably. This shows one of the deficiencies of using normal score transformations. Subsequent test back transformations using a more conservative tail length parameter of 2.5 give a value of 738 which is still unacceptable.

Visual inspection of the data plots in figures 5.15 to 5.19 is subjective but details of the clustering and anisotropy are best examined in this way. None of the individual simulations from any of the methods captures the elongated higher grade clustering obvious in the *b5404x4* data plot. However SGSIM(SK) appears to have done a better job of reproducing anisotropy than the other methods. The comparisons of ordinary kriging with the averaged point simulation data show that kriging still produces a smoother picture than the others.

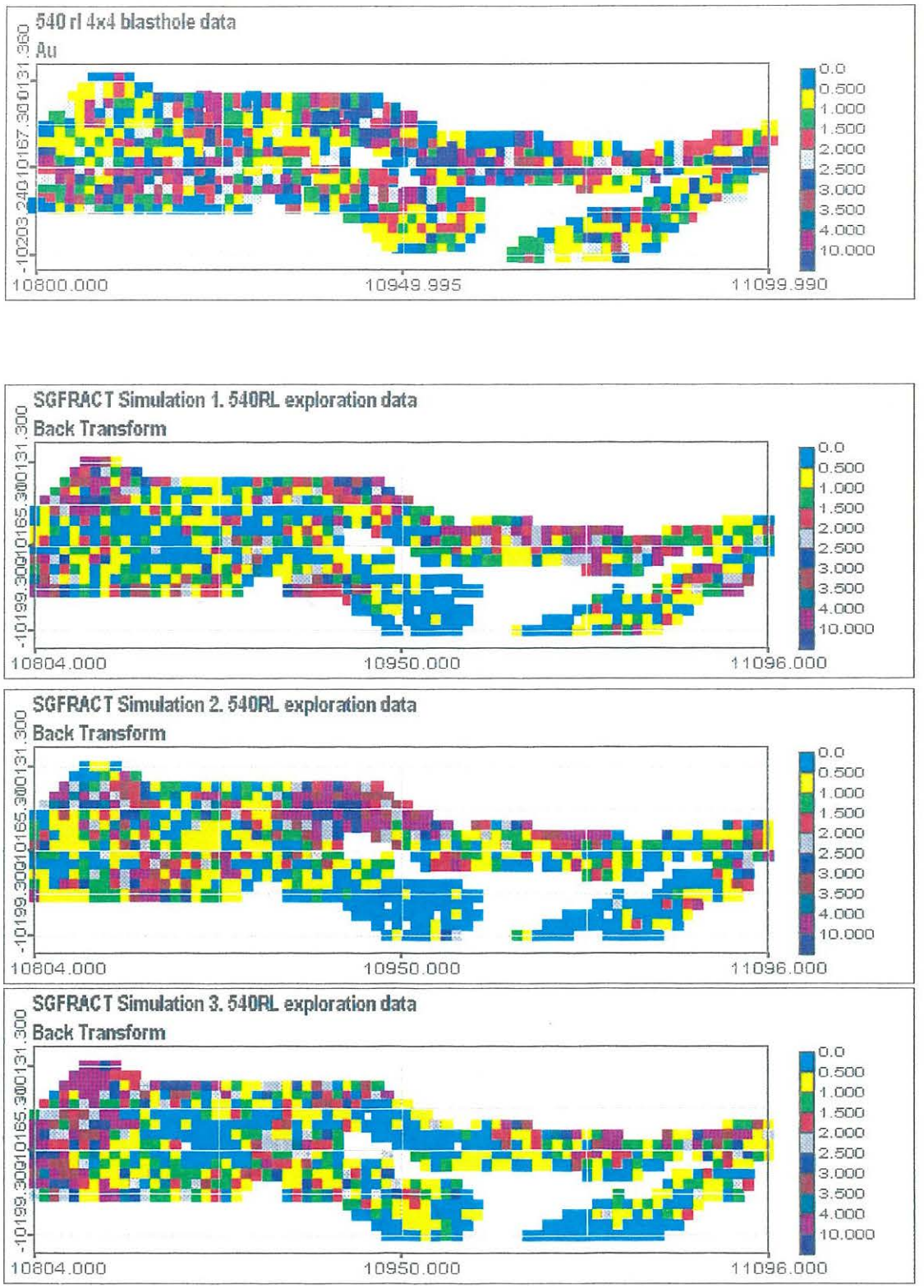

Figure 5.15. Plots of actual data values (top) compared with the three selected SGFRACT simulations.

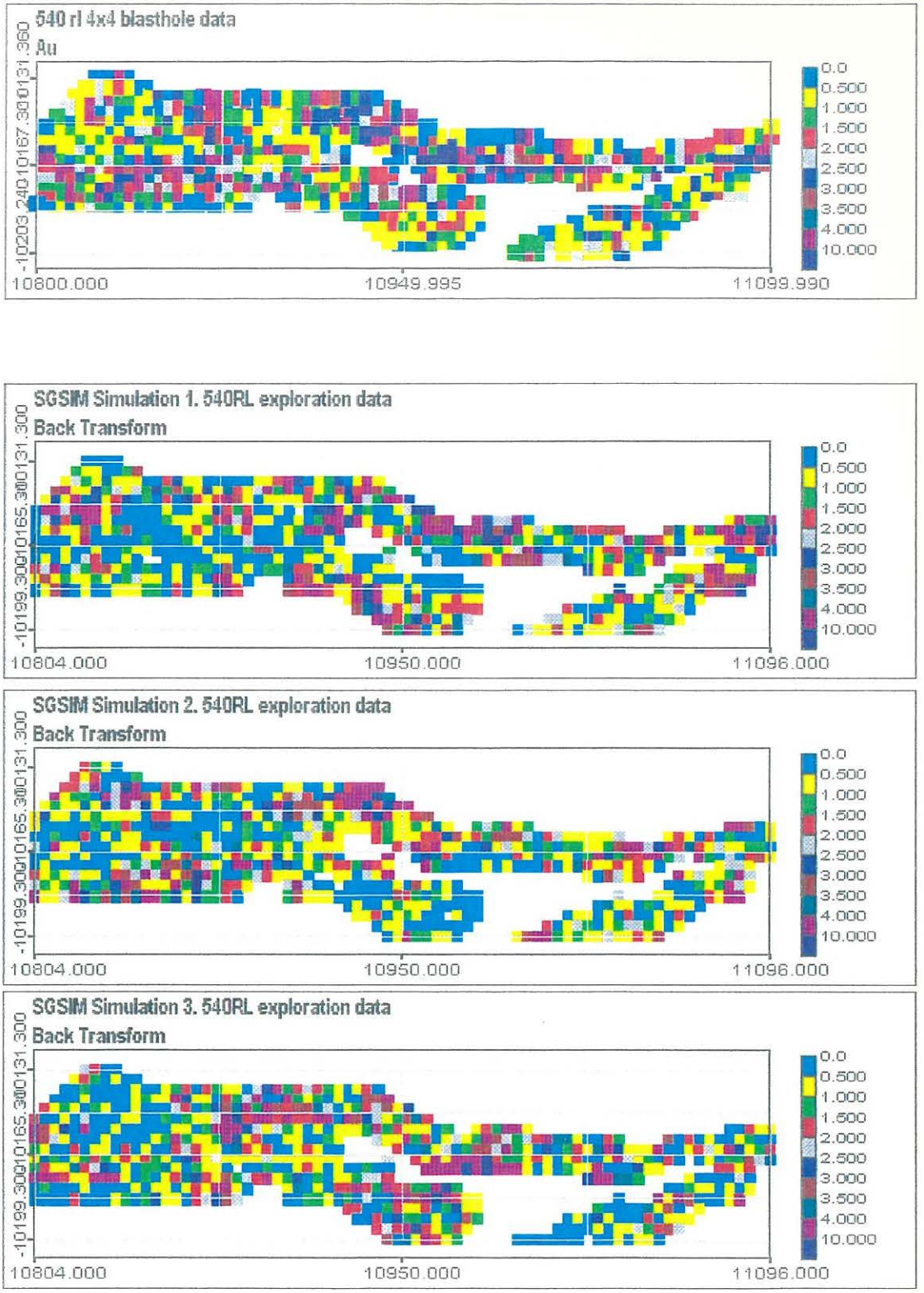

Figure 5.16. Plots of actual data values (top) compared with the three selected SGSIM(SK) simulations.

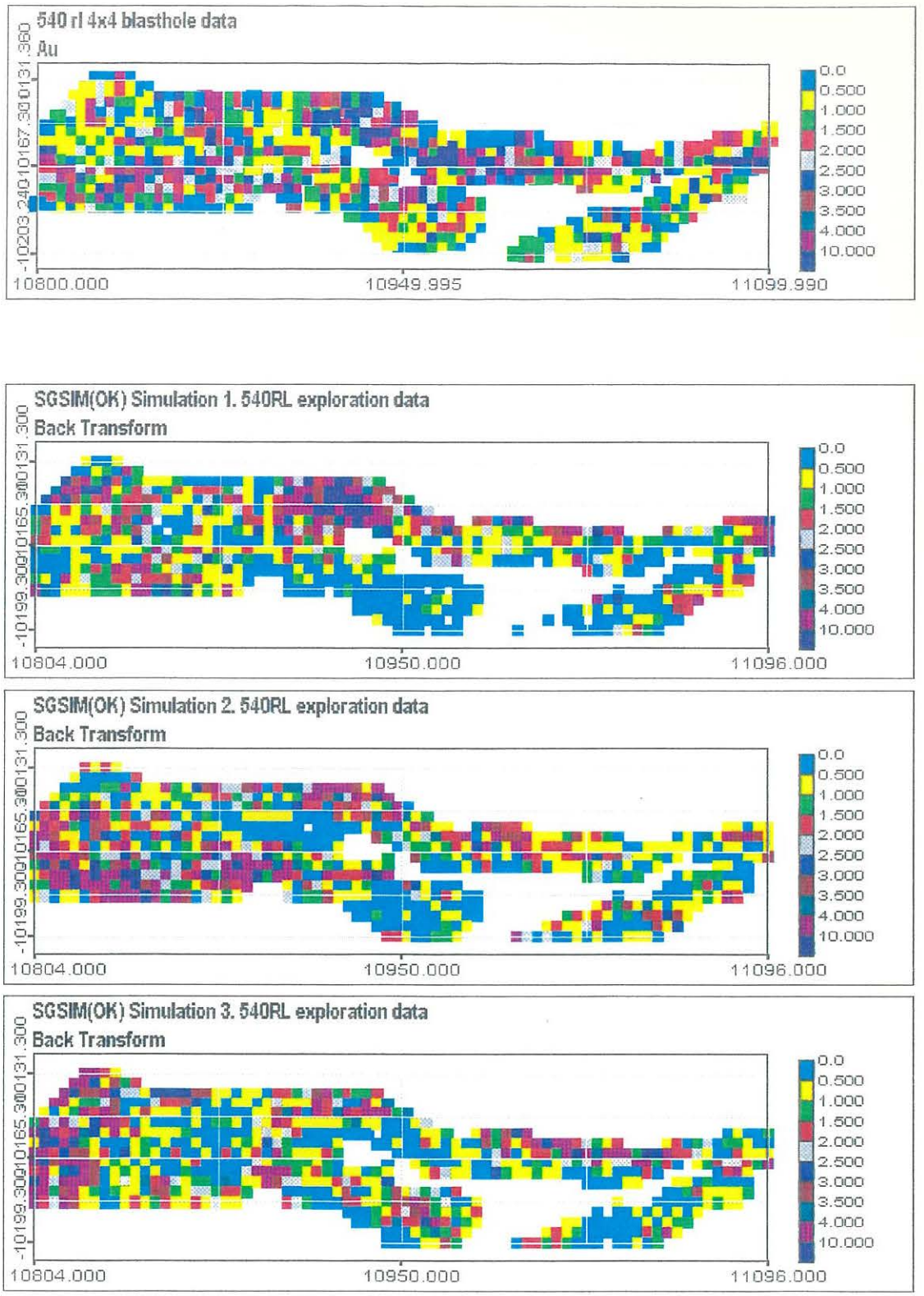

Figure 5.17. Plots of actual data values (top) compared with the three selected SGSIM(OK) simulations.

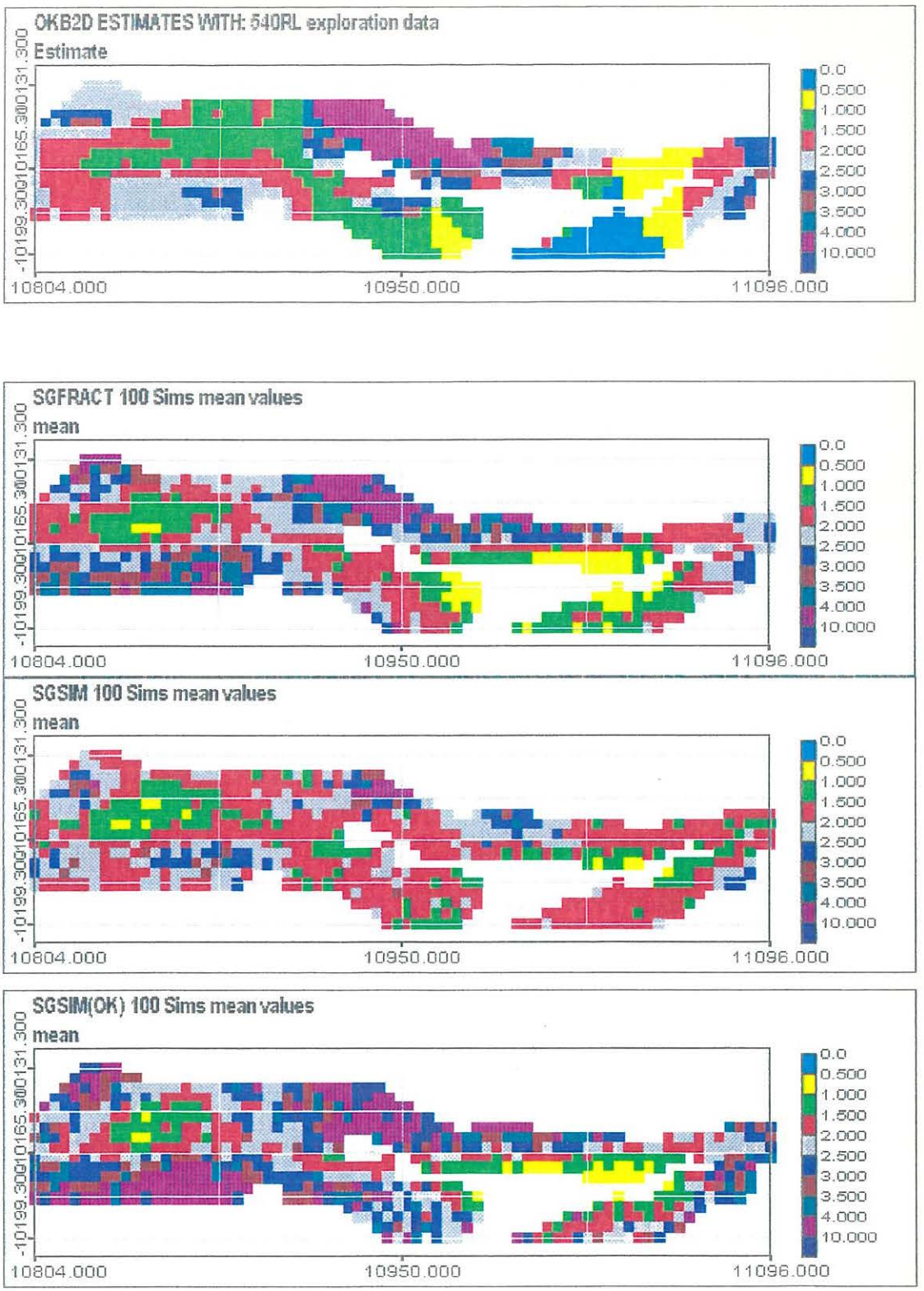

Figure 5.18. Plots of ordinary kriged data values (top) compared with the average point values over 100 simulations for SGFRACT, SGSIM(SK) and SGSIM(OK).

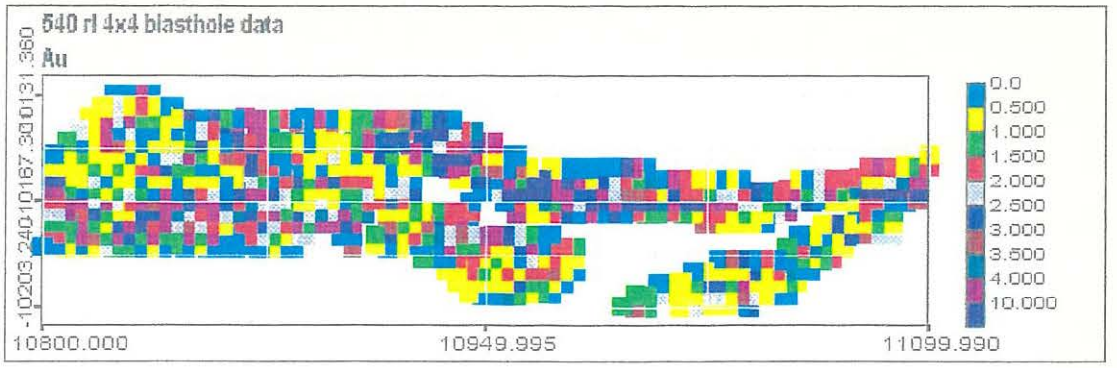

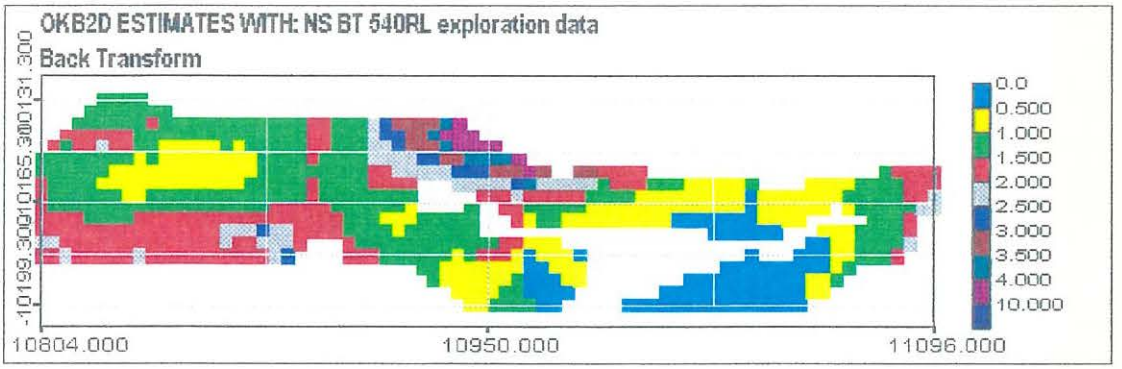

Figure 5.19. Plot of actual data values (top) compared with normal score back transformed ordinary kriging.

The results of the grade tonnage curves and their confidence limits should be considered, bearing in mind the above comments on normal score transformations and that higher average means and variances will give higher average grades at any specific cut off value. (For an explanation of how to read the grade tonnage curves refer to the text above figure 4.10 in section 4.5.) None of the kriging or point averaging methods reproduce the correct grade tonnage curve well (see figures 5.21 and 5.22). SGFRACT produces an average curve that is close to reality (see figure 5.23). Below a cut off of 2.5 g/t its average grades are very close to reality but the tonnages are lower. Above a cut off of 2.5 g/t its grades are less than in reality and its tonnages are slightly more. It can be seen from figure 5.24 that SGSIM(OK) produces grade tonnage curves that

fluctuate excessively and are unrealistic. SGSIM(SK) which gave the most acceptable normal score data back transforms to give a curve that is lower in both grade and tonnages compared with reality (see figure 5.25). Its' confidence limits are narrower than SGFRACT's and do not encompass the real curve.

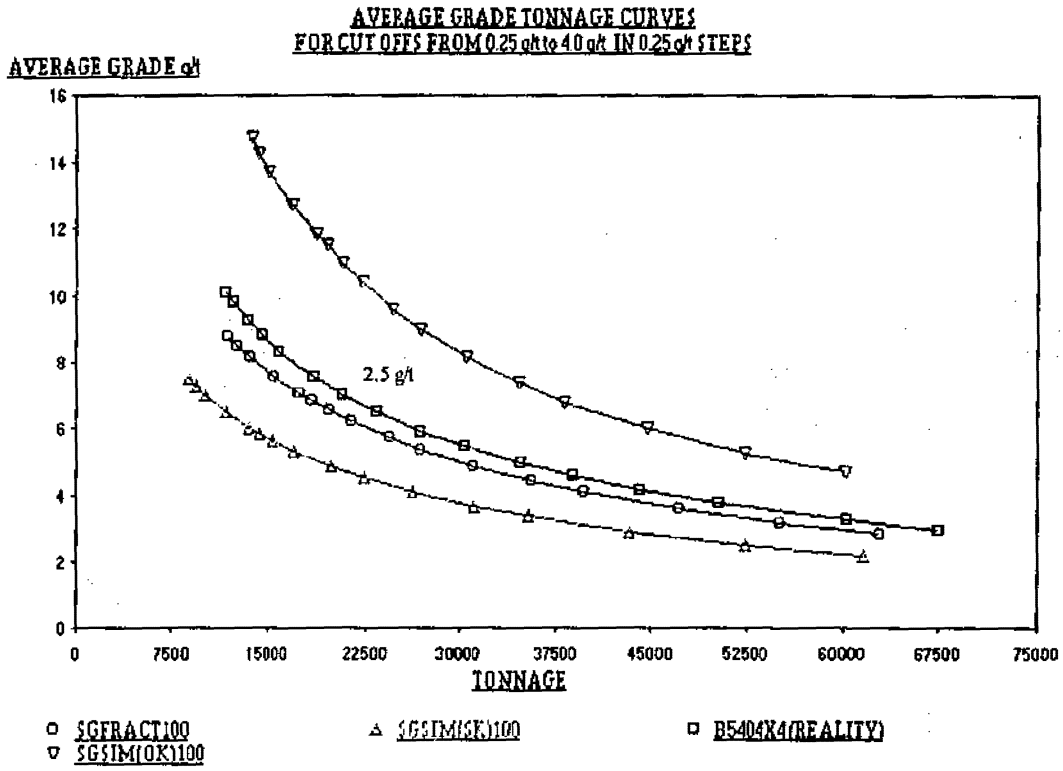

Figure 5.20. Average grade tonnage curves from SGFRACT, SGSIM(SK), SGSIM(OK) and for *b5404x4*.

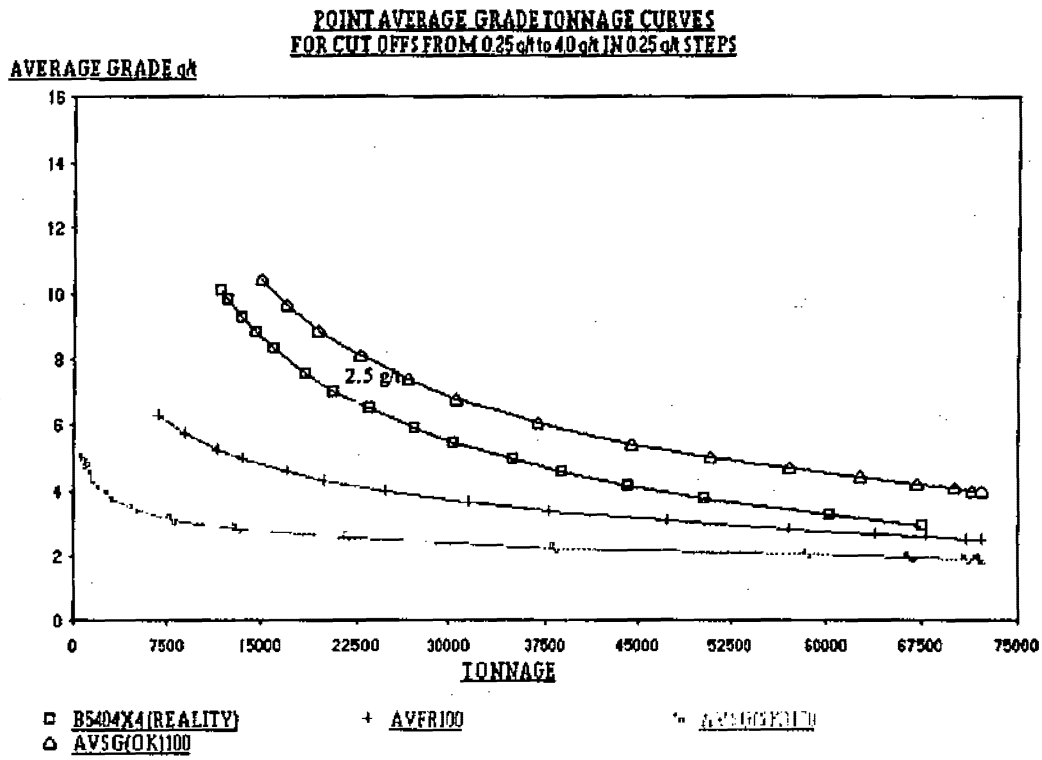

Figure 5.21. Grade tonnage curves for the point averaged simulation sets and *b5404x4*.

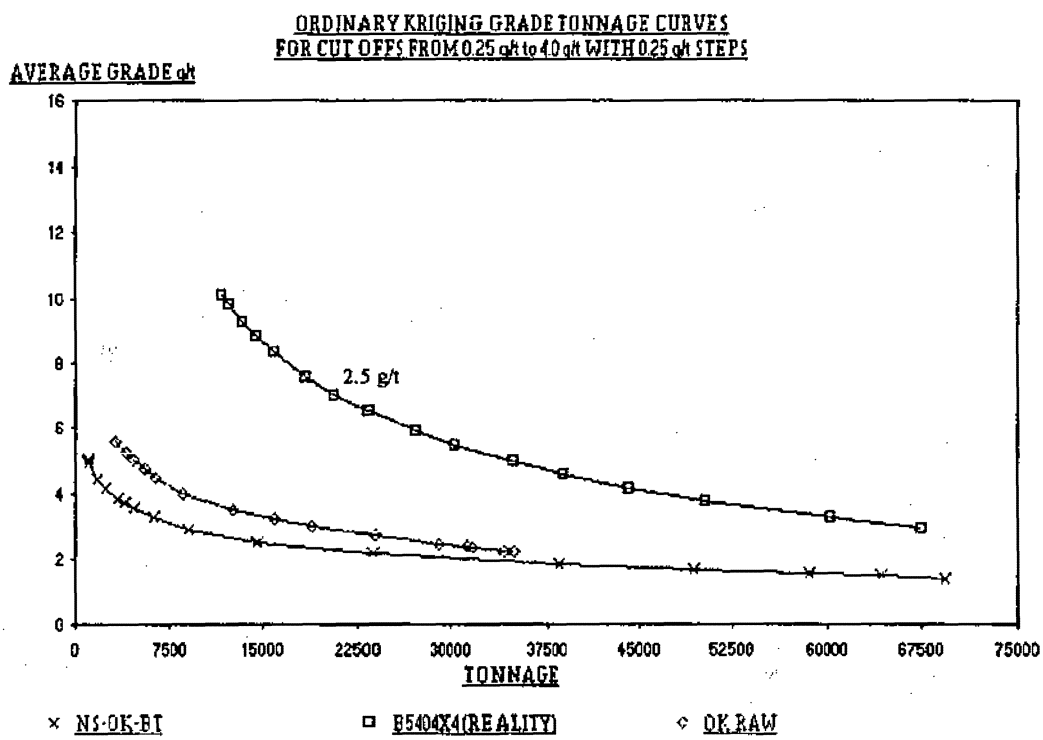

Figure 5.22. Grade tonnage curves for the kriged data and *b5404x4*.

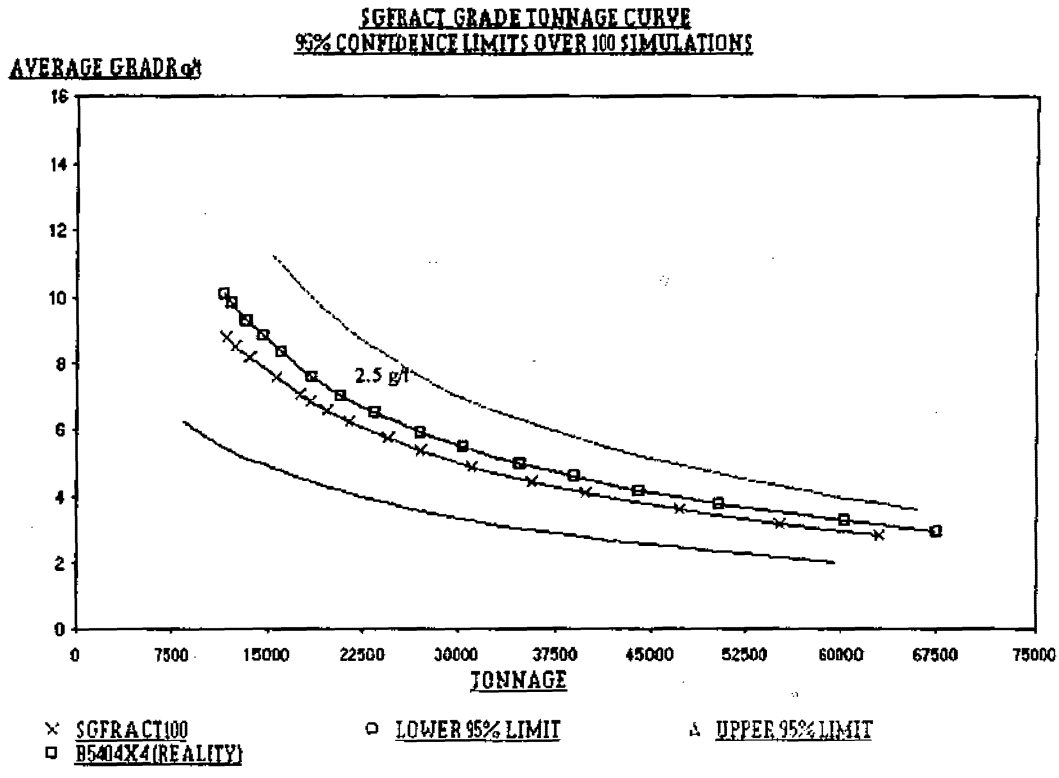

Figure 5.23. Average grade tonnage curve and 95% confidence intervals for 100 simulations of SGFRACT.

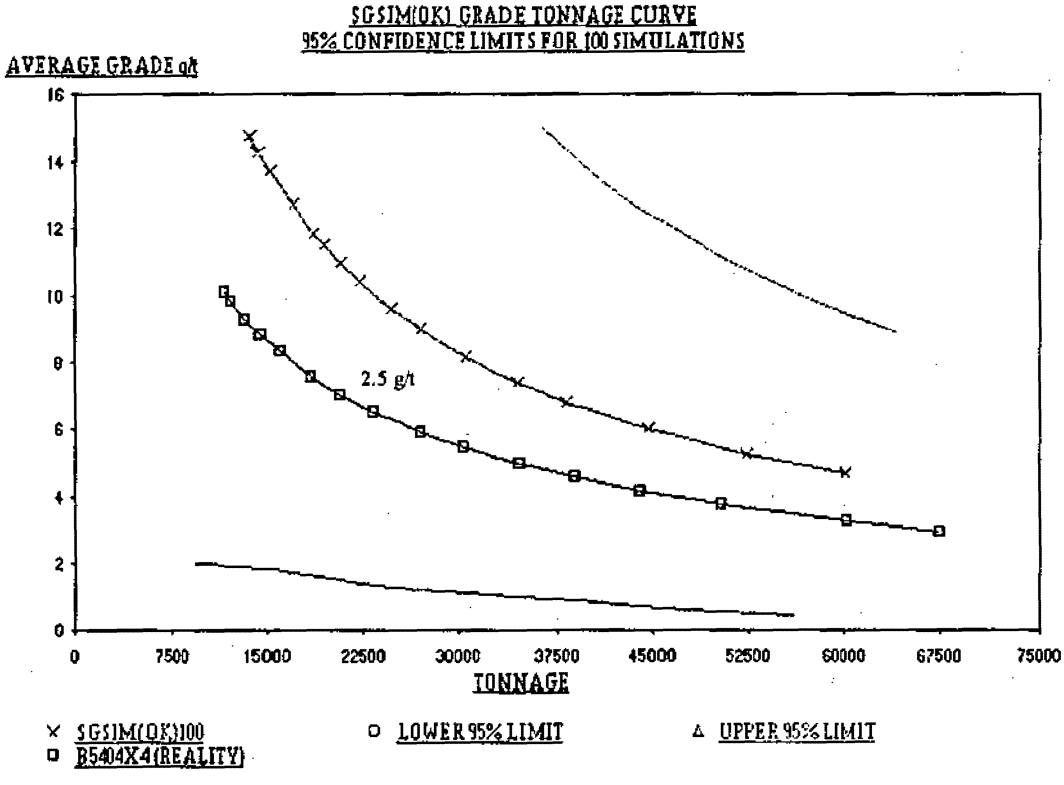

Figure 5.24. Average grade tonnage curve and 95% confidence intervals for 100 simulations of SGSIM(OK).

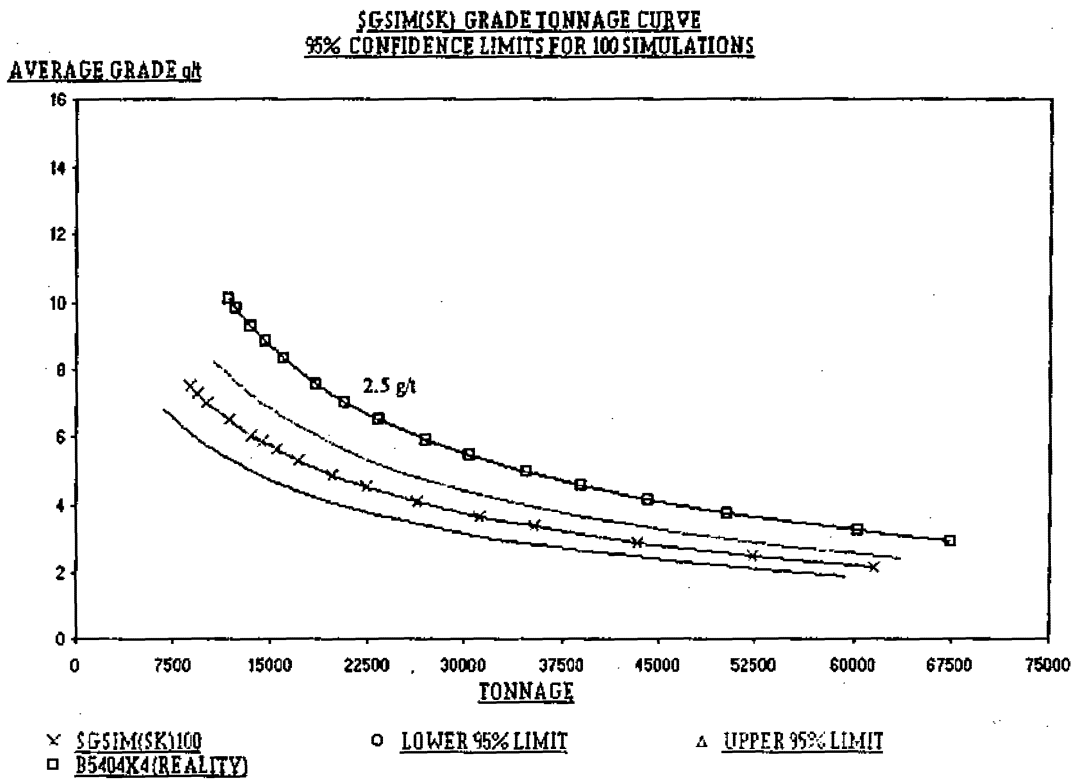

Figure 5.25. Average grade tonnage curve and 95% confidence intervals for 100 simulations of SGSIM(SK).

5.7 Summary

We have shown that fractal modelling of the spatial structure of an actual gold distribution is practical and achieves results that are, at least as good in all aspects and, for grade tonnage curves, better than sequential Gaussian simulation using a spherical model.

6 Conclusions and Recommendations

A variety of stochastic fractal simulations methods are in practical use in areas such as in computer graphics for surface visualisation and in the petroleum industry for flow simulations. However, to date, with the exception of Prasad (1991) whose Ph.D. thesis used a modified successive random additions fractal method on sulphur in coal, only theoretical applications to ore body modelling with fractal simulations have been undertaken. This is perhaps because previous fractal methods cannot handle irregularly spaced data and/or cannot quickly condition a simulation and/or do not reproduce the spatial structure. At best the spectral fractal methods available have been found to produce results that are no better or worse than traditional geostatistical methods (Bruno & Raspa, 1989 ; Chu & Journel 1992).

6.1 Conclusions

What we have achieved in this thesis is the creation of a new tool that incorporates fractal concepts into geostatistics and which can be used in geostatistical simulation and ore body modelling. This tool has been formed by drawing together simulation techniques and ideas from both geostatistics and computer graphics and combining them in a unique way. The original contributions of the thesis are:

(1) A method for the use of the (truncated) power model with bounded experimental semi-variogram models.

(2) The adaptation and extension of Rümelin's covariance equations to work with sparse irregularly spaced data while maintaining the conditionality of a simulation enabling the use of the power model with sequential Gaussian simulation, thus overcoming the two major drawbacks of most existing fractal simulation methods.

(3) The incorporation of the fractal co-dimension as an additional statistic that can be reproduced with Gaussian geostatistical simulations.

It is also the first time that we know of that a real gold mineralisation, highly skewed data set has been simulated with a fractal method. The importance of this new tool is that it creates geostatistical simulations that specifically capture the fractal nature of a distribution as well as its histogram and spatial structure. The other advantage of SGFRACT is that it does not require knowledge of spectral techniques and anyone already familiar with semi-variograms has the theoretical knowledge required to understand and implement it.

Specifically it has been shown that, for the two skewed distribution data sets, *Gslib97* and *exp540*, SGFRACT produces a simulated average grade tonnage curve that is closer to reality than sequential Gaussian simulation and ordinary kriging. Also, in the sparse data situation in chapter five SGFRACT produced a smaller range of fluctuations compared with SGSIM(OK) and is therefore less sensitive to anomalies that occur in back transforming. The method runs just as fast, in terms of computing time, as sequential Gaussian for simulations of the sizes used in the case studies.

The method has the limitation that it can provide only ordinary kriging type estimates but this is of very little concern as ordinary kriging is preferable to simple kriging in most situations. Another possible limitation is that the method can only be used with a power model. It is also restricted to using normal score data but this disadvantage is not exclusive to SGFRACT.

6.2 Extensions and Recommendations

The major aspect that needs attention is the normalisation factor. With further work the relationships between the grid size, field size, model parameters and random path used could be further analysed with the aim being to determine the normalisation factor theoretically rather than experimentally. It is possible that the normalisation factor is partly related to the introduction of a feedback loop that allows the simulation of points, from previously simulated points alone, that would otherwise remain unknown. Further studies examining the possible creation of bias by the normalisation and/or the feedback loop would be useful. The sensitivity of the simulations to the normalisation factor should also be examined.

There is still the potential for extension of this method and to date an LU version that simulates many points at once (LUFRACT) has been written but will not be discussed in detail here. The first obvious extension is to adapt both SGFRACT and LUFRACT to three dimensions. There is no theoretical reason for this not to be a simple task. The next obvious possible extension is to implement nesting so that a nugget effect, by way of $2H = 0$, can be included if desired. However, practice so far has shown that the power model alone copes quite well in situations where a nested nugget and spherical model would normally be used. Some other possible extensions and questions that need to be answered are:

(a) Can SGFRACT be adapted to indicator methods?

(b) Can it handle zonal anisotropy?

(c) Do we ever need to model a nugget effect?

(d) Can multi-fractals be incorporated?

In the sense that they all deal with nesting of models, (b), (c) and (d) are all related. Chu & Journel (1992) have shown that fractal models can be nested using spectral methods but whether the same style of nesting would work with SGFRACT requires investigation.

(e) When working with data that have a sill, could results be improved by selecting only those models that reproduce a clear sill?

Examination of many individual simulated semi-variograms showed a tendency for some to continue to increase with distance while others created by the same simulation parameters but different random path showed a definite sill. This presumably occurred because of the truncated nature of the model where the spatial structure beyond the range was uncontrolled.

(f) What is the relationship between the normal score fractal co-dimension and the actual fractal co-dimension?

In the case of the isotropic data set *True* in chapter four the fractal co-dimension for the actual and normal score data were not the same. With the anisotropic real data sets *Berea* and *b5404x4* used in chapters four and five the fractal co-dimension did remain the same after normal score transformation. This may be because these two data sets are real and the GSLIB data is a simulation that takes no account of the fractal co-dimension.

In conclusion we can say that use of the fractal co-dimension does make a useful contribution to ore body modelling and geostatistics when used in conjunction with existing methods. SGFRACT achieves this and has potential to provide even better results with future work on the topics listed above.

References

Alabert F. 1987. The practice of fast conditional simulations through the LU decomposition of the covariance matrix. *Mathematical Geology*. **19**, 5, 369 - 386.

Brooker P. 1985. Two dimensional simulations by turning bands. *Mathematical Geology*. **17**, 1, 81 - 90.

Bruno R. & Raspa G. 1989. Geostatistical characterisation of fractal models of surfaces. *Geostatistics*. **1**. 77-89. Kluwer academic publishers.

Burrough P.A. 1981. Fractal dimensions of landscapes and other environmental data. *Nature*. **294**, 240 - 242.

Carr J. & Benzer W. 1991. On the practice of estimating the fractal dimension. *Mathematical Geology*. **23**, 945 - 958.

Chilès J.P. & Delfiner P. 1996. Discrete exact simulation by the Fourier method. in Baafi E.Y. & Schofield N.A (eds.) *Geostatistics Wollongong '96*. **1**, 258 - 269. Kluwer Academic Publishers.

Chu J. 1996. Fast sequential indicator simulation: Beyond the reproduction of indicator variograms. *Mathematical Geology*. **28**, 7, 923 - 936.

Chu J. & Journel A.G. 1994. Conditional fBm simulation with dual kriging. in Dimitrakopoulos R. (ed.) *Geostatistics For The Next Century*. 407 - 421. Kluwer Academic Publishers.

Costa J.P. & Dimitrakopoulos R. 1997. Enhancing orebody delineation with fractal geostatistics. (pre-print) in *Proceedings 4th International Symposium on Mine Mechanisation and Automation*, 6-9 July 1997, Brisbane, Australia.

Cressie N.A.C. 1991. *Statistics for Spatial Data*. John Wiley & Sons Inc.

Cressie N.A.C. 1993. Aggregation in geostatistical problems. in Soares A. (ed.) *Geostatistics Tróia '92*. **1**, 25 - 36. Kluwer Academic Publishers.

Davis M.W. 1987. Production of conditional simulations via the LU decomposition of the covariance matrix. *Mathematical Geology*. **19**, 2, 91 - 98.

Deutsch C.V. & Cockerham P. W. 1994. Practical considerations in the application of simulated annealing to stochastic simulation. *Mathematical Geology*. **26**, 1, 67 - 82.

Deutsch C.V. & Journel A.G. 1992. *GSLIB: Geostatistical Software Library Users Guide*. First Edition. Oxford University Press.

Deutsch C.V. & Journel A.G. 1996. *GSLIB: Geostatistical Software Library and Users Guide*. Second Edition. (Pre-print). Oxford University Press.

Dowd P. A. & Sarac C. 1994. An extension of the LU decomposition method of simulation. in Armstrong M. & Dowd P. A. (eds.) *Geostatistical Simulations*. 23 - 36. Kluwer Academic Publishers.

Dunn J. 1997. Look for the golden lining. *Shares*. Aug. 97, 22 - 23.

Fox C.G. 1987. An inverse Fourier transform algorithm for generating random signals of a specified form. *Computers and Geosciences*. **13**, 4, 369 - 374.

Froidevaux R. 1993. Probability field simulation. in Soares A. (ed.) *Geostatistics Tróia '92*. **1**, 73 - 84. Kluwer Academic Publishers.

Galli A. et. al. 1994. The pros and cons of the truncated Gaussian method. in Armstrong M. & Dowd P.A. (eds.) *Geostatistical Simulations*. Kluwer Academic Publishers.

Gemcom Computer Services Inc. 1996. GEMCOM. Gemcom Computer Services, Vancouver B.C. Canada. (Software).

Giordano R. Slater S. & Mohanty K. 1985. The effects of permeability variations on flow in porous media. *SPE Paper 14365, 60th SPE Annual Conference*, Las Vegas.

Glacken I. 1996. Change of support and use of economic parameters for block selection. in Baafi E.Y. & Schofield N.A (eds.) *Geostatistics Wollongong '96*. **1**, 811 - 821. Kluwer Academic Publishers.

Gòmez-Hernàndez J.J. & Srivastava R.M. 1990. ISIM3D: An ANSI-C three dimensional multiple indicator conditional simulation program. *Computers and Geosciences*. **16**, 4, 395 - 408.

Goovaerts P. 1997. *Geostatistics for Natural Resources Evaluation*. Oxford University Press.

Hewett T.A. 1986. Fractal distributions of reservoir heterogeneity and their influence on fluid transport. *Paper SPE 15386 presented at the 61st Annual Technical Conference and Exhibition of The Society of Petroleum Engineers*, New Orleans.

Isaaks E.H. & Srivastava R.M. 1989. *An Introduction to Applied Geostatistics*. Oxford University Press.

James R.C. & James C.J. 1992. *Mathematics Dictionary*. Van Nostrand Reinhold.

Johnson R.A. & Wichern D.W. 1992. *Applied Multivariate Statistical Analysis*. Prentice Hall, Inc.

Journel A.G. & Alabert F. 1989. Non Gaussian data expansion in the earth science. *Terra Nova*. **1**, 123 - 134.

Journel A.G. & Alabert F. 1990. New methods for reservoir mapping. *Journal of Petrolium Technology*. **42**, 2, 212 - 218.

Journel A.G. & Deutsch C.V. 1996. Rank order geostatistics: A proposal for a unique coding and common processing of diverse data. in Baafi E.Y. & Schofield N.A (eds.) *Geostatistics Wollongong '96*. **1**, 258 - 269. Kluwer Academic Publishers.

Journel A.G. & Huijbregts Ch.J. 1978. *Mining Geostatistics*. Academic Press. London.

Kanevski M. 1997. UPFILE. Systems Analysis lab. Nuclear Safety Institute of Russian Academy of Science. (Software)

Klinkenberg B. 1994. A review of methods used to determine the fractal dimension of linear features. *Mathematical Geology*. **26**, 1, 23 - 46.

Klinkenberg B. & Goodchild M.F, 1992. Fractal properties of topography: A comparison of methods. *Earth Surface Proceedings. Landforms*. **17**, 217 - 234.

Lewis J.P. 1987. Generalised stochastic subdivision. *ACM Transactions on Graphics*. **6**, 3, 167 - 190.

Lovejoy S. & Schertzer D. 1987. Extreme variability. Scaling and fractals in remote sensing. Analysis and simulation. in Muller (ed), *Digital Image Processing In Remote Sensing*. Taylor and Francis.

Mandelbrot B.B. 1983. *The Fractal Geometry of Nature*. W. H. Freeman and company. New York.

Mandelbrot B.B. & Van Ness J.W. 1968. Brownian motions, fractional noises and applications. *SIAM Review*. **10**, 422 - 433.

Mandelbrot B.B. & Wallis J.R. 1969. Computer experiments with fractional Gaussian noises. Part 3, Mathematical appendix. *Water Resources Research*. **5**, 1, 260 - 267.

Nowak M.S. Srivastava R.M. & Sinclair A.J. 1993. Conditional simulation: A mine planning tool for a small gold deposit. in Soares A. (ed.) *Geostatistics Tróia '92*. 977 - 987. Kluwer Academic Publishers.

Pannatier Y. 1994. VARIOWIN 2.1. Institute of Mineralogy and Petrography - University of Lausanne - Switzerland. (Software).

Peitgen H-O. & Saupe D. (eds) 1988. *The Science of Fractal Images*. Springer Verlag.

Prasad K.V.K. 1991. *Variability Forecasting: Geostatistical, Spectral and Fractal Approaches*. Ph.D. Thesis. Pennsylvania State University. U.M.I. Dissertation Services.

Press W. et. al. 1986. *Numerical Recipes.* Cambridge University Press, New York.

Quick D. 1991. Geology of the Goodall gold mine. *Proceedings of the AUSIMM annual Conference, Darwin August 1991.* 75 - 82.

Ravenscroft P. J. 1994. Conditional simulation for mining: Practical implementation in an industrial environment. in Armstrong M. & Dowd P. A. (eds) *Geostatistical Simulations.* 79 - 88. Kluwer Academic Publishers.

Rivoirard J. 1990. Introduction to disjunctive kriging and non-linear geostatistics. *C-143.* Fontainebleau/CG.

Rümelin W. 1990. Simulation of fractional Brownian Motion. in Peitgen et. al. (eds) *Fractals in the Fundamental and Applied Sciences.* Elsevier.

Rümelin W. 1992. Fractal interpolation of random fields of fractal Brownian motion. in Encarnacao et. al. (eds) *Fractal Geometry and Computer Graphics.* 122 - 131. Springer Verlag.

Shibli S.A.R. 1996. Calculation of the fractal dimension. *http://java.ei.jrc.it/rem/gregoire/NEWSLETTER/13/13.2.1.html*

Srivastava R. 1992. Reservoir characterisation with probability field simulation. in *SPE Annual Conference and Exhibition, Washington DC. paper number 24753.* 927 - 938.

Tukey J. 1977. *Exploratory Data Analysis.* Addison - Wesley, Reading, MA.

Turcotte D.L. 1992. *Fractals and Chaos in Geology and Geophysics.* Cambridge University Press.

Voss R.F. 1985. Random fractal forgeries. in NATO ASI Series Vol. 17 Fundamental *Algorithms for Computer Graphics.* 805 -835. Springer -Verlag Berlin.

Voss R.F. 1988. in Pietgen H-O & Saupe D. (eds.) *The Science of Fractal Images.* Springer Verlag.

Wackernagel H. 1995. *Multivariate Geostatistics.* Springer-Verlag Berlin Heidelberg.

Walpole R.E. & Myers R.H. 1993. *Probability and Statistics for Engineers and Scientists.* Macmillan Publishing Company.

Appendix A - Notation and Symbols

The notation and symbols used throughout the thesis are listed in order of appearance in the text.

R	Region
$\mathbf{u}$	Location vector (u^x, u^y, u^z)
α, β	Location subscript indices eg. $\mathbf{u}_\alpha$
$Z(\mathbf{u}_\alpha)$	Random variable
$Z(\mathbf{u})$	Random function
$z(\mathbf{u}_\alpha)$	Regionalised value
$z(\mathbf{u})$	Regionalised variable
$m(\mathbf{u})$	Non-stationary mean of a random function, also drift
$Y(\mathbf{u})$	Stationary random function
e	Noise term
F	Cumulative frequency distribution function
$P(\,)$	Probability function
$E[\,]$	Expectation
σ^2	Variance
$Var(\,)$	Variance function
$C(\,)$	Covariance
$2\gamma(\mathbf{h})$	Variogram function
$\mathbf{h}$	Translation vector or increment
m	Stationary mean
$\gamma(\mathbf{h})$	Semi-variogram function
$\lvert\mathbf{h}\rvert$	Increment distance or lag
λ	Weight
c_0	Nugget variance

c_1	Partial sill
a	Range
b	Constant of proportionality
θ	Power of power model
φ	Principal direction of anisotropy in degrees
τ	Anisotropy ratio
$\mathbf{R}$	Rotation matrix
$\mathbf{A}$	Anisotropy transformation matrix
$v(\mathbf{u}_\alpha)$	Support volume at $\mathbf{u}_\alpha$
$z_v(\mathbf{u}_\alpha)$	Regionalised value defined on support v
$Z^*_{SK}(\mathbf{u}_i)$	Simple kriging estimator
σ^2_{SK}	Simple kriging estimation error variance
$Z^*_{OK}(\mathbf{u}_i)$	Ordinary kriging estimator
σ^2_{OK}	Ordinary kriging estimation error variance
μ	Lagrange parameter
$\mathbf{C}$	Variance covariance matrix
λ	Matrix of weights
$z^{(l)}(\mathbf{u})$	Unconditional simulation
$z^{(l)}_c(\mathbf{u})$	Conditional simulation
$N(m, \sigma^2)$	Normal distribution
$f()$	Probability density function
$G()$	Standard normal cumulative distribution function
ω	Flattening parameter for upper tail extrapolation
$\mathbf{L}$	Lower decomposition of variance covariance matrix $\mathbf{C}$
$\mathbf{U}$	Upper decomposition of variance covariance matrix $\mathbf{C}$
$\mathbf{w}$	Vector of standard normal score values

Ω	Set of points
E	Euclidean dimension
r	Scale factor
D	Fractal dimension
$\mathbf{r}$	Scaling vector where r_i is not necessarily equal to r_j
$B(\mathbf{u})$	Brownian motion
$B_H(\mathbf{u})$	Fractional Brownian motion
H	Fractal co-dimension
V_H	Proportionality constant equal to the characteristic variance at the reference unit lag for fractional Brownian motion
$W_H(\mathbf{u})$	Fractional Gaussian noise
$\mathbf{S}$	Estimation error standard deviation matrix
η	Subscript index for a specific regionalised value used for increment calculation with the covariance of increments fractal simulation method
s	Standard deviation

Appendix B - Data (sub)Set listings

Gslib97

```
GSLIB 97 conditioning data
      4
Xlocation
Ylocation
Elevation
Primary
 39.500  18.500   0.000   0.060
  5.500   1.500   0.000   0.060
 38.500   5.500   0.000   0.080
 20.500   1.500   0.000   0.090
 27.500  14.500   0.000   0.090
 40.500  21.500   0.000   0.100
 15.500   3.500   0.000   0.100
  6.500  25.500   0.000   0.110
 38.500  21.500   0.000   0.110
 23.500  18.500   0.000   0.160
  0.500  25.500   0.000   0.160
  9.500  19.500   0.000   0.170
 36.500  43.500   0.000   0.180
 21.500   5.500   0.000   0.190
 13.500   3.500   0.000   0.190
 40.500   7.500   0.000   0.190
 31.500  17.500   0.000   0.220
 46.500  40.500   0.000   0.240
 10.500   7.500   0.000   0.260
 28.500  11.500   0.000   0.280
  8.500   7.500   0.000   0.280
 47.500   0.500   0.000   0.310
  4.500  37.500   0.000   0.320
 14.500  21.500   0.000   0.330
 22.500  48.500   0.000   0.340
 18.500   6.500   0.000   0.340
  3.500  38.500   0.000   0.340
 11.500  46.500   0.000   0.400
 31.500  26.500   0.000   0.450
 14.500  29.500   0.000   0.460
 14.500  43.500   0.000   0.510
 38.500  28.500   0.000   0.570
 45.500  14.500   0.000   0.620
  4.500  30.500   0.000   0.650
  6.500  41.500   0.000   0.670
  7.500  12.500   0.000   0.710
 26.500  23.500   0.000   0.790
  8.500  45.500   0.000   0.810
 14.500  46.500   0.000   0.830
 13.500  24.500   0.000   0.840
 26.500   1.500   0.000   0.890
 33.500   7.500   0.000   0.920
 45.500  22.500   0.000   0.930
 48.500  25.500   0.000   0.940
 35.500  10.500   0.000   0.960
 34.500  14.500   0.000   0.990
 13.500  39.500   0.000   0.990
```

7.500	18.500	0.000	1.010
15.500	27.500	0.000	1.020
3.500	33.500	0.000	1.100
11.500	15.500	0.000	1.110
22.500	30.500	0.000	1.210
45.500	29.500	0.000	1.210
13.500	12.500	0.000	1.270
22.500	11.500	0.000	1.340
17.500	34.500	0.000	1.360
39.500	43.500	0.000	1.370
3.500	23.500	0.000	1.380
30.500	22.500	0.000	1.380
46.500	13.500	0.000	1.660
30.500	9.500	0.000	1.700
27.500	32.500	0.000	1.710
12.500	34.500	0.000	1.780
25.500	4.500	0.000	1.810
27.500	34.500	0.000	1.820
45.500	6.500	0.000	1.890
3.500	47.500	0.000	1.960
33.500	31.500	0.000	1.980
41.500	26.500	0.000	2.130
19.500	20.500	0.000	2.170
0.500	41.500	0.000	2.330
5.500	22.500	0.000	2.340
43.500	10.500	0.000	2.470
41.500	45.500	0.000	2.750
28.500	42.500	0.000	2.760
21.500	34.500	0.000	2.840
16.500	13.500	0.000	2.990
23.500	24.500	0.000	3.040
2.500	1.500	0.000	3.330
47.500	44.500	0.000	3.350
39.500	38.500	0.000	3.510
46.500	34.500	0.000	3.810
35.500	45.500	0.000	4.600
25.500	25.500	0.000	4.890
28.500	44.500	0.000	5.050
19.500	42.500	0.000	5.150
38.500	36.500	0.000	5.310
2.500	9.500	0.000	6.260
32.500	36.500	0.000	6.410
0.500	8.500	0.000	6.490
31.500	45.500	0.000	7.530
9.500	29.500	0.000	8.030
39.500	31.500	0.000	8.340
17.500	15.500	0.000	9.080
2.500	14.500	0.000	10.270
30.500	41.500	0.000	17.190
35.500	32.500	0.000	18.760

```
Berea64 data
      4
Xloc
Yloc
Elevation
Variable      1
25.5000 29.5000  0.0000 45.0000
26.5000 10.5000  0.0000 51.0000
36.5000 19.5000  0.0000 51.5000
 9.5000  9.5000  0.0000 59.5000
21.5000 15.5000  0.0000 59.5000
25.5000  0.5000  0.0000 42.5000
17.5000 11.5000  0.0000 54.5000
33.5000 19.5000  0.0000 56.0000
27.5000  2.5000  0.0000 34.0000
33.5000 21.5000  0.0000 45.0000
 8.5000 24.5000  0.0000 41.5000
26.5000  1.5000  0.0000 40.0000
 2.5000 31.5000  0.0000 51.0000
12.5000 34.5000  0.0000 50.5000
 9.5000 18.5000  0.0000 50.0000
30.5000 34.5000  0.0000 80.0000
28.5000 20.5000  0.0000 64.5000
 0.5000 38.5000  0.0000 60.5000
20.5000 33.5000  0.0000 49.5000
 3.5000 39.5000  0.0000 64.5000
24.5000 11.5000  0.0000 45.0000
39.5000 32.5000  0.0000 99.5000
 1.5000 30.5000  0.0000 56.0000
27.5000 14.5000  0.0000 64.0000
30.5000  3.5000  0.0000 72.0000
 7.5000 19.5000  0.0000 30.0000
32.5000  7.5000  0.0000 60.0000
20.5000  1.5000  0.0000 62.0000
 6.5000 37.5000  0.0000 65.0000
26.5000 36.5000  0.0000 80.0000
20.5000 20.5000  0.0000 62.5000
17.5000 25.5000  0.0000 55.0000
17.5000  1.5000  0.0000 45.5000
 3.5000 26.5000  0.0000 49.0000
 6.5000 39.5000  0.0000 55.0000
34.5000 23.5000  0.0000 34.0000
 2.5000 23.5000  0.0000 50.5000
24.5000 10.5000  0.0000 47.0000
20.5000 37.5000  0.0000 65.0000
 8.5000 33.5000  0.0000 70.0000
34.5000  1.5000  0.0000 71.0000
22.5000 33.5000  0.0000 48.0000
21.5000 30.5000  0.0000 36.0000
20.5000  8.5000  0.0000 24.0000
34.5000 32.5000  0.0000 82.0000
37.5000  9.5000  0.0000 88.5000
 9.5000 33.5000  0.0000 47.0000
29.5000 24.5000  0.0000 42.0000
 2.5000 11.5000  0.0000 36.5000
```

```
30.5000 14.5000  0.0000 61.5000
26.5000 20.5000  0.0000 57.5000
36.5000 36.5000  0.0000 91.0000
16.5000 31.5000  0.0000 51.0000
 1.5000  3.5000  0.0000 42.5000
31.5000  7.5000  0.0000 50.0000
18.5000  7.5000  0.0000 27.0000
17.5000 22.5000  0.0000 59.5000
29.5000  7.5000  0.0000 57.5000
13.5000 38.5000  0.0000 42.0000
10.5000 29.5000  0.0000 45.0000
19.5000 15.5000  0.0000 50.0000
35.5000 21.5000  0.0000 52.0000
 7.5000 25.5000  0.0000 41.0000
35.5000  6.5000  0.0000 69.0000
```

exp540

expl. comp. 540RL as used for simulations

4
Northing
Easting
Elevation
Au

10898.96	10154.20	538.75	1.06
11000.07	10178.87	538.74	0.05
10947.87	10171.24	538.75	1.08
10948.43	10144.03	538.75	12.68
11049.63	10175.81	538.75	0.54
10846.27	10160.30	538.75	0.31
11102.01	10181.02	538.75	5.52
11047.54	10178.34	538.76	0.23
10996.27	10157.20	538.75	4.99
10800.00	10152.24	538.75	0.76
10825.00	10146.38	538.75	5.26
10825.00	10174.72	538.75	1.93
10849.90	10148.60	538.75	0.38
10849.60	10162.85	538.75	1.25
10876.50	10143.17	538.75	1.65
10875.00	10174.95	538.75	3.97
10900.10	10139.15	538.75	1.54
10900.10	10168.95	538.75	1.50
10925.00	10168.81	538.75	0.53
10950.00	10173.54	538.75	1.42
11075.00	10161.97	538.75	1.11

Appendix C - SGFRACT Fortran 77 Code

The following two subroutines *krige* and *cova3* are part of the SGFRACT program source code and contain the essential differences between SGFRACT and SGSIM. They are not sufficient on their own to carry out a fractal simulation but are part of a much larger body of source code that was originally written by C.V. Deutsch for the SGSIM program and has been modified by D.J. Kentwell to form the SGFRACT program. Deutsch & Journel (1992) contains a full copy of the source code for SGSIM on disk and it is also available on the internet at *ftp://banach.stanford.edu/gslib/*.

```
      subroutine krige(ix,iy,iz,xx,yy,zz,cmean,cstdev)
c-----------------------------------------------------------------------
c
c          Builds and Solves the SK or OK Kriging System
c          *********************************************
c
c INPUT VARIABLES:
c
c  ix,iy,iz       index of the point currently being simulated
c  xx,yy,zz       location of the point currently being simulated
c
c
c
c OUTPUT VARIABLES:
c
c  cmean          kriged estimate
c  cstdev         kriged standard deviation
c
c
c
c EXTERNAL REFERENCES: cholfbs Cholesky LU linear system solver
c                      sqdist  anisotropic squared distance
c
c
c ORIGINAL: C.V. Deutsch                        DATE: August 1990
c MODIFIED: D.J. Kentwell                         May  1997
c-----------------------------------------------------------------------
      include 'sgfract.inc'
      flg=0
```

```
c
c Split off first node as reference value n and resize close( ):
c
    if(nclose.gt.0) then
        index=int(close(1))
        xn=x(index)
        yn=y(index)
        zn=z(index)
        vra(1)=vr(index)
        nclose=nclose-1
        if(idbg.ge.3) then
            write(ldbg,*) ' n-xy' ,xn,yn
            write(ldbg,*) ' i-xy' ,xx,yy
        endif
        do 7 k=1,nclose
            close(k)=close(k+1)
7       continue
    else
c
c  if all data is colocated with simulation nodes
c
        index=1
        xn=cnodex(index)
        yn=cnodey(index)
        zn=cnodez(index)
        vra(1)=cnodev(index)
        ncnode=ncnode-1
        flg=1
        if(idbg.ge.3) then
            write(ldbg,*) ' n-xy' ,xn,yn
            write(ldbg,*) ' i-xy' ,xx,yy
        endif
        do 8 l=1,ncnode
           icnode(l)=icnode(l+1)
8       continue
    endif
c
c Calculate the reference step size.
c
        is=1
        step=sqdist(xx,yy,zz,xn,yn,zn,is,MAXROT,rotmat)
        step=sqrt(step)
        if(idbg.ge.3) write(ldbg,*)'step= ',step
c
c Size of the linear system:
c
    na   = nclose + ncnode
    if(idbg.ge.3) then
    write(ldbg,*) 'nclose= ' ,nclose ,'ncnode= ' ,ncnode
```

```
      endif
c
c Set up kriging matrices without reference value:
c
      in=0
      do 1 j=1,na
c
c Sort out the actual location of point "j"
c
            if(j.le.nclose) then
                  index  = int(close(j))
                  x1     = x(index)
                  y1     = y(index)
                  z1     = z(index)
                  vra(j+1) = vr(index)
            else
c
c It is a previously simulated or colocated node:
c
                  index  = j-nclose
                  if(flg.eq.1) then
                        indexx = j+1
                  else
                        indexx = index
                  endif
                  x1     = cnodex(indexx)
                  y1     = cnodey(indexx)
                  z1     = cnodez(indexx)
                  vra(j+1) = cnodev(indexx)
                  ind    = icnode(index)
                  ix1    = ix + (int(ixnode(ind))-nctx-1)
                  iy1    = iy + (int(iynode(ind))-ncty-1)
                  iz1    = iz + (int(iznode(ind))-nctz-1)
            endif
            if(idbg.ge.3) then
                  write(ldbg,*) ' 1-xy' ,x1,y1
            endif
            do 2 i=1,j
c
c Sort out the actual location of point "i"
c
                  if(i.le.nclose) then
                        index  = int(close(i))
                        x2     = x(index)
                        y2     = y(index)
                        z2     = z(index)
                  else
c
c It is a previously simulated or colocated node:
```

```
c
                index  = i-nclose
                if(flg.eq.1) then
                    indexx = i+1
                else
                    indexx = index
                endif
                x2    = cnodex(indexx)
                y2    = cnodey(indexx)
                z2    = cnodez(indexx)
                ind   = icnode(index)
                ix2   = ix + (int(ixnode(ind))-nctx-1)
                iy2   = iy + (int(iynode(ind))-ncty-1)
                iz2   = iz + (int(iznode(ind))-nctz-1)
            endif
c
c Now, compute the covariance matrix values:
c
            in = in + 1
            cov=cova3(x1,y1,z1,x2,y2,z2,xn,yn,zn,step)
            a(in)=dble(cov)
 2        continue
c
c Get the RHS column matrix:
c
        cov=cova3(x1,y1,z1,xx,yy,zz,xn,yn,zn,step)
        r(j)=dble(cov)
        rr(j)=r(j)
 1    continue
c
c Get the single value "S":
c
    cov=cova3(xx,yy,zz,xx,yy,zz,xn,yn,zn,step)
    ss=dble(cov)
    if(idbg.ge.3) write(ldbg,*) 'ss= ',ss
c
c Write out the kriging Matrix if Seriously Debugging:
c
    if(idbg.ge.3) then
        write(ldbg,100) ix,iy,iz
        is = 1
        do 4 i=1,na
            ie = is + i - 1
            write(ldbg,101) i,r(i),(a(j),j=is,ie)
            is = is + i
 4        continue
 100      format(/,'Kriging Matrices for Node: ',3i4,' RHS first')
 101      format('    r(',i2,') =',f7.4,'  a= ',99f7.4)
    endif
```

```
c
c Solve the linear System:
c
          call cholfbs(a,t,lu,r,s,na,na,ierr)
c
c Write a warning if the matrix is not positive definite:
c
     if(ierr.eq.1) then
          if(idbg.ge.1) then
               write(ldbg,*) 'WARNING chol-not positive definite'
               write(ldbg,*) '              for node',ix,iy,iz
          endif
          cmean  = 0.0
          cstdev = 1.0
          return
     endif
c
c Write out the kriging Matrix if Seriously Debugging:
c
     if(idbg.ge.3) then
          do 40 i=1,na
               write(ldbg,140) i,s(i)
 40        continue
 140       format(' Kriging weight for data: ',i4,' = ',f8.4)
     endif
c
c Compute missing reference element and local variance
c
     cstdev=0.0
     bn=0.0
     do 5 i=1,na
          bn=bn+real(s(i))
          cstdev=cstdev+real(s(i))*rr(i)
 5   continue
     bn=1-bn
     cstdev=ss-cstdev
     if(cstdev.lt.0.0) then
          write(ldbg,*) 'NEGATIVE VARIANCE: ',cstdev
          cstdev = 0.0
     endif
c
c  Get the standard deviation
c
     cstdev=sqrt(cstdev)*normf
c
c Compute the estimate and return:
c
     cmean  = real(bn)*vra(1)
     if(idbg.ge.3) then
```

```
        write(ldbg,*) ' vra1' ,vra(1) ,'bn ' ,bn
      endif
      do 6 i=1,na
        cmean  = cmean  + real(s(i))*vra(i+1)
        if(idbg.ge.3) then
          write(ldbg,*) 'vra',(i+1),' ' ,vra(i+1)
        endif
6     continue
      return
      end


      real function cova3(x1,y1,z1,x2,y2,z2,xn,yn,zn,step)
c-----------------------------------------------------------------------
c
c           Covariance Between Two Points (3-D Version)
c           *******************************************
c
c This function returns the covariance associated with a fBm power model
c that is specified by possibly four different
c nested variogram structures.  The anisotropy definition can be
c different for each of the nested structures.
c
c
c
c INPUT VARIABLES:
c
c   x1,y1,z1        Coordinates of first point
c   x2,y2,z2        Coordinates of second point
c   xn,yn,zn        Coordinates of the reference point
c   nst             Number of nested structures (max. 4).
c   c0              Nugget constant (isotropic).
c   cc(nst)          Multiplicative factor of each nested structure.
c                   Slope VH for power model.
c   aa(nst)          Parameter "a" (2H = power) of each nested structure.
c   it(nst)         Type of each nested structure 6 = fBm:
c   ang1             Azimuth angle for the principal direction of
c                  continuity (measured clockwise in degrees from Y)
c   ang2             Dip angle for the principal direction of continuity
c                  (measured in negative degrees down from horizontal)
c   ang3             Third rotation angle to rotate the two minor
c                  directions around the principal direction defined
c                  by ang1 and ang2.  A positive angle acts clockwise
c                  while looking in the principal direction.
c   anis1            Anisotropy (radius in minor direction at 90
c                  degrees from "ang1" divided by the principal radius
c                  in direction "ang1")
c   anis2            Anisotropy (radius in minor direction at 90 degrees
```

```
c               vertical from "ang1" divided by the principal
c               radius in direction "ang1")
c
c
c
c OUTPUT VARIABLES: returns "cova3" the covariance obtained from the
c               variogram model.
c
c
c EXTERNAL REFERENCES: sqdist    computes anisotropic squared distance
c
c ORIGINAL  C.V. Deutsch
c MODIFIED: D.J. Kentwell                                   May 1997
c-----------------------------------------------------------------------
      parameter(PI=3.14159265,DTOR=PI/180.0,PMX=9999.)
      include 'sgfract.inc'
c
c Loop over all the structures:
c
      cova3 = 0.0
      do 2 is=1,nst
c
c Compute the appropriate structural distance:
c
            hsqd1=sqdist(x1,y1,z1,xn,yn,zn,is,MAXROT,rotmat)
            hsqd2=sqdist(x1,y1,z1,x2,y2,z2,is,MAXROT,rotmat)
            hsqd3=sqdist(xn,yn,zn,x2,y2,z2,is,MAXROT,rotmat)
            h1 = sqrt(hsqd1)
            h2 = sqrt(hsqd2)
            h3 = sqrt(hsqd3)
            if(idbg.ge.3) then
              write(ldbg,*) 'h1-3 ' ,h1,h2,h3
            endif
c
c Calculate the fBm model covariances  as per Rumelin 1991.
c 'Simulation of fractional Brownian motion' in Peitgen et.al. (eds)
c Fractals in the Fundamental and applies Sciences. Elsevier. 1991.
c
            tmp=cc(is)*(h1**aa(is)-h2**aa(is)+h3**aa(is))
            cova3=cova3+tmp
 2    continue
      return
      end
```

Appendix D - Proof: Covariance of the increments of Fractional Brownian Motion

The increments or fractional Brownian motion are stationary and have mean 0. Hence

$$\begin{aligned} C(\Delta B(\mathbf{u}) &= E[\Delta B_H(\mathbf{u})\Delta B_H(\mathbf{u}+\mathbf{h})] \\ &= E[\Delta B_H(\mathbf{u}_\alpha)\Delta B_H(\mathbf{u}_\beta)] \end{aligned}$$

The covariance of the increment with respect to a known but arbitrary value at location $\mathbf{u}_\eta$ is then

$$= E[(B_H(\mathbf{u}_\alpha) - B_H(\mathbf{u}_\eta))(B_H(\mathbf{u}_\beta) - B_H(\mathbf{u}_\eta))]. \quad \text{(D.1)}$$

From equation 4.10 we have

$$E[|B_H(\mathbf{u}_\alpha) - B_H(\mathbf{u}_\beta)|^2] = V_H|\mathbf{u}_\alpha - \mathbf{u}_\beta|^{2H} \quad \text{(D.2)}$$

where V_H is a constant of proportionality. Alternatively

$$\begin{aligned} E[(B_H(\mathbf{u}_\alpha) - B_H(\mathbf{u}_\beta))^2] &= E[((B_H(\mathbf{u}_\alpha) - B_H(\mathbf{u}_\eta) + B_H(\mathbf{u}_\eta) - B_H(\mathbf{u}_\beta))^2] \\ &= E[(B_H(\mathbf{u}_\alpha) - B_H(\mathbf{u}_\eta))^2] + E[(B_H(\mathbf{u}_\eta) - B_H(\mathbf{u}_\beta))^2] \\ &\quad + 2E[(B_H(\mathbf{u}_\alpha) - B_H(\mathbf{u}_\eta))(B_H(\mathbf{u}_\eta) - B_H(\mathbf{u}_\beta))]. \quad \text{(D.3)} \end{aligned}$$

From equations D.1 and D.3 we get

$$\begin{aligned} &E[(B_H(\mathbf{u}_\alpha) - B_H(\mathbf{u}_\eta))(B_H(\mathbf{u}_\eta) - B_H(\mathbf{u}_\beta))] = \\ &\quad 0.5V_H(|\mathbf{u}_\alpha - \mathbf{u}_\beta|^{2H} - |\mathbf{u}_\alpha - \mathbf{u}_\eta|^{2H} - |\mathbf{u}_\eta - \mathbf{u}_\beta|^{2H}). \quad \text{(D.4)} \end{aligned}$$

Alternatively

$$\begin{aligned} &E[(B_H(\mathbf{u}_\alpha) - B_H(\mathbf{u}_\eta))(B_H(\mathbf{u}_\eta) - B_H(\mathbf{u}_\beta))] = \\ &\quad -E[(B_H(\mathbf{u}_\alpha) - B_H(\mathbf{u}_\eta))(B_H(\mathbf{u}_\beta) - B_H(\mathbf{u}_\eta))]. \quad \text{(D.5)} \end{aligned}$$

From equations D.1, D.4 and D.5 we the have the result

$$C(\Delta B_H(\mathbf{u})) = 0.5V_H(|\mathbf{u}_\alpha - \mathbf{u}_\eta|^{2H} - |\mathbf{u}_\alpha - \mathbf{u}_\beta|^{2H} + |\mathbf{u}_\eta - \mathbf{u}_\beta|^{2H}). \quad \text{(D.6)}$$

Appendix E - Goodall data set 'Evolution'